AN INTRINSIC, HETEROGENEOUS MODEL OF COMPOSITE SOLID PROPELLANT COMBUSTION

by

BRYAN MICHAEL RASMUSSEN

A THESIS

Submitted in partial fulfillment of the requirements

for the degree of Master of Science in Engineering in

The Department of Mechanical and Aerospace Engineering

of

The School of Graduate Studies

of

The University of Alabama in Huntsville

HUNTSVILLE, ALABAMA

1999

THESIS APPROVAL FORM

Submitted by Bryan M. Rasmussen in partial fulfillment of the requirements for the degree of Master of Science in Engineering with a major in Mechanical Engineering.

Accepted on behalf of the Faculty of the School of Graduate Studies by the thesis committee:

_____Committee Chair
(Date)

_____

_____

_____Department Chair

_____College Dean

_____Graduate Dean

ABSTRACT

School of Graduate Studies
The University of Alabama in Huntsville

Degree: Master of Science in Engineering College/Dept.: Engineering / Mechanical and Aerospace Engineering

Name of Candidate: Bryan Michael Rasmussen

Title: An Intrinsic, Heterogeneous Model of Composite Solid Propellant Combustion

This thesis is a theoretical study of composite solid propellant combustion, built around a computational model of AP/HTPB propellants. The purpose of the thesis is to investigate the effect of composite solid structure on nonsteady, nonlinear combustion processes. Of particular interest is the effect of heterogeneity on the nonlinear, pressure-coupled frequency response of the system. The model is a system of eight equations, two of which depend on an implicit solution of temperature profiles in the propellant binder and oxidizer. It is very complicated and computationally intense, but it can potentially show trends and dependencies that disappear under the assumptions of other models.

Two issues have become significant in the development of the current model. First, the model seems to show an over-dependence of flame structure on the burning rates of the propellant. Second, the concept of "frequency response" appears to be ambiguous for wholly nonlinear analyses. The thesis contains recommendations on how to address the issues. It also contains preliminary results, which show how AP mass percentage, mean pressure, pressure oscillation magnitude, AP particle diameter, and other parameters affect the frequency response.

Abstract Approval: Committee Chair _____

(Date)

Department Chair _____

Graduate Dean _____

Advisor: Dr. Robert A. Frederick, Jr. Assistant Professor

ACKNOWLEDGEMENTS

This work was sponsored by the California Institute of Technology Multidisciplinary University Research Initiative under ONR Grant No. N00014-95-1-1338.

I dedicate this thesis to my cat, Harbinger.

TABLE OF CONTENTS

Page

Page

LIST OF FIGURES

Page

LIST OF TABLES

LIST OF SYMBOLS

Symbol	Definition
A	pre-exponential factor; constant in response function; area; constant
a	factor in burning rate equation
B	constant in response function
C_p	constant-pressure specific heat
$C;\ c$	constants
D	diameter
d	distribution coefficient
D	diffusion coefficient
E	activation energy
F	mass distribution function in PEM
f	function
G	mass flux
i	imaginary number specifier; space vector index
j	time vector index
K	turbulent diffusion coefficient
k	ratio of motor throat area to burning surface area; ZN parameter
ℓ	length
M	total mass; molecular weight; coefficient in matrix equation
$\dot{m}$	mass flow rate
n	pressure exponent; total number of points in a matrix
P	pressure
q	specific energy
R_P	pressure-coupled frequency response function
r	burning rate; ZN parameter
S	surface fraction
s	Laplace variable, second

T	temperature
t	time
V	volume
v	solution in matrix equation
x	distance

a	mass fraction; thermal diffusivity
b	diffusion exponent
D	change in
d	x-spacing coefficient
z	non-dimensional exponent for reaction
q	non-dimensional temperature
l	thermal conductivity
m	non-dimensional mass flux; ZN parameter
n	exponential modifier
x	non-dimensional distance
p_k	pressure temperature sensitivity
r	density
s	mode width parameter in PEM
s_p	temperature sensitivity
t	non-dimensional time
f	non-dimensional function
W	non-dimensional frequency
w	frequency

Modifier	Description
$( )^{\pm}$	just above/below
$(\bar{?})$	mean or steady-state

$( )'$	differential, or nonsteady part
$( )_{ap}$	ammonium perchlorate
$( )_{b}$	binder
$( )_{d}$	diffusion
$( )_{eff}$	effective
$( )_{f}$	flame
$( )_{f\text{-}s}$	flame-to-surface
$( )_{g}$	gas
$( )_{i}$	initial
$( )_{lam}$	laminar
$( )_{max/min}$	maximum/minimum
$( )_{ox}$	oxidizer
$( )_{p}$	total propellant
$( )_{r}$	reaction
$( )_{s}$	solid; surface
$( )_{tr}$	transitional
$( )_{tot}$	total
$( )_{turb}$	turbulent
$( )_{v}$	total vaporization
$( )_{vap}$	surface vaporization
bold	indicates matrix or vector

Chapter I

INTRODUCTION

A. Solid Combustion

Solid Rockets are the simplest types of rockets, and for that reason they have been in use for centuries longer than any other type of mechanical propulsion device. For over 800 years, military engineers and pyrotechnic enthusiasts have added various and sundry solid ingredients to rocket cases in a confusing search for the best propellants. Modern scientific and engineering techniques have vastly improved on this trial-and-error approach. Research conducted during the 20^{th} century has resulted in better solid motor manufacturing methods and has added to a basic understanding of solid combustion.

Whereas the primary ingredient in almost all older rockets was gunpowder, modern solid propellants generally fall into one of two categories:

- *Double-base* propellants have a heterogeneous solid phase. They consist of solid nitrocellulose dissolved in nitroglycerin, possibly with a few minor additives. Double-base propellants are detonable, so they pose a safety risk during manufacturing or storage.
- *Composite* propellants have a heterogeneous solid phase. They consist of oxidizer particles suspended in a polymer binder. The most popular oxidizer is ammonium perchlorate (NH_4ClO_4), and most binders are polybutadiene variations. Most practical composite propellants also contain a powdered metallic fuel, such as aluminum. The binder itself will usually oxidize and burn during combustion, so the term “fuel” often refers to the binder and not the aluminum.

Regardless of the type of propellant, all solid propellants have some specific properties that are of interest to motor designers. One of the most important properties is the *burning rate*. Solid fuels ideally burn normal to the burning surface, an assumption that leads to a

linear burning rate in the units of distance/time. Figure 1.1 contains a simplified sketch of a burning solid rocket motor to illustrate the concept of a lindear burning rate.

Experiments have shown that macroscopic burning rates typically depend on a power of pressure through the equation

$$r = aP^n . \tag{1.1}$$

The relationship in Equation 1.1 is usually accurate over a local pressure range. It indicates an important parameter in solid motor design: the *pressure exponent*, *n*. If the pressure exponent is low, the propellant will be stable in the particular pressure range. If the exponent is high (approaching unity), then the propellant could potentially become unstable with a small change in pressure. Gunpowder, for example, has a high pressure exponent, so it explodes when pressurized.

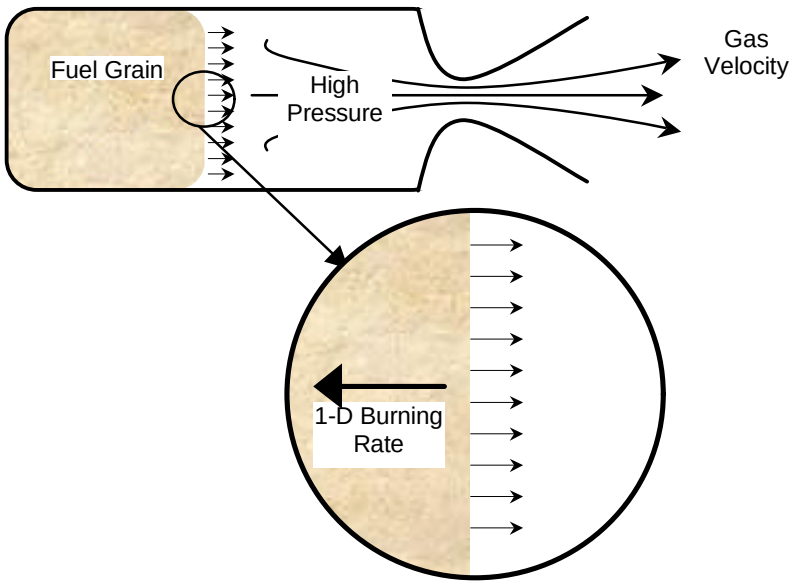

Figure 1.1: Sketch of Burning Solid Motor

Solid propellant burning rate is also a function of initial temperature of the propellant. Two variables, σ_p and π_k, describe the temperature sensitivity[1]. The sensitivity of the burning rate to initial temperature at constant pressure is σ_p. Its mathematical definition is

$$\sigma_p = \left.\frac{\partial \ln r}{\partial T_i}\right|_p = \left.\frac{\partial \ln aP^n}{\partial T_i}\right|_p = \frac{1}{a}\left.\frac{\partial a}{\partial T_i}\right|_p . \tag{1.2}$$

The temperature sensitivity of the pressure to initial temperature at a constant throat/burning surface area (k) is denoted π_k. It represents the sensitivity of the mean motor pressure to the initial temperature of the motor. Note that π_k only applies to whole motors, while σ_p can be an intrinsic property of the propellant. The definition of π_k is

$$\pi_k = \left.\frac{\partial \ln P}{\partial T}\right|_k = \frac{1}{P}\left.\frac{\partial P}{\partial T}\right|_k . \tag{1.3}$$

A system as complicated as a burning solid propellant will clearly have many other quantifiable elements that affect the system. Properties such as flame structure, deflagration-detonation-transition (DDT) environment, and composition of combustion products are all important to motor designers. A complete list of all parameters that could possibly be significant would require twenty or more pages.

One final property that is important in this paper, however, is the pressure-coupled frequency response function. Response functions in combustion are exactly like response functions in mechanics. They are ratios of the magnitude of an output function to the magnitude of a driving function. In the case of the pressure-coupled response, the driving function is pressure, and the output function is burning rate. The pressure-coupled response function, R_P, is

$$R_p = \frac{\dot{m}'/\bar{\dot{m}}}{P'/\bar{P}}, \tag{1.4}$$

where $\dot{m}$ is the mass burning rate, $(')$ denotes a differential change and $(\bar{})$ denotes a mean quantity. Pressure-coupled frequency response is an intrinsic property of the propellant that is very important in motor design. It is a function of frequency of pressure oscillations, so peaks in

R_P indicate areas where the propellant could easily become unstable. In Figure 1.2, for example, the propellant has a peak at around 675 Hz, and motor designers should not use the propellant in a motor that has a natural acoustic mode anywhere between 400 and 800 Hz.

Most of the rest of this thesis is an attempt to theoretically predict burning rates, temperature sensitivities, and pressure-coupled frequency response functions of a particular class of composite propellants. The following two sections introduce experimental and theoretical means of calculating these three properties.

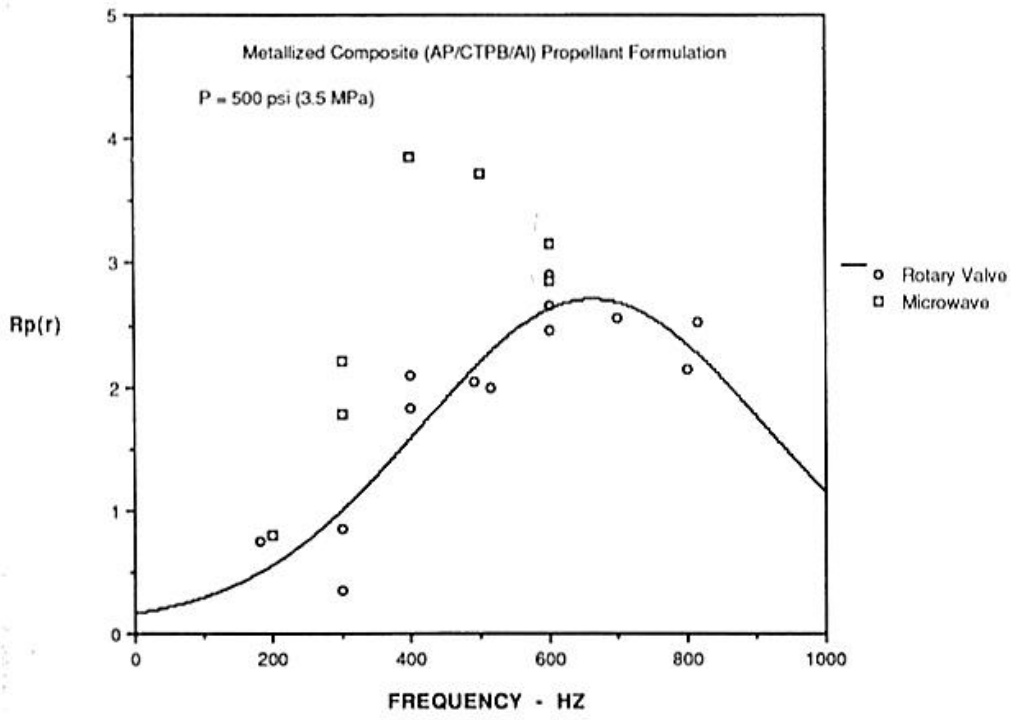

Figure 1.2: Example of Pressure-Coupled Frequency Response Function[2]

B. Experimental Research

1. Burning Rate

The most common way to obtain burning rates has traditionally been the Crawford strand burner[3]. This device, shown in Figure 1.3, is very simple. A propellant strand with an inhibiting outer coating has two or more wires threaded through it. As the surface regresses (linearly, by assumption), it burns through the wires, changing the resistance in the system. Knowing the time between the resistance change and the initial spacing of the wires allows for a calculation of the burning rate of the propellant.

There are many other techniques for finding burning rates in a laboratory. One relatively new technique is to use an ultrasonic transducer to bounce a sound wave off the propellant surface[4,5]. By measuring the time it takes to travel from the transducer to the surface and back, it is possible to calculate the position of the surface in a 50-200μs time interval. The ultrasonic method has two advantages: 1) it allows for many measurements in one test, and 2) it allows for measurements under pressure transients. Figure 1.4 is a simplified diagram of the ultrasonic technique.

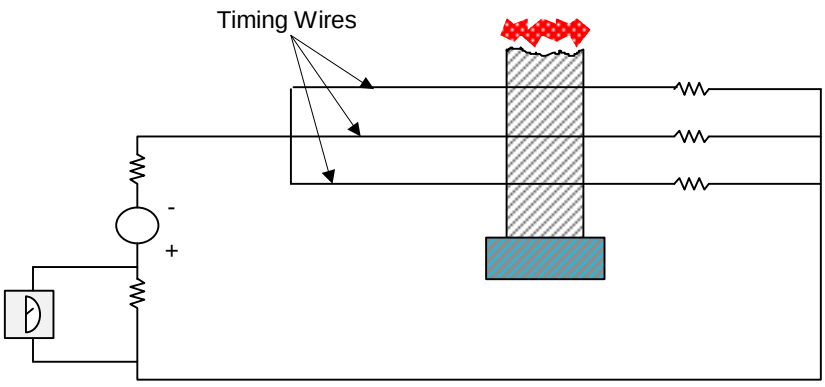

Figure 1.3: Crawford Strand Burner

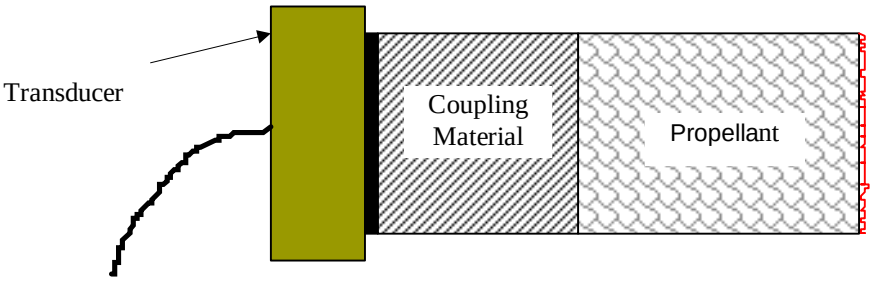

Figure 1.4: Ultrasonic Burning Rate Measurement

Unfortunately for motor designers, solid propellants do not always burn in an operational motor as they do in a laboratory. In a motor, hot, high-velocity gases are flowing over the surface of the propellant, thus increasing the burning rate and causing other difficulties. Expensive measurement methods, such as x-ray pictures[6], are usually necessary for measuring burning rates in motors although heavily instrumented experimental motors often contain ultrasonic transducers, thermocouples, pressure transducers, and an array of other instruments.

2. Temperature Sensitivity

In theory, finding temperature sensitivity is easy once the burning rate is known. If the burning rates are r_1 and r_2 at initial temperatures T_1 and T_2 respectively, then s_p is a simple relationship. For discrete data, s_P is

$$s_p = \left.\frac{\partial \ln r}{\partial T_i}\right|_p \cong \frac{\ln r_2 - \ln r_1}{T_2 - T_1}, \tag{1.5}$$

or, alternatively,

$$s_p = \left.\frac{\partial \ln r}{\partial T_i}\right|_p \cong \frac{1}{\bar{r}}\frac{r_2 - r_1}{T_2 - T_1}. \tag{1.6}$$

Similar relationships exist for p_k. The problem is that s_p and p_k are differential quantities, and discrete data do not generally translate well into smooth differences. Consequently, experimentally measured values of s_p and p_k typically have a great deal of scatter[7].

3. Frequency Response

By far the most widely used device for measuring propellant frequency response is the T-burner, which has a record of over 50,000 tests[8]. The T-burner is a length of tube with one propellant grain at each end. Gas flows out of the tube through a nozzle in the center of the tube, and the two propellant grains force pressure on each other to produce oscillations. The length of the tube determines the oscillation frequency. Figure 1.5 is a sketch.

T-burners have several disadvantages. Among other problems, they use a large amount of propellant per test, they do not generally generate reproducible results, and they do not accurately mimic internal motor conditions. As a consequence, other methods for determining the pressure-coupled frequency response are now under development. They include, but are not limited to, microwave burning rate measurements[9], exhaust modulation[10], magnetohydrodynamic flow measurement[11], and direct modulated mass-injection (now under development at UAH). Modern experimental methods still require significant development before they can produce accurate, cheap, reproducible response predictions.

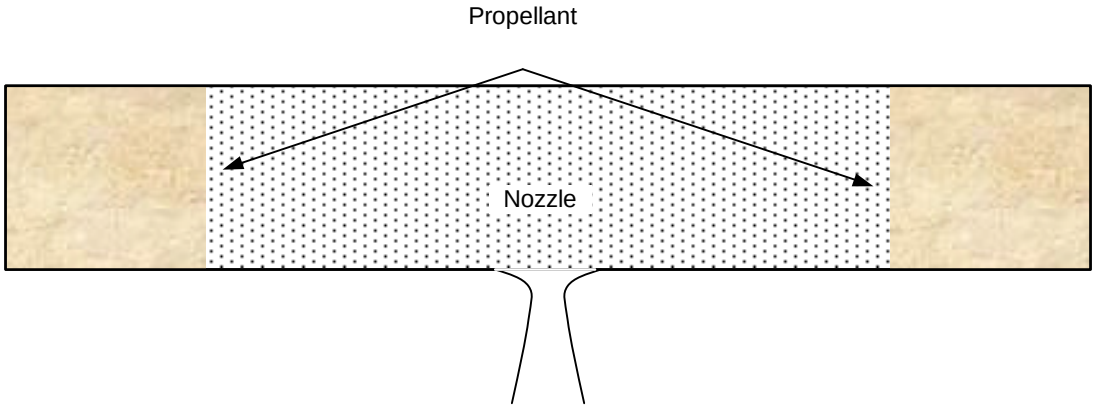

Figure 1.5: T-Burner

C. Theoretical Research — Steady-state Models

Combustion is a very complicated phenomenon, and modeling efforts are rarely able to quantitatively reproduce experimental data. A few models have been precise enough to stimulate burning rate "tailoring" for specific motors, but most models predict only qualitative behavior and trends. The most practical justification for spending money on theoretical combustion modeling is that theoretical procedures may lead to a better understanding of physical processes. That is, modeling has scientific value, not necessarily engineering value.

To make matters even more difficult, the heterogeneous structure of composite propellants complicates the combustion process, making a nearly intractable problem even worse. This additional complication generally prohibits analytic solutions of burning rate as a function of pressure and propellant properties. Most composite steady-state models, such as those listed below, require numerical solutions on computers.

1. Beckstead-Derr-Price Framework

The first successful heterogeneous model for composite propellants was probably the Beckstead-Derr-Price (BDP) multiple flame model[12]. This model was the first to recognize that the flame structure of a composite propellant was not homogeneous. Indeed, diffusion processes associated with heterogeneity often dominate the combustion process in BDP models.

The BDP concept involves three combustion regions: two kinetics-dominated (reaction) flames and one diffusion flame. The oxidizer, usually ammonium perchlorate (AP), breaks down in one reaction flame and sends approximately 30% O_2 into the diffusion flame. Binder decomposition products pre-react in the other reaction flame then rush into the diffusion flame, where they react further with the oxygen.

Examples of influential parameters in BDP models include the heat of vaporization, the heat conduction into the solid phase, and the flame standoff distances. In a BDP-type model, *where* the combustion occurs is as important as *how* it occurs.

2. Separate Surface Temperatures

Researchers have added numerous improvements to the original BDP model since its original publication[13]. One of the most important improvements is the consideration of separate surface temperatures for binder and oxidizer. Because the flame structure is different

over the binder and oxidizer, there is no reason why their surface temperatures or heat fluxes should be the same. Separate surface temperature models are necessarily more elaborate because they incorporate the solid-phase relationships of two original BDP models — one for the AP and one for the binder. Nevertheless, they can reproduce observed behavior that other, simpler models cannot[14].

3. Multi-modal Composite Propellants

Another limitation of the original BDP model was that it could only simulate propellants with a single oxidizer particle size. Most composite propellants, in contrast, contain a wide dispersal of oxidizer particle diameters. Such a scattering is actually desirable because propellants with a single oxidizer particle diameter are limited to slightly more than an 80% theoretical maximum oxidizer mass fraction. Simply put, small oxidizer particles are necessary to fit in between the large ones in order to have a high oxidizer percentage.

Most propellants have essentially two or three particle sizes, with a scattering of other sizes around the mean. Propellants with only one particle size are called mono-modal, those with two are called bi-modal, and so on. The plot in Figure 1.6, for example, is a bi-modal propellant with a large scatter around the coarse oxidizer size.

Glick, Condon, and Renie created a new statistical formalism to deal with multi-modal propellants[15,16]. The result of their research is called the Petite Ensemble Model (PEM). The PEM is still a one-dimensional model, but it incorporates a three-dimensional picture of burning oxidizer particles. The PEM method is to track the evolution of an oxidizer particle from the time it breaks the surface until its final consumption. Each particle has a separate life cycle, but all particles for a particular mode can reduce to a representative "petite ensemble" for that mode. Glick et al. proposed that each oxidizer mode has a mass distribution function, $F_{ox,d}$, defined as

$$F_{ox,d} = \frac{1}{\sqrt{2p}\, s} exp\left[-\frac{1}{2}\left(\frac{ln D - ln \overline{D}}{s} \right)^2 \right], \qquad (1.7)$$

where s is a mode width parameter that roughly corresponds to standard deviation, D is the diameter of a particular particle, and $\overline{D}$ is the diameter of the oxidizer mode itself.

In Figure 1.6, for instance, the propellant has two distinct modes. The small-diameter mode is around 15μm with a small s, and the large diameter is around 150μm with a large s. A value of s that is greater than unity indicates a "polydisperse" propellant.

The total burning rate is therefore the following integral over all the modes of the propellant:

$$\bar{r} = \int_D \frac{\bar{r}_d}{a_d} F_d \, d(\ln D). \tag{1.8}$$

The PEM has been moderately successful in modeling the effects of particle size distribution on steady-state properties[15,16].

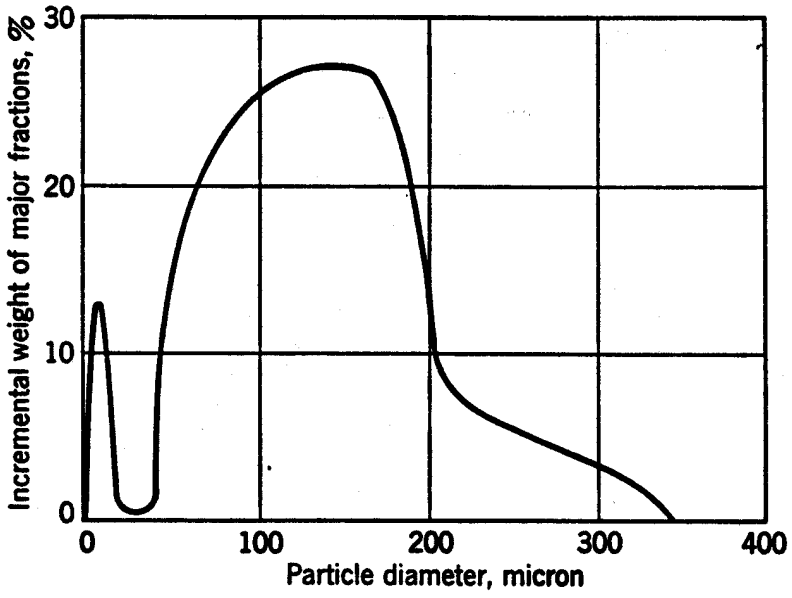

Figure 1.6: Oxidizer Particle Size Distribution in a Sample Propellant[17]

D. Theoretical Research — Nonsteady Models

Nonsteady-simulation of combustion processes is a very tedious endeavor. In addition to the normal complexities encountered in steady-state modeling, nonsteady models must also account for thermal lags in the solid phase.

Under most normal pressure transients, the gas phase reacts very quickly. Thermal capacitance in the gas phase is usually negligible compared to heat accumulation in the solid phase. Thus, the solid phase thermal relaxation time is the most important factor in determining the nonsteady response of burning rate to pressure differences. It is what ultimately drives the pressure-coupled frequency response of the propellant.

This thermal relaxation time, or "characteristic response time", is a function of the thermal diffusivity of the propellant, a, and its burning rate. Denoted t, the thermal relaxation time is

$$t = \frac{a}{r^2} . \tag{1.9}$$

Under a positive pressure transient, the temperature profile in the propellant is artificially steep, causing the propellant to burn faster than it would under the exact same pressure at steady-state. The essence of nonsteady modeling is to determine exactly how the thermal relaxation time affects the burning rate, given a known driving pressure function.

Because solid combustion processes are so intricate, most models incorporate **Q**uasi-**S**teady gas phase, **H**omogeneous solid phase, **O**ne **D**imensional (QSHOD) assumptions to simplify the problem. The acronym is disingenuous, however, because some of the more advanced models, including this one, do accommodate some properties of **H**eterogeneous (i.e., composite) propellants.

1. Linear Models

Linear pressure-coupled frequency response models have been in existence since the 1940's. There are essentially two main categories: those that rely on Flame Models (FM) and those that rely on the Zeldovich-Novozhilov (ZN) method.

Every nonsteady analysis, regardless of its classification, starts with the same basic relationship. The *transient heat conduction equation* is a second-order, parabolic partial differential equation that represents an energy balance at some point x in the solid phase. Its most general form is

$$rC_p \frac{\partial T}{\partial t} = \frac{\partial}{\partial x}\left(l \frac{\partial T}{\partial x} \right) - rr \frac{\partial \left(C_p T \right)}{\partial x}, \tag{1.10}$$

where $x = 0$ at the burning surface and is positive above the surface. At steady-state, Equation 1.10 becomes a second-order ordinary differential equation. Assuming that the thermal properties of the propellant are constant, that the temperature is T_s at the surface, and that the temperature is T_i well below the surface at $x = -\infty$, the steady-state heat conduction equation becomes

$$a \frac{\partial^2 T}{\partial x^2} - r \frac{\partial T}{\partial x} = 0 . \tag{1.11}$$

The ODE has the following solution, which defines the steady-state temperature profile:

$$T(x) = T_i + (T_s - T_i) exp\left(\frac{rx}{a} \right). \tag{1.12}$$

Note that Equation 1.12 is not linear, as the steady-state profile would be in a normal heat conduction equation. This nonlinearity results from the burning rate contribution term in the transient heat conduction equation. In colloquial terms, the burning rate "bends" the normal linear profile into an exponential one.

The next step in the development of a linear model is to define a function for the mass flow rate. A simple Arrhenius expression gives the mass flow rate as a function of surface temperature only[18]. The Arrhenius expression is

$$G = A_s \cdot exp\left(- \frac{E}{RT_s} \right) \quad . \tag{1.13}$$

The following are some useful non-dimensional terms:

$$m = \frac{G}{\bar{G}}, \tag{1.14}$$

$$q = \frac{T}{\bar{T}_s}, \tag{1.15}$$

$$x = \frac{xC_{p,s}}{l_p}, \tag{1.16}$$

and

$$W = tw. \tag{1.17}$$

The linearized and non-dimensional form of the Arrhenius expression (Equation 1.13) is therefore

$$\mu' = \zeta_s \theta_s', \tag{1.18}$$

where the steady-state portion has been subtracted out, and the exponential ζ_s, is given by

$$z_s = \frac{E_s}{R\bar{T}_s}. \tag{1.19}$$

If the reader is unfamiliar with the process of linearization, the next section contains an example using an exponential function. The non-dimensional form of Equation 1.10 is

$$\frac{\partial^2 q}{\partial x^2} - (1 + m')\frac{\partial q}{\partial x} - \frac{\partial q}{\partial t} t = 0. \tag{1.20}$$

The steady-state solution of the above PDE is Equation 1.12 again. Using the new notation, Equation 1.12 becomes

$$\bar{q} = q_i + (1 - q_i) exp(x). \tag{1.21}$$

Now two assumptions become necessary: 1) pressure input is a sine wave with frequency; and 2) the surface temperature oscillates at the same frequency as the input, though not necessarily in the same phase. One can represent this assumption with the familiar complex exponential,

$$q = \bar{q} + |q'_{max}| exp(iwt). \tag{1.22}$$

Substituting Equations 1.22 and 1.21 into Equation 1.20, subtracting off the steady-state portion, assuming that $\partial q'/\partial x$ is on the same order as q', and linearizing, the new transient heat conduction equation is

$$\frac{\partial^2 q'}{\partial x^2} - \frac{\partial q'}{\partial x} - iWq' = m'(1-q_i)exp(x), \tag{1.23}$$

which has the solution,

$$q' = q'_s exp(sx) + m'(1-q_i)\frac{i}{W}[exp(x) - exp(sx)], \tag{1.24}$$

where *s* is the familiar Laplace variable, the positive solution to the quadratic equation,

$$s^2 - s - iW = 0. \tag{1.25}$$

Another simplifying constant would be useful here. Let *A* be defined by

$$A = (1-q_i)/_s \quad . \tag{1.26}$$

The next step is to draw an energy balance from $x = 0^-$ to $x = +\infty$ as follows:

$$GC_pT_s + Gq_{tot} = l_s \left.\frac{\partial T}{\partial x}\right|_{x=0^-} + GC_{p,g}T_f \quad . \tag{1.27}$$

After substituting Equations 1.24, 1.25, and 1.26 into Equation 1.27, and after considerable manipulation, the nonsteady energy balance becomes

$$\frac{m'}{z_s}\left[(s-1) + \frac{A}{s} - A\right] = -\frac{C_{p,g}}{C_{p,s}}q'_f. \tag{1.28}$$

Here is where the American and Russian approaches have traditionally diverged. Equation 1.28 contains two variables: q_f and μ'. Another equation is necessary in order to obtain a solution. One approach is to simply assume an equation based on an exponential, pressure-related model of the flame. This is the so-called flame model approach.

For example, Denison and Baum[19] used a simple expression to link the gas phase to the burning rate. They proposed

$$G = cP^n \exp\left(-\frac{E_f}{2RT_f}\right), \tag{1.29}$$

or, linearized,

$$m' = n\frac{P'}{\bar{P}} + \zeta_f \frac{q_f'}{\bar{q}_f}, \tag{1.30}$$

where ζ_f is analogous to ζ_s. The definition of ζ_f is

$$\zeta_f = \frac{E_f}{2R\bar{T}_f} \tag{1.31}$$

Yet another constant will simplify the notation even more. "B" has the definition

$$B = \frac{C_{p,g}}{C_{p,s}}\frac{\zeta_s}{\zeta_f}\bar{q}_f, \tag{1.32}$$

Solving Equations 1.28 and 1.30 together leads to the following definition for the pressure-coupled response function:

$$R_p = \frac{nB}{(s-1)+\frac{A}{s}-A+B}. \tag{1.33}$$

(Equation 1.33 often takes different forms in the literature, with slightly different definitions for A and B.)

The Zeldovich-Novozhilov method[20] is an alternative approach for creating linear models. It is a phenomenological description that depends on steady-state properties of the propellant to replace Equation 1.29.

One form of the ZN response function looks very similar to the flame model result[21]. It is

$$R_p = \frac{n + (nr - \mu k)(s-1)}{1 + r(s-1) - k(s-1)/s}, \tag{1.34}$$

where k, r, and μ are combinations of rate properties as follows:

$$k = (\bar{T}_s - T_i)s_p, \tag{1.35}$$

$$r = \left.\frac{\partial \bar{T}_s}{\partial T_i}\right|_P, \tag{1.36}$$

and

$$m = \frac{1}{\bar{T}_s - T_i}\left(\frac{\partial \bar{T}_s}{\partial \ln P}\right)_{T_i}. \tag{1.37}$$

Ideally, the ZN approach would yield a better response function because it does not rely on an *a priori* flame model. In practice, however, ZN models often suffer from lack of accurate data because the parameters r, k, and μ are very difficult to measure precisely in the laboratory.

Brewster and Son thoroughly analyzed both ZN and flame models in 1994 and concluded that the simple Arrhenius expression with no pressure dependence was inadequate for nonsteady analysis[22]. They proposed the use of a different expression, called zeroth order decomposition, which had been in use since the early 1970's[23].

The zeroth order decomposition relationship is

$$r^2 = \frac{A_s \rho_s T_s^2 C_{p,s} \alpha_s \exp\left(-\frac{2E_s}{RT_s}\right)}{2E_s\left[C_p(T_s - T_i) - Q_s/2 - f_s q/\rho r_s\right]}. \tag{1.38}$$

Equation 1.38, however, really applies only at steady-state. Because of the consideration of condensed-phase energy storage, a proper unsteady version must include an integral term to account for solid phase capacitance, shown here as

$$r^2 = \frac{A_s \rho_s T_s^2 C_{p,s} \alpha_s \exp\left(-\frac{2E_s}{RT_s}\right)}{2E_s\left[C_p(T_s - T_i) - \rho_s \int_{-\infty}^{0} C_p \frac{\partial T}{\partial t} dx - Q_s/2 - f_s q / \rho r_s\right]}. \tag{1.39}$$

Brewster is continuing work in this area by modifying the initial temperature in the zeroth order decomposition equation[24].

Another question for linear models is how to extend them to heterogeneous propellants. One tactic is to perturb and linearize a BDP-type steady-state model. This approach usually leads to a functional form similar to Equation 1.33, but with significantly more complicated constants[25].

Glick et al. tried a different approach by extending the PEM to unsteady situations[26]. Their work implies that a multi-modal propellant will behave like a series of homogeneous propellants, so it is possible to combine the end results of several homogeneous response functions. Indeed, they did report multi-peaked response functions that were consistent with several QSHOD models in series.

2. Nonlinear Models

As mentioned above, all nonsteady solid combustion models employ the transient heat conduction equation and share some of the same basic assumptions. Linear models, however, generally have an analytic solution, due to the simplification process.

The standard way to linearize a function is to take the Taylor series expansion and disregard everything higher than order two. For example, consider the following function:

$$f(x) = A\exp(Bx). \tag{1.40}$$

At any given x, it is possible to represent the independent variable using a mean and a perturbation around the mean. Let $x = \bar{x} + x'$. Substituting and expanding the original function in a Taylor series, one obtains

$$f = A + AB(\bar{x} + x') + \frac{1}{2} AB^2 (\bar{x} + x')^2 + \frac{1}{6} AB^3 (\bar{x} + x')^3 + \dots \quad . \tag{1.41}$$

The perturbations around the mean are, by assumption, relatively small. Surely, then, the square of the perturbations would be even smaller, in fact negligible. Neglecting everything of second-order or higher, the linearized form of f is

$$f = A + AB(\bar{x} + x'). \tag{1.42}$$

Setting $f = \bar{f} + f'$ and subtracting off the steady portion, one obtains

$$f' = ABx'. \tag{1.43}$$

Equation 1.43 is linear and thus is much simpler than the transcendental Equation 1.40. If a model contains a system of linear equations, it will have a simple analytic solution, whereas a system of transcendental equations may not have an analytic solution and will require numerical solution techniques.

Nonlinear models do not consider the perturbations to be necessarily small, and thus they include second-order or higher terms. These additional terms do complicate models significantly, but nonlinear models can account for effects that linear models cannot.

Nonlinear models can, for instance, account for large pressure spikes and possibly predict extinguishment and deflagration-to-detonation thresholds. They can predict the evolution of a system over time, and they can give response functions in terms of both amplitude and frequency.

To create a nonlinear model, it is necessary to preserve at least some effects of order two or greater. One approach is to take the Taylor series expansions of functions, as in the linear case, but leave in terms of progressively higher order[27]. Another approach is to perform no reduction whatsoever. These are the most complicated attempts, and they require relatively sophisticated computers and programming techniques. Researchers have been able to attack the nonlinear problem since the 1970's, but modern computing power has sped up the process[28].

Because of the added complexity of the *mathematical* circumstances, nonlinear models typically incorporate many simplifying assumptions about the *physical* circumstances. No nonlinear models in the open literature have been able to account for the complex gas phase and heterogeneous solid phase of a BDP-type analysis. Some nonlinear models, however, have been able to account for changing thermo-physical properties in the solid phase[28,29,30]. Variable-property models have shown a reduction of amplitude in the frequency response function, as well as a shift to higher frequencies. The observed effects are probably due to temperature profiles that are steeper in variable-property simulations than in fixed-property simulations. As discussed in Chapter IV, steeper temperature profiles typically diminish response amplitude and shift the peak to higher frequencies.

3. A New Approach

The purpose of this thesis is to combine some of the best aspects of the different types of models into one comprehensive model with an intrinsically heterogeneous view of composite solid combustion. The following chapters describe a model of solid propellant combustion that is very similar to the BDP steady-state description, but with time-dependent terms to account for thermal lags in the solid phase.

The model is a completely nonlinear analysis that contains no Taylor series expansions. It is a description of mono-modal propellants only although a PEM or other surface description might not be too difficult to merge into the model at some later date. The model does not account for changes in constant-pressure specific heat and thermal conductivity in the solid phase. Essentially, it is an attempt to marry the mathematical and numerical complexity of a nonlinear model to the more physically accurate view of a BDP steady-state model.

Chapter II

STEADY-STATE COMBUSTION MODEL

A. Theoretical Framework

The theoretical model presented here is a modification of the original BDP multiple flame model for composite propellants. As in the BDP, the present model contains three types of flames, as shown in Figure 2.1.

The *pre-mixed* flame is a kinetics flame that emerges due to the exothermic decomposition of AP. The most reactive product of this flame is the approximately 30% O_2 that results from AP decomposition. The *reaction* flame is also a kinetics flame, but it receives its chemical energy through a reaction between perchloric acid from the AP flame and gaseous decomposition products from the polymer binder. Finally, the flame occurs above the kinetics region where the products of the previous two flames diffuse into each other and form the final decomposition products.

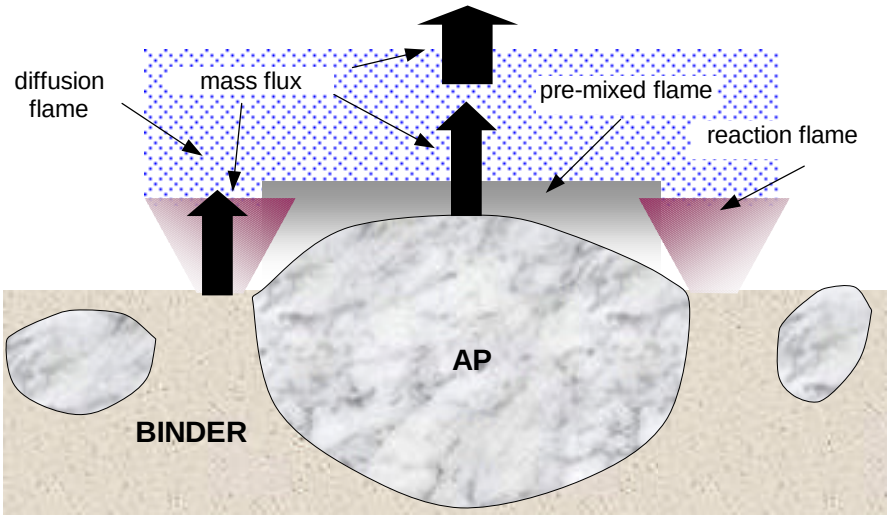

Figure 2.1: Conceptual Picture

B. Mathematical Development

The model comprises eight interrelated, dependent variables, which are elucidated below. In all the following equations, the coordinate system is one-dimensional, with $x = 0$ at the surface, $x = -\infty$ far below the surface, and $x = +\infty$ far above the surface. This Lagrangean coordinate reference frame moves relative to a "laboratory" reference frame. Rather than picturing a propellant surface that regresses to a base, the simplest way to view the system is to picture a "river" of propellant that flows to the surface, where it vaporizes.

1. Mass Flux of AP

Because the model is one-dimensional, a mass flux (mass flow rate per unit area) can represent the mass flow. The mass flux is the same, by assumption, at any point on the surface of an AP particle.

The burning rates of many materials seem to be related almost solely to surface temperature. In this model, the Arrhenius surface pyrolysis relationship[18] is

$$G_{ap} = A_{s,ap}\, exp\left(-\frac{E_{s,ap}}{RT_{s,ap}} \right). \tag{2.1}$$

Although this expression does not account for sub-surface effects as in Equations 1.38 and 1.39, other expressions in the model do account for them. Thus, the Arrhenius expression is probably adequate in this case.

2. Mass Flux of Binder

The mass flux of the binder is essentially the same expression as Equation 2.1 with different thermo-physical constants. The binder Arrhenius expression is

$$G_b = A_{s,b}\, exp\left(-\frac{E_{s,b}}{RT_{s,b}} \right). \tag{2.2}$$

There has been some recent discussion about the activation energy for HTPB under combustion heating conditions[31]. The binder seems to have a lower activation energy under higher heating rates. This is probably due to physical processes, not changes in polymer

chemistry. The activation energy used here is 8.8 kcal/mole, a value that corresponds to a relatively low heating rate[32].

3. Total Mass Flux

Because the model is one-dimensional, another equation is necessary to combine the mass fluxes of binder and AP. Modelers have used several different relationships in the past, some more elaborate than others. The PEM, for example, is probably the most accurate, but, of course, it is also one of the most tedious.

The purpose of this model is not to create a perfect steady-state description. Hence, simplicity wins out in this situation, and the simplest relationship that conserves physical principles is the best.

The mass flux of the propellant must be an algebraic combination of the mass fluxes of the binder and oxidizer. Assuming that the propellant burns linearly, the average combined burning rate should be the total amount of time that a propellant burns, divided by the total length. Figure 2.2 shows the concept graphically.

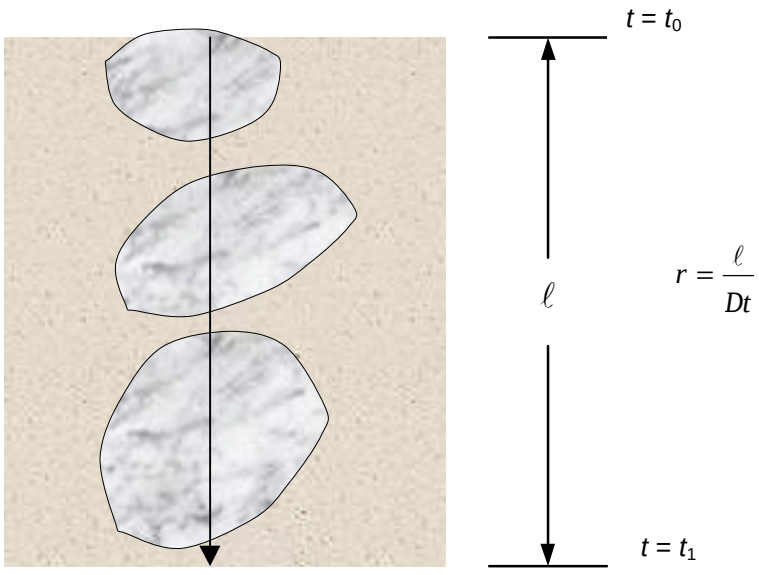

Figure 2.2: Total Burning Rate

Simply picking a characteristic length of ℓ, the total mass flux over that length becomes

$$G_p = \frac{r_p \ell}{\frac{M_{ap}}{G_{ap}A} + \frac{M_b}{G_b A}} = \frac{1}{\frac{a_{ap}}{G_{ap}} + \frac{1-a_{ap}}{G_b}}. \tag{2.3}$$

4. AP Flame Height

The reaction flames of the model are, by assumption, second-order flames. In common terms, this assumption means that the reactions result from two particles colliding, not from commingled reactions involving three or more particles. Mathematically, the assumption means that the total flame height is inversely proportional to the square of the pressure.

The pre-mixed flame height is also a function of the gas velocity moving through it. It is therefore directly proportional to the mass flux of AP. It also depends on the activation energy of the reaction in an Arrhenius-type expression. The expression for $x_{f,ap}$ in the current model is

$$x_{f,ap} = \frac{G_{ap}}{P^2 A_{g,ap}\, exp\left(-\frac{E_{g,ap}}{RT_{f,ap}}\right)} \quad , \tag{2.4}$$

which is similar to kinetics-dominated flame heights in many other models[12,13,14].

5. Total Flame Height

The expression for total flame height is somewhat more complicated. It too has a kinetics-related component that is proportional to the inverse square of the pressure, but it has a diffusion component as well. The reaction flame height is very similar to Equation 2.4, and its equation is

$$x_r = \frac{G_p}{P^2 A_r\, exp\left(-\frac{E_r}{RT_f}\right)}. \tag{2.5}$$

Diffusion flames, as their names imply, result from mixing processes where one material diffuses into another. Bunsen burners and cigarette lighters are examples of diffusion flames.

Burke and Schumann were probably the first researchers to thoroughly analyze diffusion flames in macroscopic environments, and they accomplished this in 1928[33]. Their analysis is still in common use today.

Under relatively fast burning rates, the Burke-Schumann analysis reduces to

$$x_d = \frac{G_p D_{ap}^{*\,2}}{A_{diff}\left(r_g \mathsf{D}_g\right)_{eff}}, \tag{2.6}$$

where D_{ap}* is the characteristic diameter of an oxidizer particle. It represents the average diameter of an oxidizer particle while the propellant is burning. It is related to the mass fluxes of AP and binder, as well as the surface geometry, through the following:

$$D_{ap}^{*} = \frac{2D_{ap}}{\sqrt{6\dfrac{r_p G_{ap}}{r_{ap} G_p}}}. \tag{2.7}$$

Two effects contribute to the value of the diffusion coefficient. The dominant contribution at low pressures is ordinary laminar diffusion mixing, which is itself related to a reference diffusion coefficient and temperature[34]. It has the form

$$\left(r_g \mathsf{D}_g\right)_{lam} = r_g \mathsf{D}_0 \frac{T_{f,ap}^{\;b}}{P}. \tag{2.8}$$

Substituting the ideal gas law to write the laminar diffusion coefficient as a function of temperature alone, the laminar coefficient is

$$\left(r_g \mathsf{D}_g\right)_{lam} = \mathsf{D}_0 T_{f,ap}^{\;b-1} \frac{M}{R}. \tag{2.9}$$

The second effect on the diffusion coefficient is turbulent mixing. This is a relatively high-pressure phenomenon that is near zero below a threshold. The following equation represents turbulent mixing in the model:

$$\left(r_g \mathsf{D}_g\right)_{turb} = KG_p D_{ap}^{*}\left(tan^{-1}\left(C_1 C_2\right) + tan^{-1}\left[C_2\left(\frac{1}{x_r} - C_1\right)\right]\right). \tag{2.10}$$

In the above equation, K is a constant that is on the order of one, C_1 and C_2 are constants that control the onset of turbulence, and the arctangent function is a convenient way to model the growing effects of turbulent mixing on the system.

A postulate of the model is that turbulence commences in the diffusion flame as reaction height falls. When the reaction height is large, turbulence is negligible, but when it shortens at higher pressures, the arctangent function in Equation 2.10 becomes significant. This is a purely utilitarian assumption, as it is necessary to define some sort of criterion for when turbulence should appear and a full turbulence analysis would be too complicated for the current project. In Equation 2.10, C_1 controls the point at which turbulence begins, and C_2 determines the length of the transitional region. Figure 2.3 is a graphical representation.

Setting $(r_g \mathsf{D}_g)_{eff} = (r_g \mathsf{D}_g)_{lam} + (r_g \mathsf{D}_g)_{turb}$ and $x_f = x_r + x_d$ (that is, by combining Equations 2.5, 2.6, 2.7, 2.9, and 2.10), the total flame height equation becomes

$$x_f = \frac{G_p D_{ap}^{*\,2}}{A_{diff}\left[\mathsf{D}_0 T_{f,ap}{}^{b-1}\frac{M}{R} + KG_p D_{ap}^{*}\left(tan^{-1}\left(C_1 C_2\right) + tan^{-1}\left[C_2\left(\frac{1}{x_r} - C_1\right)\right]\right)\right]} + \frac{G_p}{P^2 A_r\, exp\left(-\frac{E_r}{RT_f}\right)} \tag{2.11}$$

.

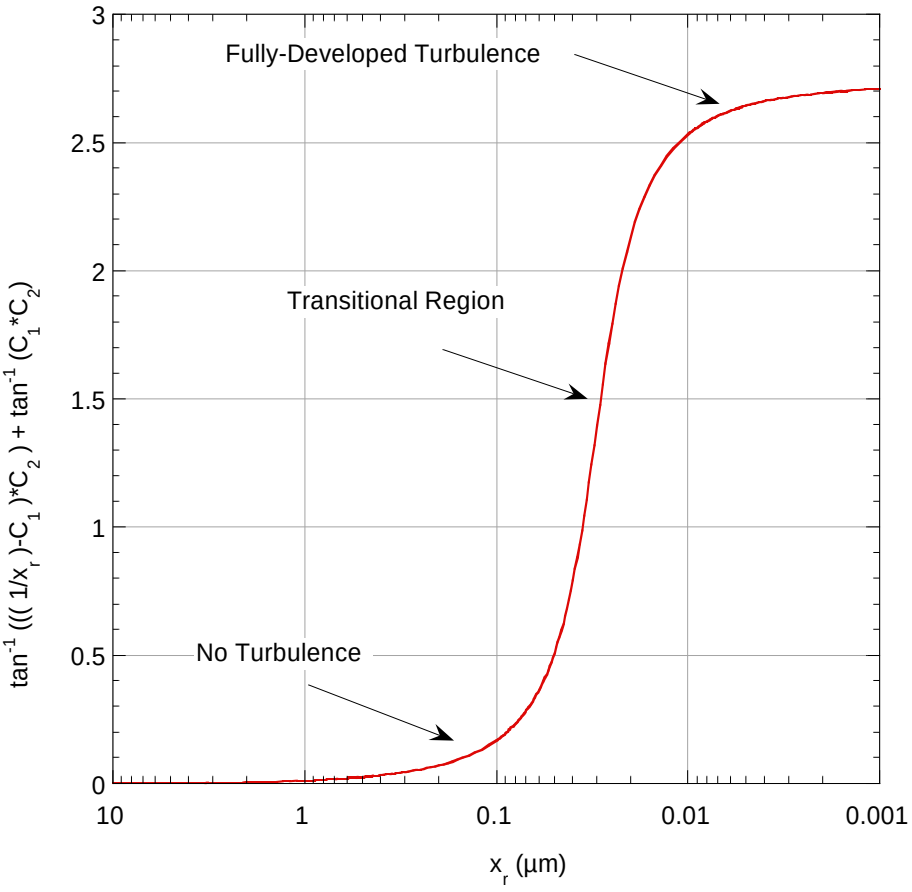

Figure 2.3: Turbulence as a Function of Reaction Flame Height

6. AP Surface Temperature

The oxidizer and binder have separate surface temperatures in the model, and equations for both come from energy balances. Consider an energy balance from deep in an oxidizer grain ($x = -\infty$) to just above the surface ($x = 0^+$). Assuming that the only energy going into the surface is conduction from the gas phase, the energy balance is

$$G_{ap} C_{p,s,ap} T_i + l_{g,ap} \left. \frac{\partial T}{\partial x} \right|_{x=0^+} + G_{ap} q_{v,ap} = G_{ap} C_{p,s,ap} T_{s,ap} + \int_{-\infty}^{0} r_{s,ap} C_{p,s,ap} \frac{\partial T}{\partial t} \partial x \quad . \tag{2.12}$$

Ammonium perchlorate has three distinct crystal phases. The first phase is only present at very low temperatures and is not of interest in practical rocket applications. The second phase is an orthorhombic phase, which is the natural state from cold temperatures up to approximately 513K. The third phase is a cubic phase that persists until sublimation/melting. For the purpose of this model, however, use an average specific heat at reference temperature, T_{ref}=500K.

From a steady-state viewpoint, the phase transition does not matter, except that it draws energy out of the system. The $q_{v,ap}$ is positive (exothermic), and it is the sum of three energies:

$$q_{v,ap} = q_{tr} + q_{vap,ap} + q_r \quad , \tag{2.13}$$

where q_{tr} is the specific energy required to force the phase transition, $q_{vap,ap}$ is the energy required to vaporize the AP at the surface assuming 70% sublimation and 30% degradation, and q_r is the energy of exothermic reactions in the thin melt layer[12].

Now the only remaining unknown term is the derivative that defines conduction into the surface. To obtain it, one can reasonably postulate an exponential temperature profile in three regions in the flame.

One can postulate a profile above the oxidizer and below $x_{f,ap}$,

$$T = T_{f,ap} - \left(T_{f,ap} - T_{s,ap}\right) exp\left(-n \frac{x}{x_{f,ap}} \right) \quad , \tag{2.14}$$

above the binder,

$$T = T_f - (T_f - T_{s,b}) \exp\left(-\nu \frac{x}{x_f}\right), \tag{2.15}$$

and between $x_{f,ap}$ and x_f,

$$T = T_f - (T_f - T_{f,ap}) exp\left(-n \frac{x - x_{f,ap}}{x_f - x_{f,ap}}\right). \tag{2.16}$$

In the three profiles above, n is a constant that modifies the steepness of the profile. Use n=2.5 because that will get the temperature to within $1/e^{2.5}$ of the maximum temperature difference at the characteristic height. For example, at $x = x_{f,ap}$ over the oxidizer, the temperature is

$$T = T_{f,ap} - \frac{(T_{f,ap} - T_{s,ap})}{exp(2.5)} = T_{f,ap} - 0.082(T_{f,ap} - T_{s,ap}). \tag{2.17}$$

Now it is possible to calculate the derivative term from the assumed profile as follows:

$$\left.\frac{\partial T}{\partial x}\right|_{x=0^+} = \frac{n}{x_{f,ap}}(T_{f,ap} - T_{s,ap}). \tag{2.18}$$

Assuming that the integral term in Equation 2.12 is zero (steady-state), the solution for oxidizer surface temperature is

$$T_{s,ap} = \frac{G_{ap} C_{p,s,ap} T_i + l_{g,ap} T_{f,ap} \dfrac{n}{x_{f,ap}} + G_{ap} q_{v,ap}}{G_{ap} C_{p,s,ap} + l_{g,ap} \dfrac{n}{x_{f,ap}}} \quad . \tag{2.19}$$

7. Binder Surface Temperature

The expression for the surface temperature of the binder is almost exactly the same as the one for the oxidizer. Start again with the binder energy balance. Polymer binders are obviously not crystalline, and there is no phase transition until the surface, so the balance reduces to

$$G_b C_{p,s,b} T_i + l_{g,b} \left.\frac{\partial T}{\partial x}\right|_{x=0^+} + G_b q_{v,b} = G_b C_{p,s,b} T_{s,b} + \int_{-\infty}^{0} r_{s,b} C_{p,s,b} \frac{\partial T}{\partial t} \partial x \quad . \tag{2.20}$$

Differentiate Equation 2.15 to get the derivative term and solve, again assuming that the integral term in Equation 2.20 is zero. The solution for $T_{s,b}$ is

$$T_{s,b} = \frac{G_b C_{p,c,b} T_i + l_{g,b} T_f \dfrac{n}{x_f} + G_b q_{v,b}}{G_b C_{p,s,b} + l_{g,ap} \dfrac{n}{x_f}} \quad . \tag{2.21}$$

8. Pre-mixed Flame Temperature

One way to calculate the pre-mixed flame temperature is simply to define it as the adiabatic flame temperature of self-deflagrating ammonium perchlorate. Such an assumption might not be realistic, however, because of the effects of the diffusion flame.

If the AP were burning without a separate fuel, then $T_{f,ap}$ would clearly be the adiabatic flame temperature. The addition of a fuel to the mix adds extra chemical energy, some of which must flow back into the pre-mixed flame. Thus, an energy balance in the diffusion part of the gas phase is necessary to calculate the pre-mixed flame temperature. The energy balance is, in fact, very similar to Equations 2.12 and 2.20:

$$G_p C_{p,g,p} T_f + l_g \left.\frac{\partial T}{\partial x}\right|_{x=x_{f,ap}} + G_p q_{f,d} = G_p C_{p,g,p} T_f \, . \tag{2.22}$$

The above equation does not contain an unsteady integral term. The gas phase is assumed to bea quasi-steady, a reasonable assumption except under very high pressure transients.

Again, using the assumed temperature profile in the diffusion flame to get the derivative term and solve for $T_{f,ap}$, the final expression is

$$T_{f,ap} = \frac{T_f \left[G_p C_{p,g,p} + \dfrac{n l_{g,p}}{x_f - x_{f,ap}} \right] - G_p q_f}{G_p C_{p,g,p} + \dfrac{n l_{g,p}}{x_f - x_{f,ap}}}. \tag{2.23}$$

Equation 2.23 leads to an important point — the gas phase does *not* move immediately to steady-state, even though it is "quasi-steady". It moves instead to a state that would be steady-state for a particular value of G_p. In other words, the total propellant mass flux is not quasi-steady, so it "drags" the gas phase with it. This point will become significant in the unsteady portion of the model.

C. Solution

The steady-state model developed in the previous section is a system of eight equations that must be solved simultaneously. Equations 2.1, 2.2, 2.3, 2.4, 2.11, 2.19, 2.21, and 2.23 represent the system. Table 2.1 contains a list of the dependent variables and their relationships to one another.

The model contains six "floating" parameters: K, C_1, C_2, $A_{diff,}$ A_r, and $A_{g,ap}$. The first three parameters define the turbulent onset (the shape of the curve in Figure 2.3), so they effectively constitute one floating parameter. That is, the model really has four floating parameters- A_{diff}, A_r, $A_{g,ap}$, and the shape of the turbulent mixing transition.

These floating parameters help to "calibrate" the model. Because it is generally impossible to find accurate values of the parameters from experiments, they are completely adjustable. Increasing or decreasing the parameters can move the final result of the model to a reasonable approximation of the experimental data. See Table 2.2 for a list of all physical/mechanical/chemical properties in the model, including the deduced floating parameters. Table 2.2 contains some properties, such as solid-phase thermal conductivity, that

Table 2.1: Dependent Variables in the Steady-State Model

Variable	Eq. #	Function of Variable							
		G_p	G_{ap}	G_b	$x_{f,ap}$	x_f	$T_{s,ap}$	$T_{s,b}$	$T_{f,ap}$
G_p	2.3		P	P					
G_{ap}	2.1						P		
G_b	2.2							P	
$x_{f,ap}$	2.4		P						P
x_f	2.11	P	P						P
$T_{s,ap}$	2.19		P		P				P
$T_{s,b}$	2.21			P		P			
$T_{f,ap}$	2.23	P			P	P			

Table 2.2: Physical Constants in the Model

Constant	Value
A_{diff} †	11
$A_{g,ap}$ †	$5.0 \cdot 10^{-4}$ m
A_r †	$2.2 \cdot 10^{-4}$ m
$A_{s,ap}$	$9.6 \cdot 10^{5}$ kg·m^{-2}·s^{-1}
$A_{s,b}$	$1.225 \cdot 10^{3}$ kg·m^{-2}·s^{-1}
C_1 †	30 m^{-1}
C_2 †	0.075 m
$C_{p,cu,ap}$	T·(1.717)+669.9 J·kg^{-1}·K^{-1}
$C_{p,g,ap}$	1254 J·kg^{-1}·K^{-1}
$C_{p,g,b}$	2100 J·kg^{-1}·K^{-1}
$C_{p,g,p}$*	1787-2870 J·kg^{-1}·K^{-1}
$C_{p,or,ap}$	T·(1.717)+586.2 J·kg^{-1}·K^{-1}
$C_{p,s,b}$	T·(3.559)+1047 J·kg^{-1}·K^{-1}
D_o	$7.585 \cdot 10^{-5}$ m^2·s^{-1}
$E_{g,ap}$	$6.28 \cdot 10^{4}$ J·mole^{-1}
E_r	$1.26 \cdot 10^{5}$ J·mole^{-1}
$E_{s,ap}$	$9.6 \cdot 10^{4}$ J·mole^{-1}

Constant	Value
$E_{s,b}$	$3.43 \cdot 10^{4}$ J·mole^{-1}
K †	2
M	0.0262 J·mole^{-1}·K^{-1}
q_f*	$2.07 \cdot 10^{6}$-$3.63 \cdot 10^{6}$ J·kg^{-1}
q_r	0 J·kg^{-1}
q_{tr}	$-8.78 \cdot 10^{4}$ J·kg^{-1}
$q_{v,b}$	$-2 \cdot 10^{5}$ J·kg^{-1}
$q_{vap,ap}$	$5.1 \cdot 10^{5}$ J·kg^{-1}
T_f*	1587-2993 K
$l_{g,ap}$	T·$(7.2 \cdot 10^{-5})$+$6 \cdot 10^{-3}$ W·m^{-1}·K^{-1}
$l_{g,b}$	T·$(4.33 \cdot 10^{-4})$-0.15 W·m^{-1}·K^{-1}
$l_{g,p}$	T·$(1.08 \cdot 10^{-4})$+0.0133 W·m^{-1}·K^{-1}
$l_{s,ap}$	T·$(-3.854 \cdot 10^{-4})$+0.628 W·m^{-1}·K^{-1}
$l_{s.b}$	T·$(5.43 \cdot 10^{-5})$+0.184 W·m^{-1}·K^{-1}
r_{ap}	1950 kg·m^{-3}
r_b	920 kg·m^{-3}

* Linearly interpolated from thermo-chemical-equilibrium calculations at various oxidizer mass percentages.

† Floating parameter.

are not necessary in the steady-state model but do contribute to the nonsteady model. Also, some of the properties in Table 2.2 are averages of various results reported in the literature.

There are of course, many different numerical techniques for solving the system of equations. It is not a simple problem, due to the non-linearity of the equations and the wide range of conditions under which they must be solved.

The next section contains some preliminary results from the steady-state model. Results come from Mathcad 7.0.3 calculations over a wide range of pressures and initial temperatures. Mathcad's numerical solution algorithm is a variation of the MINPACK public domain algorithm published by the Argonne National Laboratory. The MINPACK algorithm is itself a version of the Levenberg-Marquardt method[35].

Appendix A contains the steady-state solution sheet.

D. Preliminary Steady-state Results

This section contains some general results of the steady-state model. For more explicit results showing the effect of changes in specific variables, along with discussion of the physical meaning of those results, see Chapter IV.

1. Burning Rate vs. Pressure

Figure 2.4 is a plot of burning rate vs. pressure. All propellants are 80% AP / 20% HTPB at an initial temperature of 298K. Experimental data were available for 5µm and 90µm oxidizer particle diameters, so the model is calibrated to those data. The experimental data come from ultrasonic tests conducted at the *Office Nationale d'Etudes et de Recherches Aérospatiales* (ONERA) in 1996 in Palaiseau, France. The extra trends at 50µm and 200µm are purely theoretical predictions. Figures 2.5 and 2.6 show the data from Figure 2.4 in a different way. They are plots that show the percentage difference between theoretical predictions and experimental data for (90, 80/20, 298)[‡] and (5, 80/20, 298) propellants respectively. The theoretical predictions are a baseline for the difference calculations.

[‡] If a propellant is (a, b/c, d), then the oxidizer particle diameter is "a" µm, the oxidizer/binder mass fraction is "b/c", and the initial temperature is "d"K.

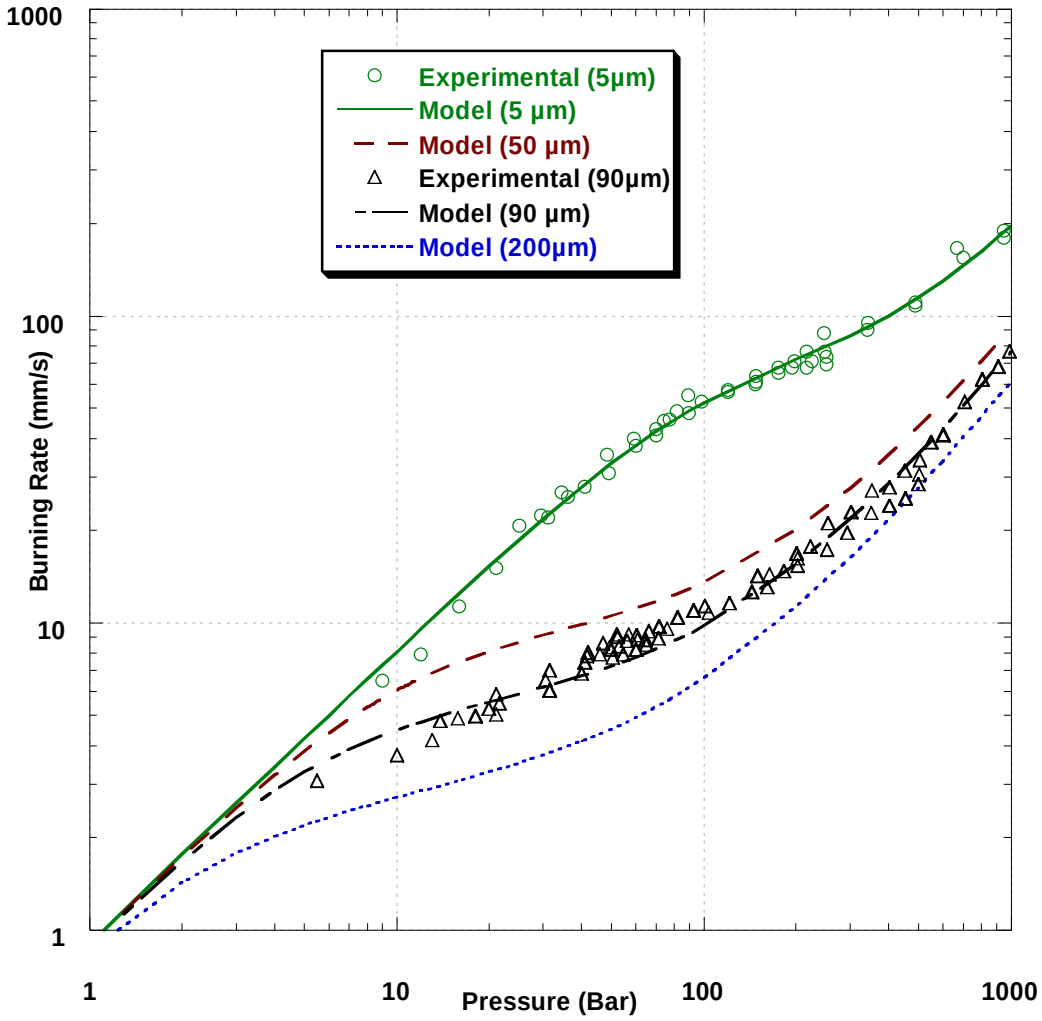

Figure 2.4: Burning Rate vs. Pressure

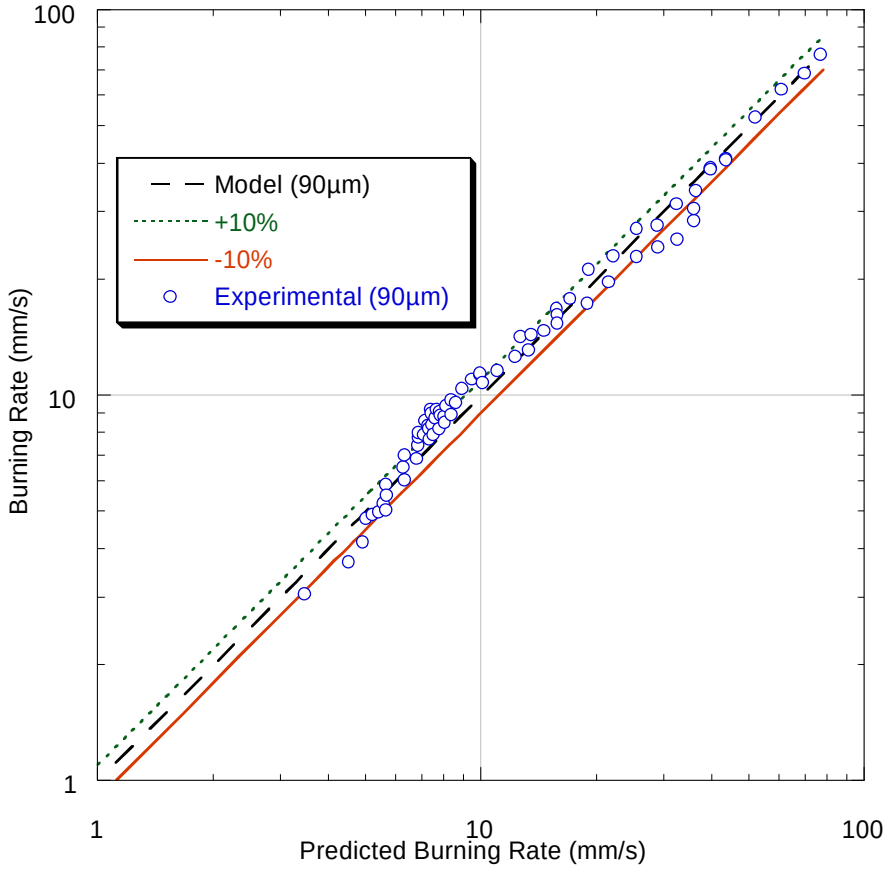

Figure 2.5: Theoretical vs. Experimental, (90 80/20, 298)

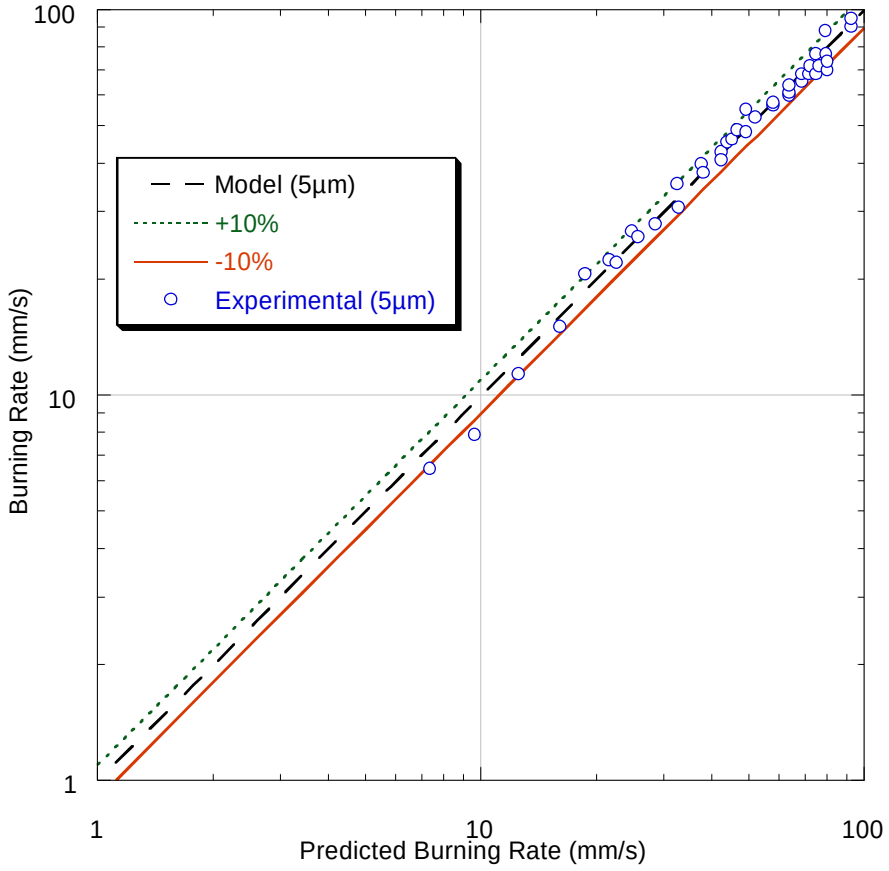

Figure 2.6: Theoretical vs. Experimental, (5, 80/20, 298)

2. Initial Temperature Sensitivity

Figure 2.7 is a plot of predicted initial temperature sensitivity as a function of pressure. The three traces are for 80%AP / 20%HTPB at three different particle diameters. Values of σ_p come from applying Equation 1.5 to two separate simulations at 219K and 333K initial temperature.

Theoretical initial temperature sensitivity predictions do agree generally with experimental data. Practical AP/HTPB propellants occasionally exhibit higher sensitivities, but mono-modal propellants are probably less sensitive than others. The general trend in composite propellants is for propellants with wide oxidizer particle diameter distributions to have higher sensitivities[7]. Obviously, mono-modal propellants have the tightest distribution possible, so they should have lower values of σ_p.

3. Evolution of System Variables

The rest of the charts in this section represent system variables as functions of pressure for (90, 80/20, 298) propellant. All data are theoretical, and in fact some of the following variables would be nearly impossible to find experimentally.

Figure 2.8 is a plot of the relative mass fluxes in the system. The mass flux for AP grows much higher than that of the binder at high pressures, even though total mass is conserved. Dividing by the densities, one obtains Figure 2.9, a plot of the linear burning rates.

Figure 2.10 is a plot of the flame heights in the system. The total flame height, x_f, is the sum of the reaction flame height, x_r, and the diffusion flame height, x_d. This plot will become important in the following chapter, as quasi-steady flame heights and temperatures are necessary for calculating reasonable response amplitudes.

Figure 2.11 is a plot of $T_{f,ap}$, $T_{s,ap}$, and $T_{s,b}$ as functions of pressure. The surface temperatures approach the flame temperatures as the pressure builds and the flame heights fall, bringing more conductive energy into the propellant surface. The surface temperature of the AP is a function of $x_{f,ap}$, and surface temperature of the binder is a function of x_f. The adiabatic flame temperature is a constant 2309K for the 80/20 formulation.

Finally, Figure 2.12 is a plot of oxidizer surface fraction as a function of pressure for a (90, 80/20, 298) propellant, where the surface fraction comes from a mass balance,

$$G_{AP}S_{AP} + G_b(1 - S_{AP}) = G_p . \tag{2.24}$$

Rearranging, the mass balance becomes

$$S_{AP} = \frac{G_p - G_b}{G_{AP} - G_b} . \tag{2.25}$$

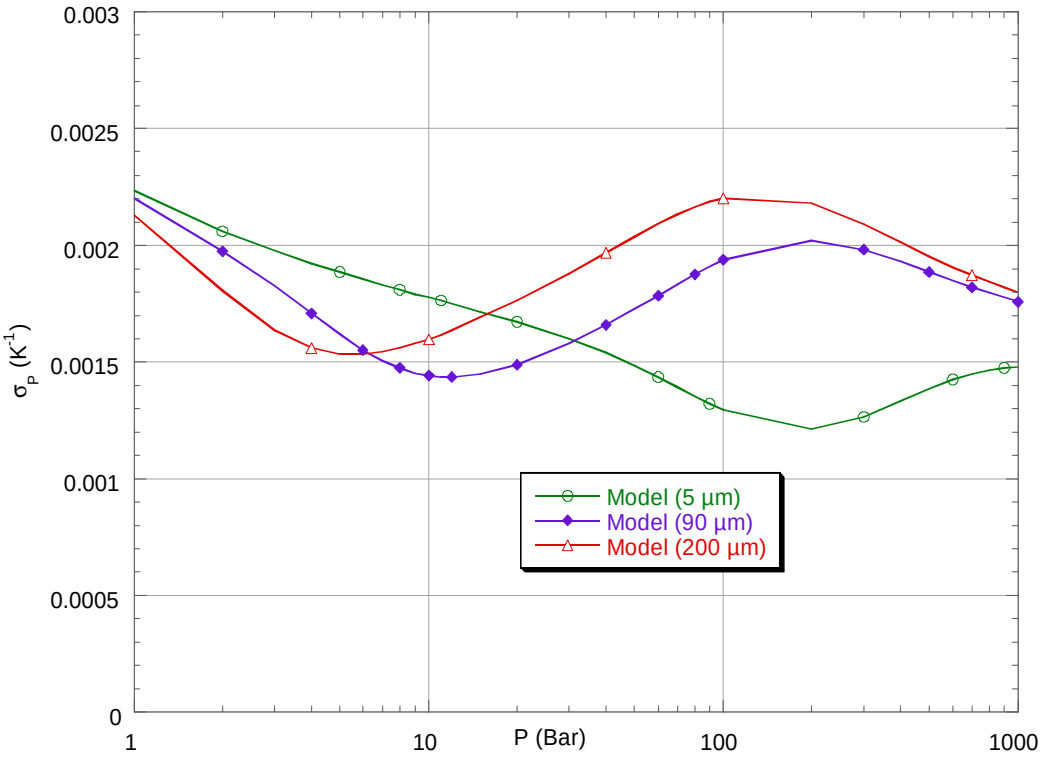

Figure 2.7: Predicted Initial Temperature Sensitivity

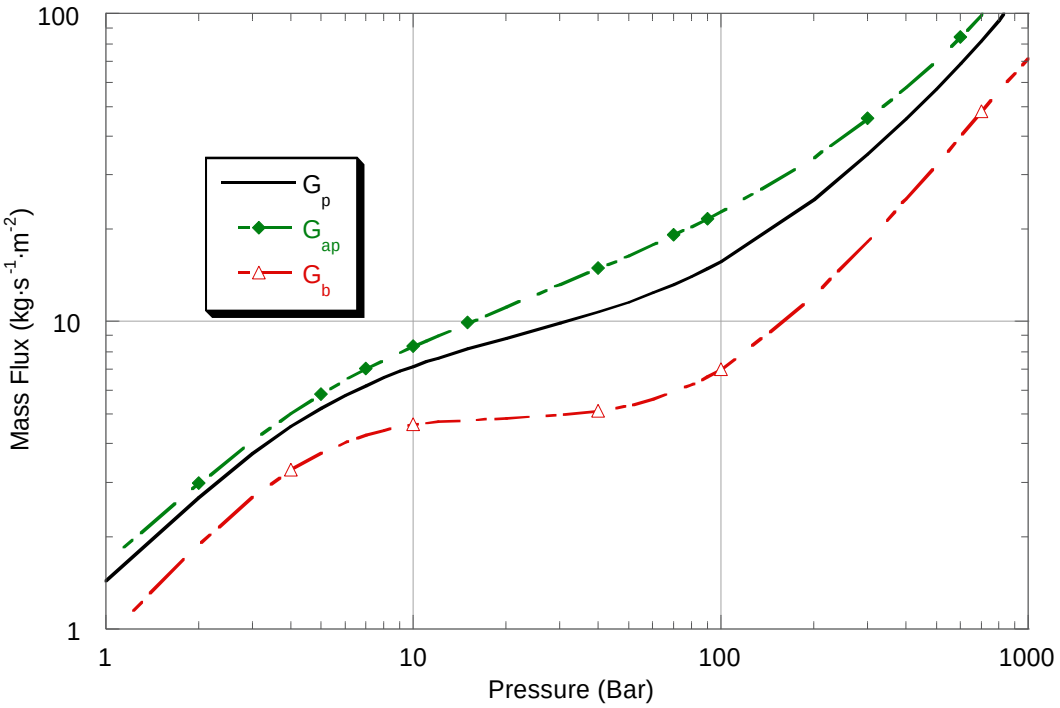

Figure 2.8: Mass Fluxes of (90, 80/20, 298) Propellant

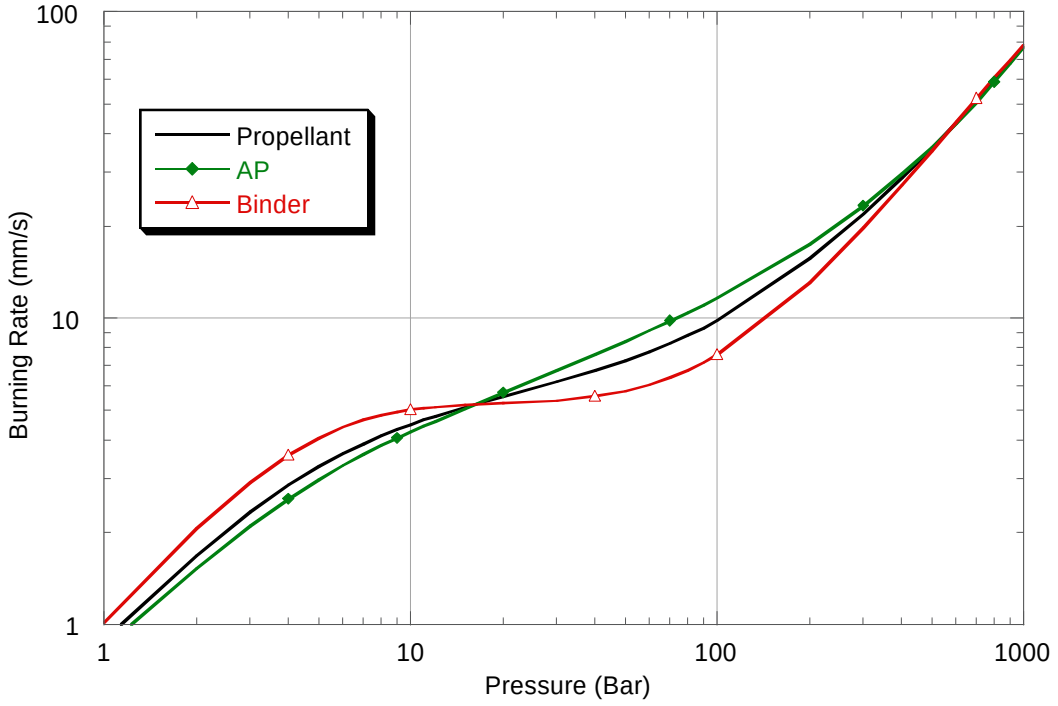

Figure 2.9: Linear Burning Rates of (90, 80/20, 298) Propellant

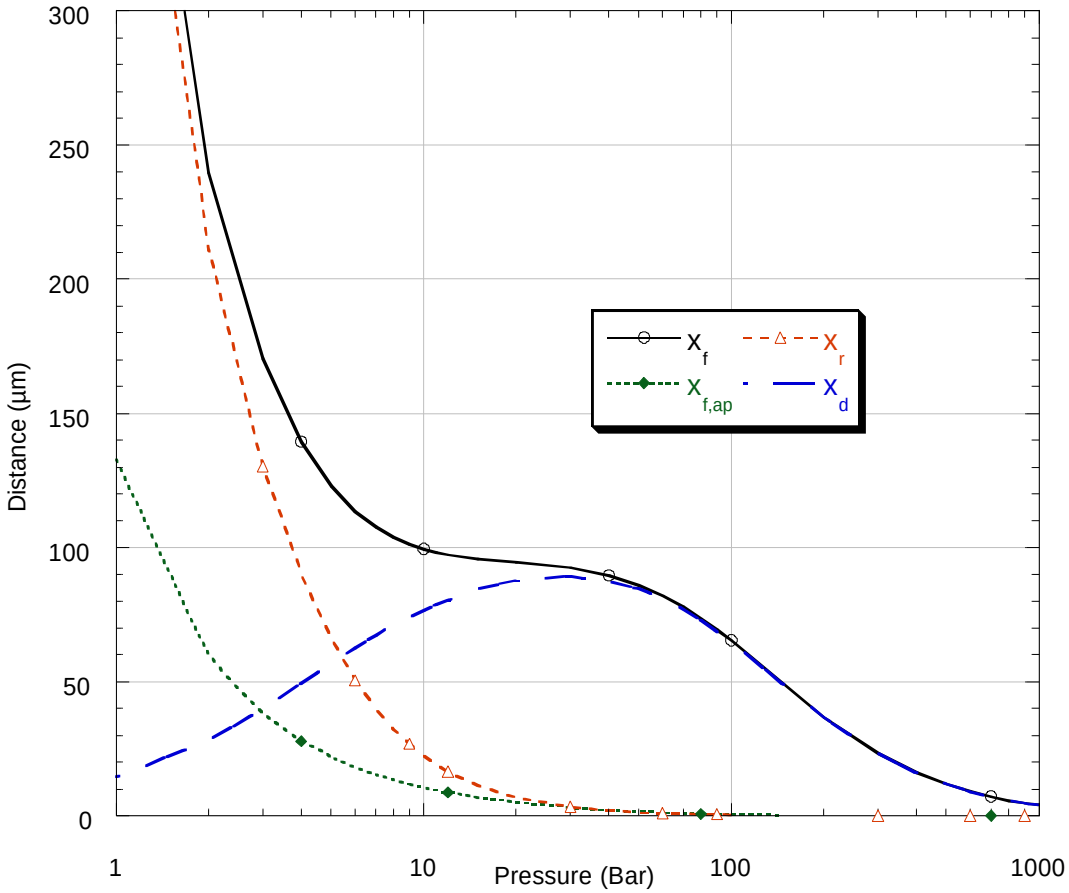

Figure 2.10: Flame Heights of (90, 80/20, 298) Propellant

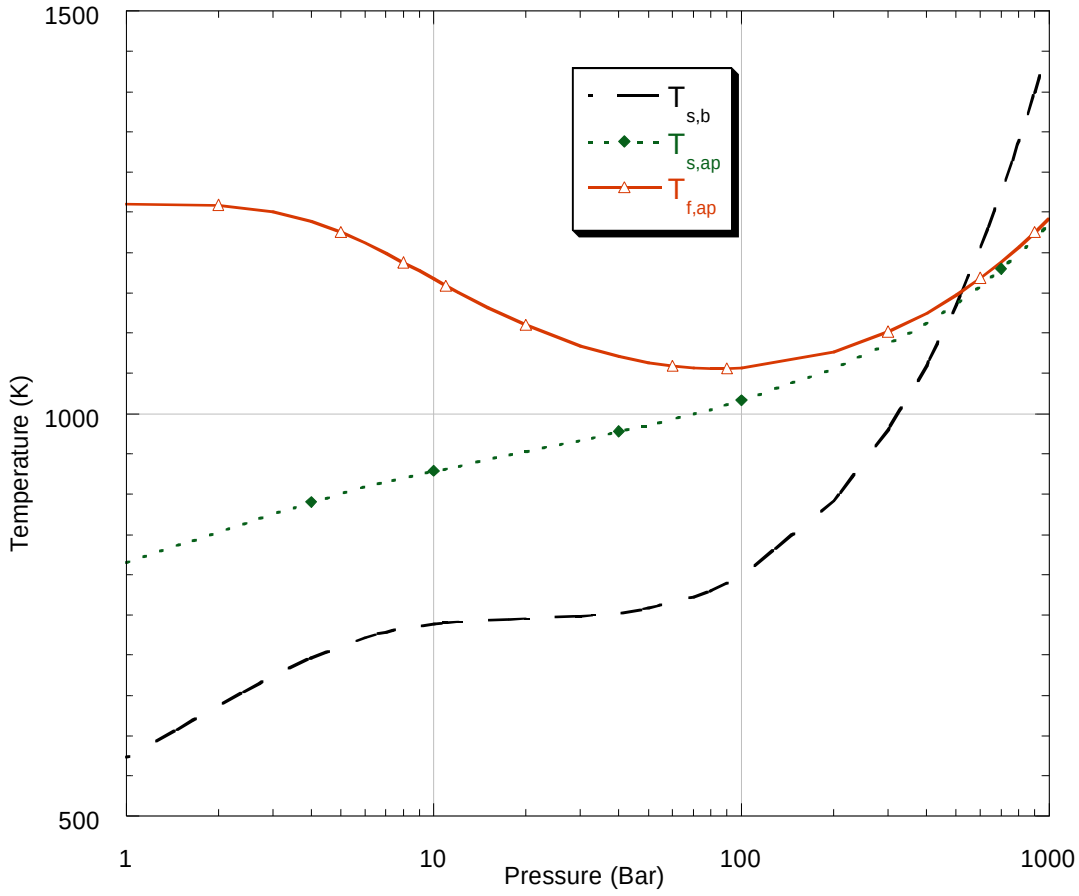

Figure 2.11: Flame and Surface Temperatures of (90, 80/20, 298) Propellant

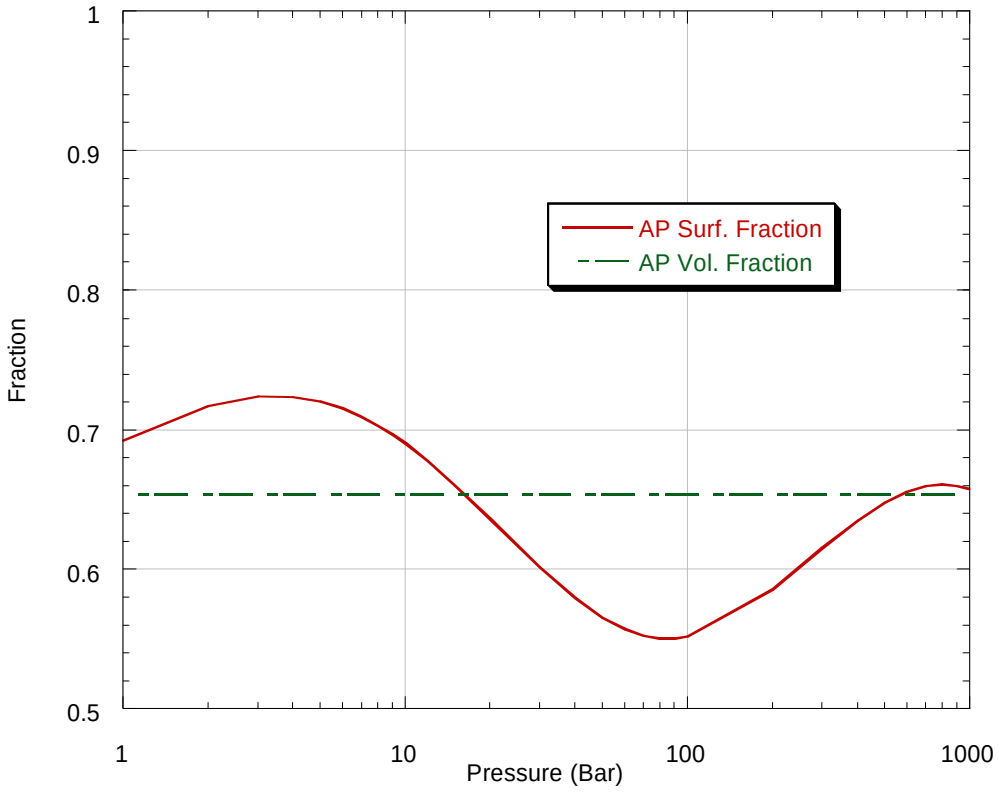

Figure 2.12: Surface Fraction of AP as a Function of Pressure

Chapter III

NONSTEADY-STATE COMBUSTION MODEL

A. Nonsteady Foundations

Equations 2.12 and 2.20 contain two integral terms that are zero under steady-state conditions. Leaving them in the energy balances leads to two different expressions for the surface temperatures of the oxidizer and binder:

$$T_{s,ap} = \frac{G_{ap} C_{p,s,ap} T_i + \lambda_{g,ap} T_{f,ap} \dfrac{\nu}{x_{f,ap}} + G_{ap} q_{v,ap} - \displaystyle\int_{-\infty}^{0} \rho_{s,ap} C_{p,s,ap} \frac{\partial T}{\partial t} dx}{G_{ap} C_{p,s,ap} + \lambda_{g,ap} \dfrac{\nu}{x_{f,ap}}}, \tag{3.1}$$

and

$$T_{s,b} = \frac{G_b C_{p,c,b} T_i + \lambda_{g,b} T_f \dfrac{\nu}{x_f} + G_b q_{v,b} - \displaystyle\int_{-\infty}^{0} \rho_{s,b} C_{p,s,b} \frac{\partial T}{\partial t} dx}{G_b C_{p,s,b} + \lambda_{g,b} \dfrac{\nu}{x_f}}. \tag{3.2}$$

The integral terms in the numerators represent the only difference between these two equations and the previous expressions for surface temperature. In fact, the integral terms are the only two nonsteady contributions in the model.

Essentially, the two integral terms represent a “capacitance” in the solid phase of the propellant. Solid materials store energy through their temperatures and specific heats, and, just as in an electrical capacitor, it takes time to discharge this stored energy. The heat discharge time is

related to the thermal conductivity of the system, just as the discharge time of a capacitor in an RC circuit is related to the total impedance.

The best way to solve the integrals is to go back to the transient heat conduction equation. The following explanation considers either the binder or the oxidizer as a homogeneous propellant for now, though the temperature profiles in both must be solved simultaneously, according to the eight variables in the model. At any given point *x* in the solid phase of a homogeneous propellant with constant thermal properties, the heat conduction equation reduces to

$$\frac{\partial T}{\partial t} = \alpha \frac{\partial^2 T}{\partial x^2} - r \frac{\partial T}{\partial x} . \tag{3.3}$$

Hence, if the temperature profile at any given time is known, it is then possible to calculate $\partial T/\partial t$ across the whole propellant.

In the model presented in this paper, however, the propellant is certainly not homogeneous. There are in fact two temperature profiles in the system — one in the binder and one in the oxidizer Hence, the model must incorporate two different versions of Equation 3.3 in order to come to a solution. The equations are structurally identical, but they have different thermo-physical constants and different burning rates.

To reiterate, the unsteady model is almost exactly the same as the steady-state model, except that Equations 2.12 and 2.20 have been replaced by Equations 3.1 and 3.2 respectively. The trick here is to calculate the integral terms that make the unsteady equations unique, using a different version of Equation 3.3 for both the binder and the oxidizer.

B. Solution Method

There is no analytic solution for the two integral terms in Equations 3.1 and 3.2. To solve the system of eight equations, one must numerically calculate the binder and oxidizer temperature profiles at each time step.

From a conceptual standpoint, the easiest way to calculate temperature profiles is to use the temperature profile from the previous time step in Equation 3.3 to get the $\partial T/\partial t$ at each x. The

next temperature profile is the old profile, plus ∂T/∂t multiplied by the length of the time step. Explicit methods such as these have a very serious limitation in heat transfer problems. The time step must be very small in order for the equations to converge[36]. Specifically,

$$Dt \le \frac{(Dx)^2}{2a}. \tag{3.4}$$

For example, consider a propellant with a thermal diffusivity of $1 \cdot 10^{-7}$ $m^2 \cdot s^{-1}$. Say the particle diameter is 100μm, so that near the surface, the *Dx* should be at least as small as 0.05μm. The maximum time step size is

$$Dt \le \frac{(Dx)^2}{2a} = \frac{\left(5 \cdot 10^{-8}\right)^2}{2 \cdot 10^{-7}} = 1.25 \cdot 10^{-8} \text{ seconds (!).} \tag{3.5}$$

Considering that the response time of the system, as given by Equation 1.9, is on the order of a few milliseconds, the *Dt* calculated above would require thousands of explicit solutions for even a very short simulation. Computation time for an explicit method is therefore prohibitively large, especially because the temperature profile must be calculated many times at each time step in the course of finding a simultaneous solution to the eight nonlinear equations of the model. Clearly, a better method is necessary.

One common numerical technique for calculating transient temperature profiles is the Crank-Nicolson method[37]. It has many variations, but the underlying idea is very simple. To calculate a temperature profile at time t_{j+1}, use an average of the temperature profile at t_j and t_{j+1} in all of the ¶/¶*x* terms. The temperature profile at t_{j+1} is unknown, so one must solve for the whole profile at once. This type of solution is known as an *implicit* solution, and it is stable even for large time steps. Of course, smaller time steps do lead to better numerical accuracy.

The best way to elucidate the idea is to show a sample case. Consider, for example, the AP and binder temperature profiles known at *n* points in the solid phase of the propellant at time t_j. The task is to calculate the new temperature profiles, given the old profiles and new surface temperatures at time t_{j+1}. Figures 3.1 and 3.2 are representative steady-state temperature profiles in the binder and AP for a (90, 80/20, 298) propellant.

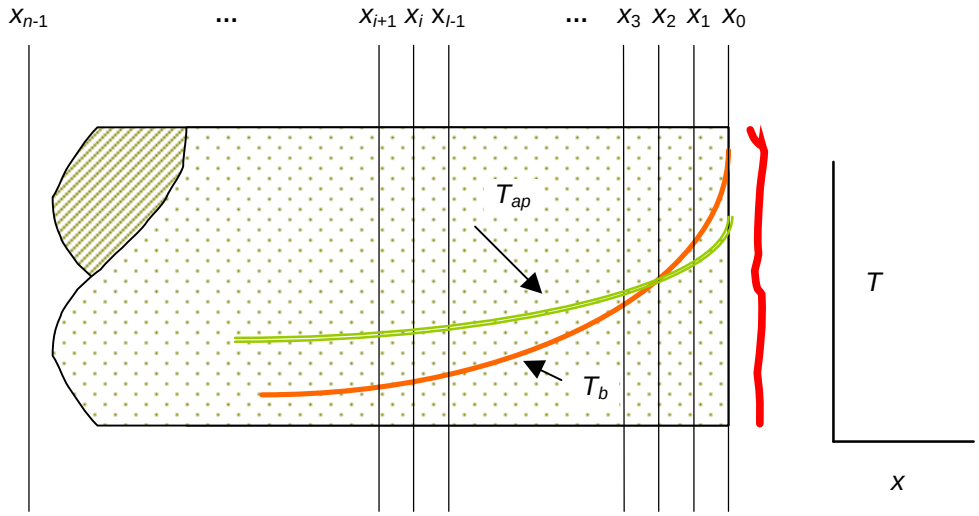

Figure 3.1: Sample Temperature Profile in Propellant (Ideal)

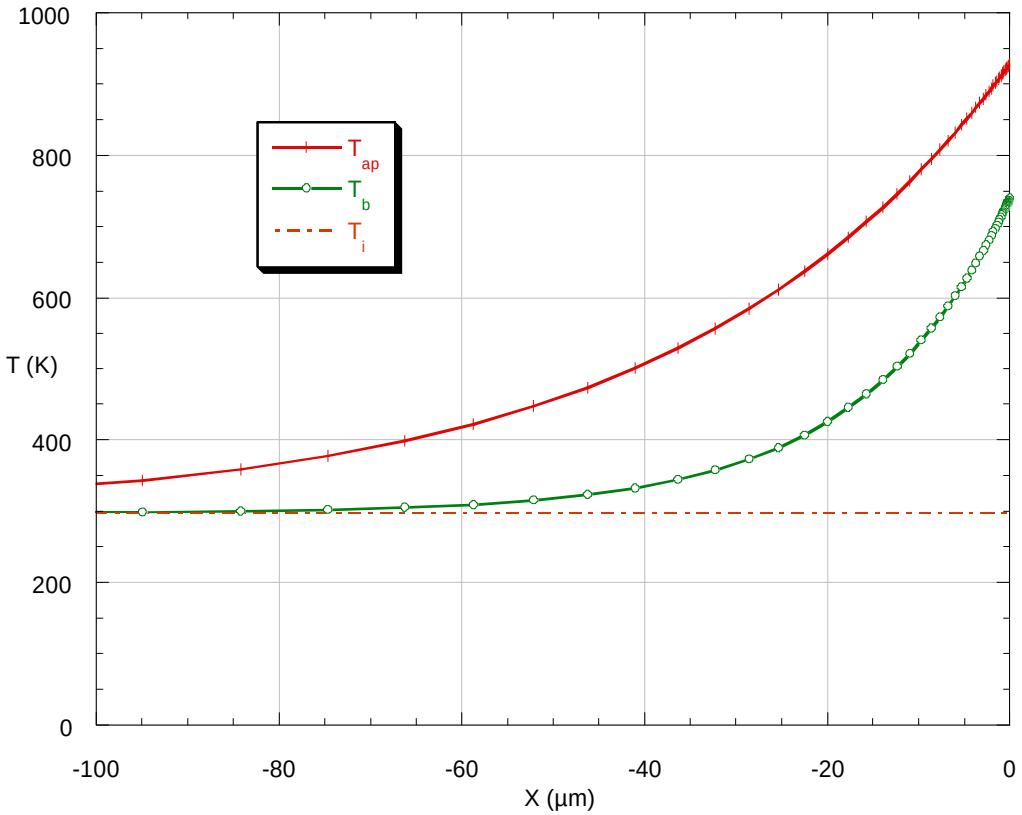

Figure 3.2: Sample Temperature Profile in Propellant (Actual)

First, note that the *x*-spacing in the calculated profile is not constant. (The circles and lines represent calculation points.) The reason for the non-constant spacing is that the temperature, as shown in Equation 1.12, grows exponentially near the surface. An *x*-spacing that becomes exponentially smaller near the surface is therefore preferable because it has a fine resolution near the surface where it is needed and a coarse resolution deep inside the propellant where the temperature changes slowly with distance. For the present model, the equation describing the *x*-spacing is

$$x_i = x_{depth} \cdot exp\left[\left(i+1-n\right)\cdot n_X\right] - x_{depth} \cdot exp\left[\left(1-n\right)\cdot n_X\right]. \tag{3.6}$$

The following derivation considers just one generic profile for now, though the model contains two solid-phase calculations. Denoting, $T_{i,j+1}$ as the new temperature and $T_{i,j}$ as the previous temperature at some x_i, the discrete mathematical environment looks like Figure 3.3.

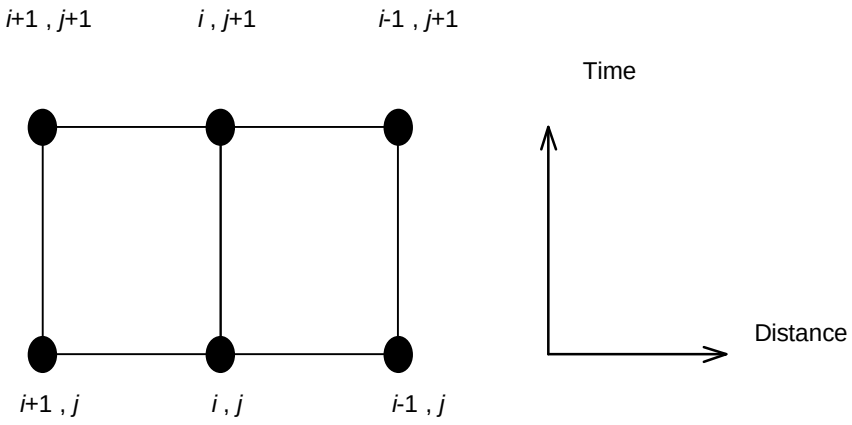

Figure 3.3: Discrete Computational Grid

Equation 3.3 now becomes a discrete algebraic problem. The derivatives come from an average between time t_{j+1} and time t_j. In finite-difference form, the derivatives are

$$\left.\frac{\partial T}{\partial t}\right|_{x=x_i} \approx \frac{1}{Dt}\left(T_{i,j+1} - T_{i,j}\right), \tag{3.7}$$

$$\left.\frac{\partial T}{\partial x}\right|_{x=x_i} \approx \frac{1}{2}\left(\frac{T_{i-1,j} - T_{i+1,j}}{x_{i-1} - x_{i+1}}\right) + \frac{1}{2}\left(\frac{T_{i-1,j+1} - T_{i+1,j+1}}{x_{i-1} - x_{i+1}}\right), \tag{3.8}$$

and

$$\left.\frac{\partial^2 T}{\partial x^2}\right|_{x=x_i} \approx \frac{1}{2}\left(\frac{\dfrac{T_{i-1,j} - T_{i,j}}{x_{i-1} - x_i} - \dfrac{T_{i,j} - T_{i+1,j}}{x_i - x_{i+1}}}{\dfrac{x_{i-1} - x_{i+1}}{2}}\right) + \frac{1}{2}\left(\frac{\dfrac{T_{i-1,j+1} - T_{i,j+1}}{x_{i-1} - x_i} - \dfrac{T_{i,j+1} - T_{i+1,j+1}}{x_i - x_{i+1}}}{\dfrac{x_{i-1} - x_{i+1}}{2}}\right). \tag{3.9}$$

Let $\Delta x_i = x_{i-1} - x_{i+1}$. Substituting Equations 3.7 - 3.9 into Equation 3.3 and placing all the j+1 (unknown) terms on one side, the final form is

$$\begin{aligned} &T_{i-1,j+1}\left(\frac{-a}{\Delta x_i \cdot \left(x_{i-1} - x_i\right)} + \frac{r_{j+1}}{2 \cdot \Delta x_i}\right) + \\ &T_{i,j+1}\left(\frac{1}{Dt} + \frac{a}{x_{i-1} - x_i} + \frac{a}{x_i - x_{i+1}}\right) + \\ &T_{i+1,j+1}\left(-\frac{r_{j+1}}{2 \cdot \Delta x_i} - \frac{a}{x_i - x_{i+1}}\right) \quad = \quad \frac{T_{i,j}}{Dt} - \frac{r_j}{2}\left(\frac{T_{i-1,j} - T_{i+1,j}}{x_{i-1} - x_{i+1}}\right) + \\ &\qquad\qquad \frac{a}{x_{i-1} - x_{i+1}}\left(\frac{T_{i-1,j} - T_{i,j}}{x_{i-1} - x_i} - \frac{T_{i,j} - T_{i+1,j}}{x_i - x_{i+1}}\right). \end{aligned} \tag{3.10}$$

Replacing the coefficients with constants, Equation 3.10 reduces to

$$T_{i-1,j+1}A_i + T_{i,j+1}B_i + T_{i+1,j+1}\mathrm{C_i} = \mathrm{V_i}. \tag{3.11}$$

Boundary conditions dictate that $V_0=T_s$, $A_0=A_{n-1}=1$, and $V_{n-1}=T_i$. To simplify the equation further, define a new matrix, ***M***, by

$$\mathbf{M} = \begin{bmatrix} B_0 & 0 & 0 & 0 & \cdots & 0 \\ A_1 & B_1 & C_1 & 0 & \cdots & 0 \\ 0 & A_2 & B_2 & C_2 & \cdots & 0 \\ 0 & 0 & A_3 & B_3 & \cdots & 0 \\ \vdots & \vdots & \vdots & \vdots & \ddots & 0 \\ 0 & 0 & 0 & 0 & 0 & B_{n-1} \end{bmatrix}. \tag{3.12}$$

The new temperature profile, as a function of the previous temperature profile and new surface temperature, is therefore the solution of the matrix equation,

$$\boldsymbol{MT} = \boldsymbol{V}. \tag{3.13}$$

Because ***M*** is a tri-diagonal matrix, a large number of very efficient and quick algorithms for solving Equation 3.13 are available[38].

C. Solution Criteria

Now, finally, there exists a nonsteady, nonlinear model. It consists of Equations 2.1, 2.2, 2.3, 2.4, 2.11, 2.23, 3.1, and 3.2, all solved simultaneously. Moreover Equations 3.1, and 3.2 depend on simultaneous temperature profile solutions, determined from different versions of Equation 3.13. Table 3.3 contains a list of the dependent variables, with their equation numbers and dependencies.

The only remaining questions from a computational standpoint are how to apply the model to a given input and how to maintain stability in a time-dependent solution. Here, the characteristic response time is a critical parameter. Its definition, from Chapter I, is

$$t = \frac{a}{r^2}. \tag{1.9}$$

Table 3.3: Dependent Variables in Nonsteady Model

Variable	Eq. #	Function of Variable							
		G_p	G_{ap}	G_b	$x_{f,ap}$	x_f	$T_{s,ap}$	$T_{s,b}$	$T_{f,ap}$
G_p	2.3		P	P					
G_{ap}	2.1						P		
G_b	2.2							P	
$x_{f,ap}$	2.4		P						P
x_f	2.11	P	P						P
$T_{s,ap}$	3.1		P		P		P		P
$T_{s,b}$	3.2			P		P		P	
$T_{f,ap}$	2.23	P			P	P			

The system obviously has two characteristic response times: one in the AP and one in the binder. Denote t_{max} as the larger of the two and t_{min} as the smaller. The smallest possible time step, therefore, should be the smallest characteristic response time divided into sufficiently small increments. "Sufficiently small" in this case might mean at least 59 increments per response time, i.e.,

$$Dt \le \frac{t_{min}}{59}. \tag{3.14}$$

In practice, however, numerical stability requirements are more restrictive, so the above criterion rarely dominates. Characteristic response times are on the order of a few milliseconds, yet the simulation usually requires a Dt of around 10^{-5} seconds to maintain stability.

Different types of simulations, too, require different step sizes. In a simulation of a step- or exponentially increasing pressure function, the lower of 10^{-5} or $t_{min}/59$ would certainly suffice. Harmonic pressure oscillations at high frequency, however, might require a smaller step size in order to obtain the appropriate number of increments per pressure oscillation.

For a simulation of a harmonic pressure input of frequency w, the time step should be the minimum of 10^{-5} s, $1/(w \cdot 59)$, and $t_{min}/59$. In other words, the criterion is

$$Dt = min\left(\frac{t_{min}}{59}, 10^{-5}, \frac{1}{w \cdot 59}\right). \tag{3.15}$$

Just as t_{min} governs the step size, t_{max} governs the length of the simulation. Under a step- or exponentially-increasing pressure, the transient behavior is the region of interest. Thus, the simulation should run until the transient behavior dies down, usually at three or four times t_{max}.

In oscillatory burning, however, the region of interest is after the response has developed a condition of dynamic equilibrium. Again considering a harmonic pressure input of frequency w, run the simulation to either $10*t_{max}$ or 10 pressure oscillations, whichever is longer.

Figure 3.4 is an example of a step pressure input from 10 bar to 20 bar. Figure 3.5 is an example of an oscillatory pressure at 2000 Hz, 10 bar mean and 20% oscillation amplitude. The time scale for both figures is t/t_{max} with (90, 80/20, 298) propellant. Both figures incorporate the "curve-fit" method of flame feedback, discussed in the following section.

The nonsteady model resides as a Mathcad 7.0.3 file, with some of the more computationally intensive routines written in Microsoft Visual C^{++}. The nonsteady Mathcad solution sheet is in Appendix B.

D. Solution Issues

Completely nonlinear nonsteady models present a set of challenges to the programmer that test the limits of both computational accuracy and theoretical validity. Several notable difficulties have appeared during the course of the current study.

1. Issue One: Burning Rate "Dragging" of the Gas Phase

Perhaps the most troubling issue is the apparent over-influence of burning rate on the gas phase. In Equations 2.4, 2.11, and 2.23, the flame heights and flame temperatures are linearly related to the mass fluxes and quadratically related to the pressure.

Even a linear dependence on burning rate, however, seems to override much of the nonsteady behavior of the propellant system. Figure 3.6 is a simplified sketch of the feedback from the flame into the propellant surface. Both the heat flux into the solid phase and the heat flux out of the gas phase are functions of burning rates in the current model. Each functional dependency acts like a form of damping, which tends to drag the model, shifting the response into shorter times with smaller amplitudes.

Some modelers have completely disregarded the dependency of $q_{f\text{-}s,ap}$ and $q_{f\text{-}s,b}$ on burning rate[29,30] while others have included it in a simplified form[28]. Many researchers have investigated the effect of flame modeling on transient response, but to the author's knowledge, no one has yet investigated multiple-flame, BDP-type flame structures in nonlinear, nonsteady regimes. The over-dependence observed here is not encouraging.

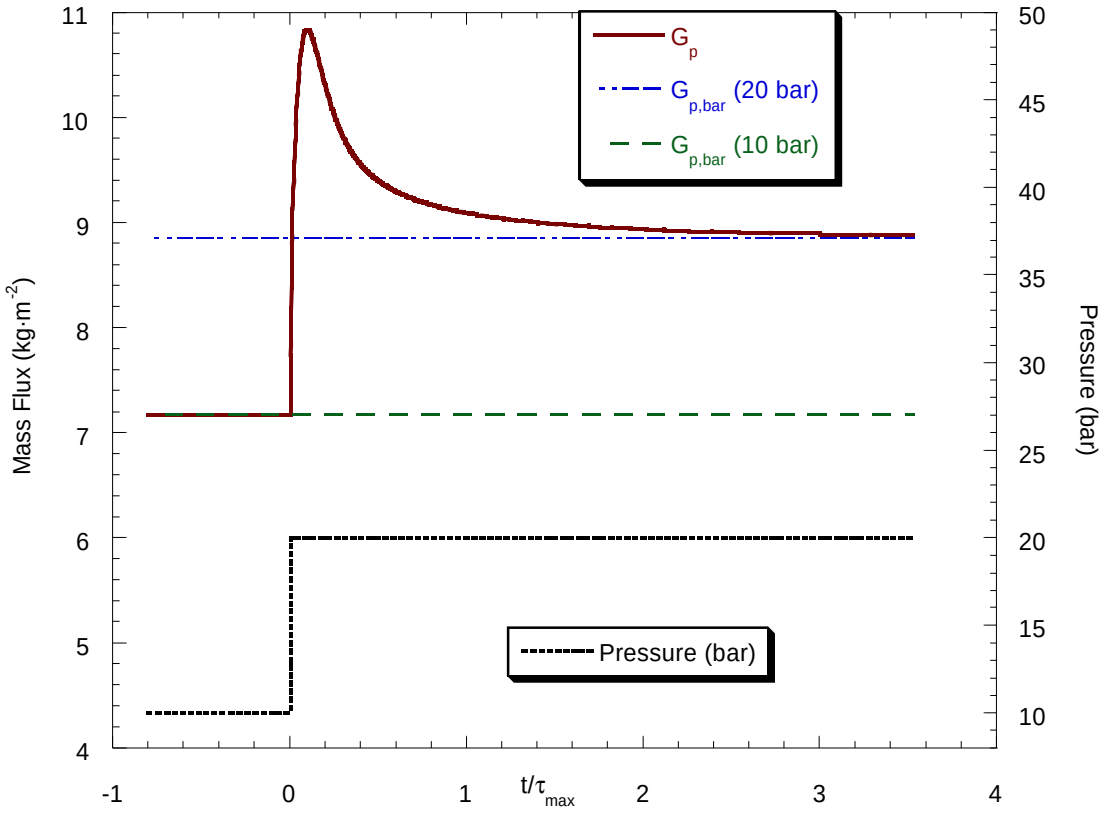

Figure 3.4: Response to Step Pressure Input

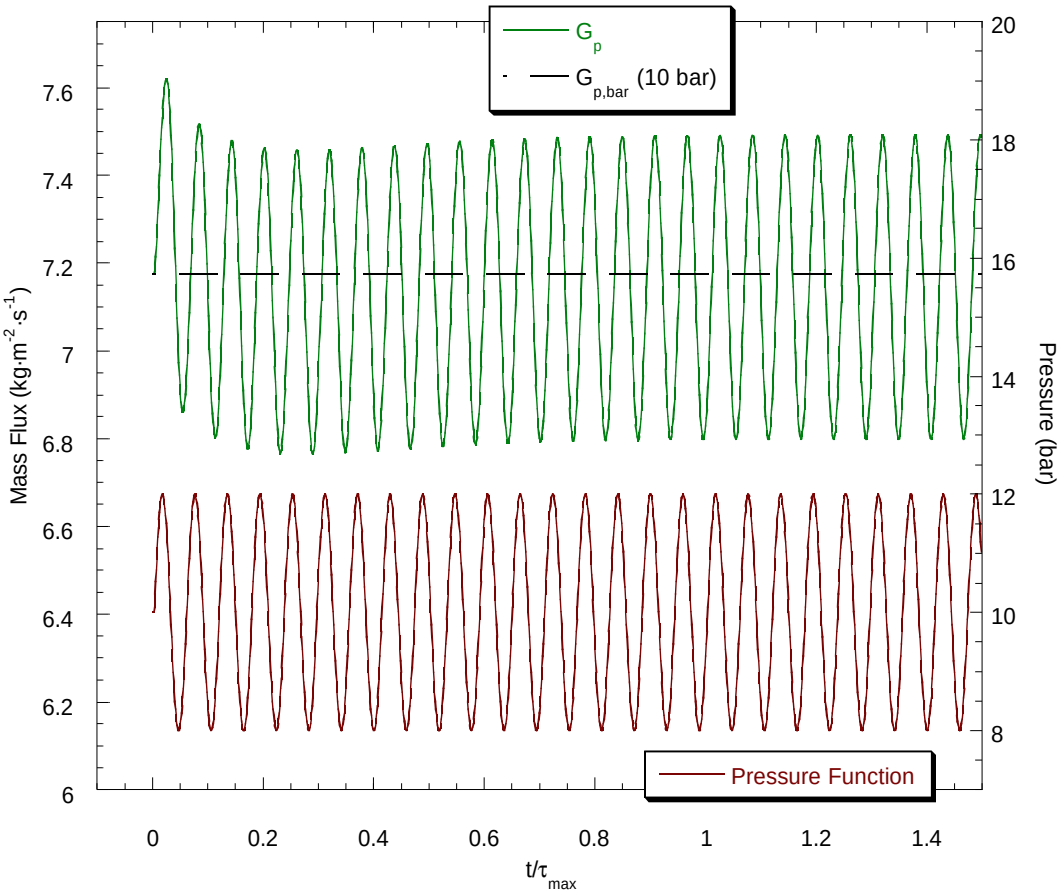

Figure 3.5: Response to Oscillatory Pressure Input

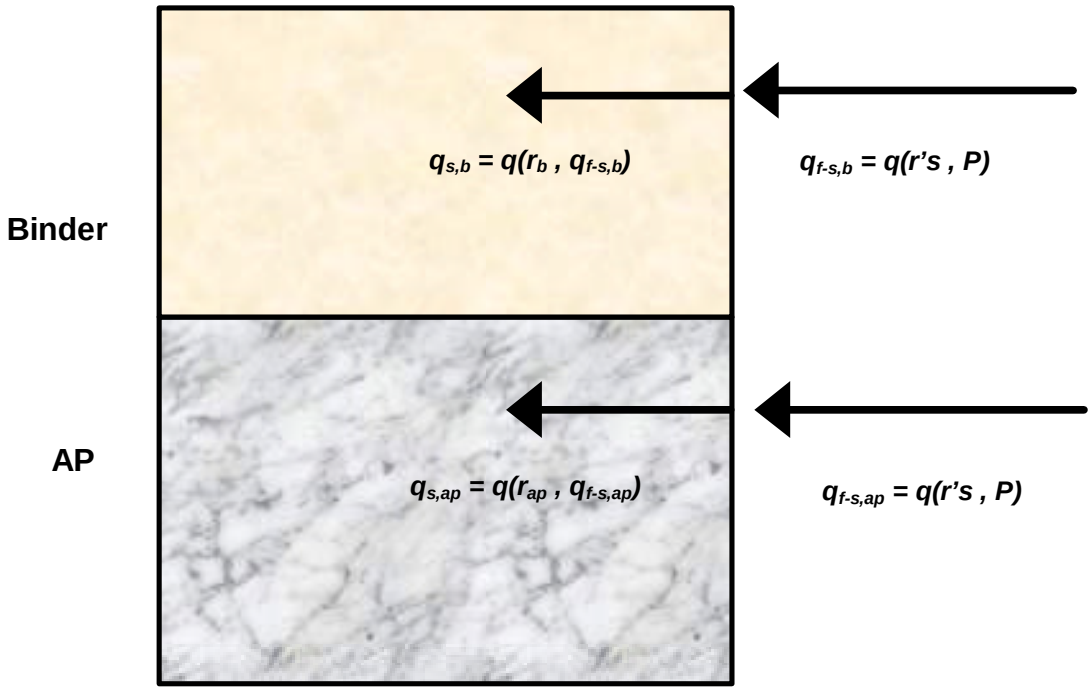

Figure 3.6: Heat Feedback Model

All is not lost, however, as it is still possible to obtain response results that compare favorably to those of other models. The method is simple; it involves eliminating some of the dependencies shown in Figure 3.6 to minimize the damping in the system. Specifically, the following algorithm will eliminate the gas phase dragging:

- Run a steady-state simulation.
- Fit the output of x_f, x_r, $x_{f,ap}$, and $T_{f,ap}$ as functions of pressure.
- Substitute these curve-fits into the nonsteady model in place of Equations 2.4, 2.11, and 2.23.

The above procedure effectively decouples the gas phase from the burning rate. Although this may not be an ideal simplification, it will produce results until a better method comes along. Figure 3.7 is a plot of various methods of calculating response of a (90, 80/20, 298) propellant to a step pressure input from 10 bar to 20 bar. "Full calculation" means that the quantity depends on burning rate through the proper equation , and "curve-fit" means that the quantity comes from a curve-fit of the steady-state data as a function of pressure only.

Figure 3.8 shows the same effect as Figure 3.7 in a frequency-response plot. The propellant is (90, 80/20, 298) subjected to harmonic pressure oscillations at a mean of 10 bar, with 20% oscillation magnitude. All curves come from a "peak-average" calculation method, as discussed in the following section.

The figures indicate that the equations for $T_{f,ap}$ and $x_{f,ap}$ are the most significant contributions to damping in the system. This result matches expectations because $T_{f,ap}$ and $x_{f,ap}$ define the heat feedback to the AP, which is approximately 80% of the system. The large difference between the full gas phase calculation and the curve-fit gas phase calculation in Figure 3.7 and Figure 3.8 is interesting. Clearly, the burning rate dependence adds significant damping to the system.

All simulations for the remainder of the paper will use a curve-fit gas phase, unless stated otherwise. To reiterate, this is not a perfect assumption, but it gets results.

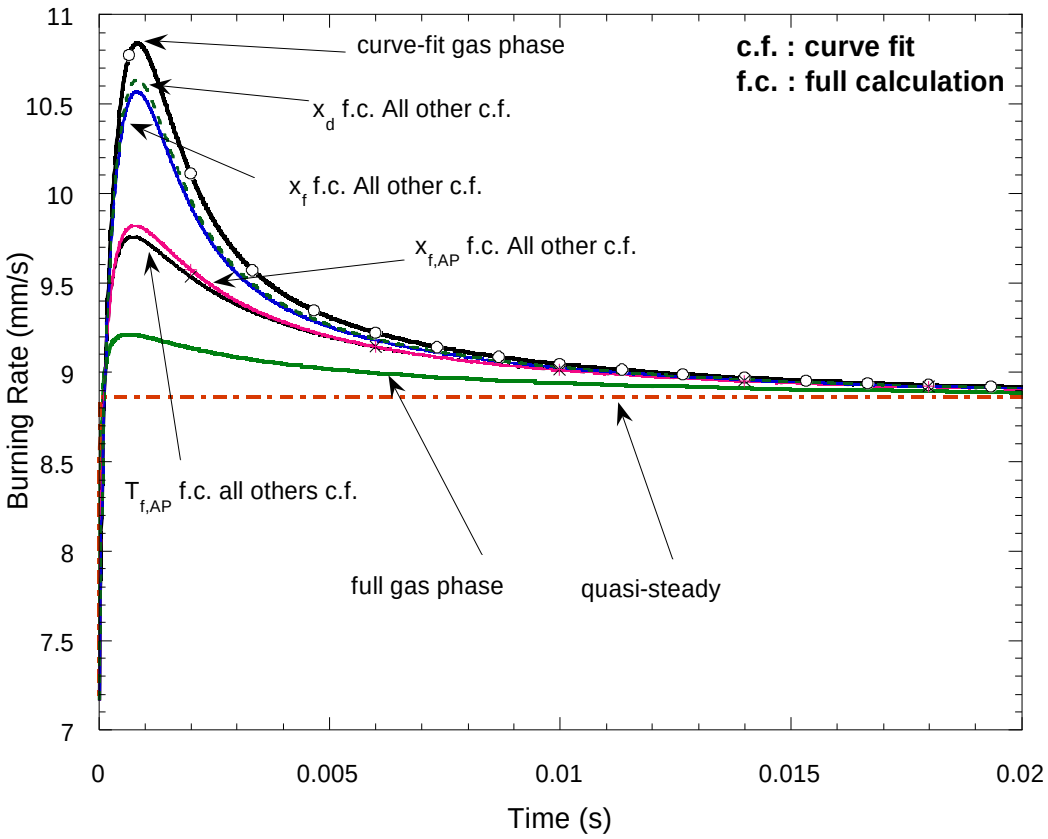

Figure 3.7: Effect of Curve-Fitting on Step Input

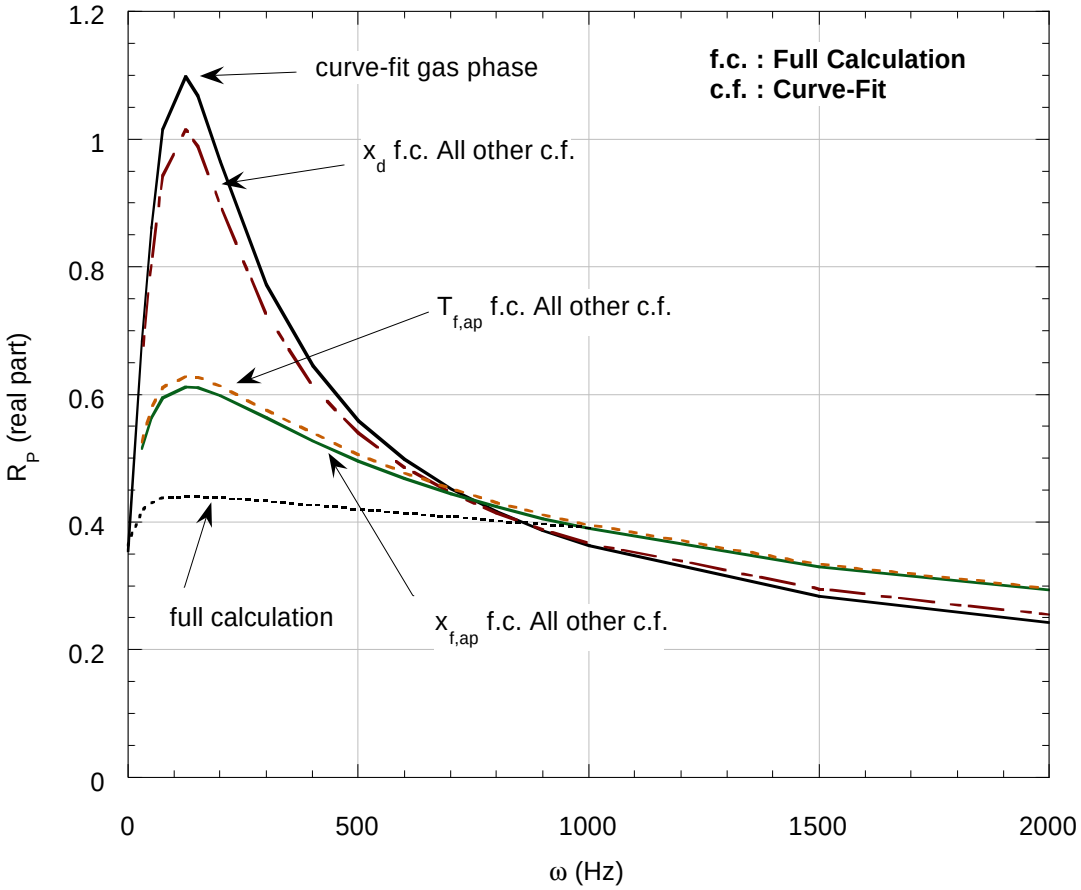

Figure 3.8: Effect of Curve-Fitting on Frequency Response

2. Issue Two: Response Function Definition

The pressure-coupled response function, as previously mentioned, is the ratio of a percentage change in burning rate to the percentage change in pressure. From Chapter I, the pressure-coupled frequency response is

$$R_p = \frac{\dot{m}'/\overline{\dot{m}}}{P'/\overline{P}} = \frac{r'/\bar{r}}{P'/\overline{P}}. \tag{1.4}$$

The difficulty comes in the definition of $\bar{r}$ and r'. Linear models do not have a problem. The output of a linear model, based on a harmonic input, is harmonic itself around the mean steady-state solution. Thus, $\bar{r}$ and r' are well-defined and the definition in Equation 1.4 is unambiguous.

In nonlinear models, the output due to a harmonic forcing function is not itself harmonic, the "mean" is not necessarily the steady-state solution at the mean of the forcing function, and the peaks of the output are not symmetric about the arithmetic mean. Fortunately, in most cases the output is *periodic* with a frequency equal to that of the driving function. Such periodicity does not eliminate the ambiguous nature of Equation 1.4, but it does allow for an answer.

For example, Figure 3.9 is a plot of the final oscillation of G_p in response to a 125 Hz harmonic driving pressure with a mean of 10 bar and 20% oscillation magnitude. The propellant is (90, 80/20, 298), and the simulation has run to ten times the maximum characteristic response time.

The "steady-state" line is simply the solution at $P = \overline{P}$ (10 bar). The "arithmetic mean" is the average of all the points in the curve, and the "peak-average" is the sum of the top and bottom peaks divided by two. All three of these methods are candidates for calculating the $\bar{r}$ in Equation 1.4.

Although difficult to see in Figure 3.9, the arithmetic mean does not exactly equal the peak average. Thus, there are at least five different ways to calculate R_P from the Figure 3.9:

1) $\bar{r}$ = arithmetic mean; $r' = r_{max} - \bar{r}$.
2) $\bar{r}$ = arithmetic mean; $r' = \bar{r} - r_{min}$.
3) $\bar{r} = (r_{min} + r_{max})/2$; r' = either .
4) $\bar{r}$ = steady-state at $\overline{P}$; $r' = r_{max} - \bar{r}$.
5) $\bar{r}$ = steady-state at $\overline{P}$; $r' = \bar{r} - r_{min}$.

Method 3 is the recommended method because it usually returns an answer that is between the extremes of the four other methods and because it returns only one value of R_P for a given $\bar{r}$. Figure 3.10 is a plot of R_P vs. frequency for all five of the calculation methods. The two lines plotted against the secondary abscissa show the percentage difference between $\bar{r}$ and the mean burning rate, using the mean burning rate as a baseline. The methods differ the most at low frequency, and the percentage difference between the means is largest below 100Hz. Figure 3.10 represents a (90, 80/20, 298) propellant excited by a pressure oscillation of 20% about a mean of 10 bar.

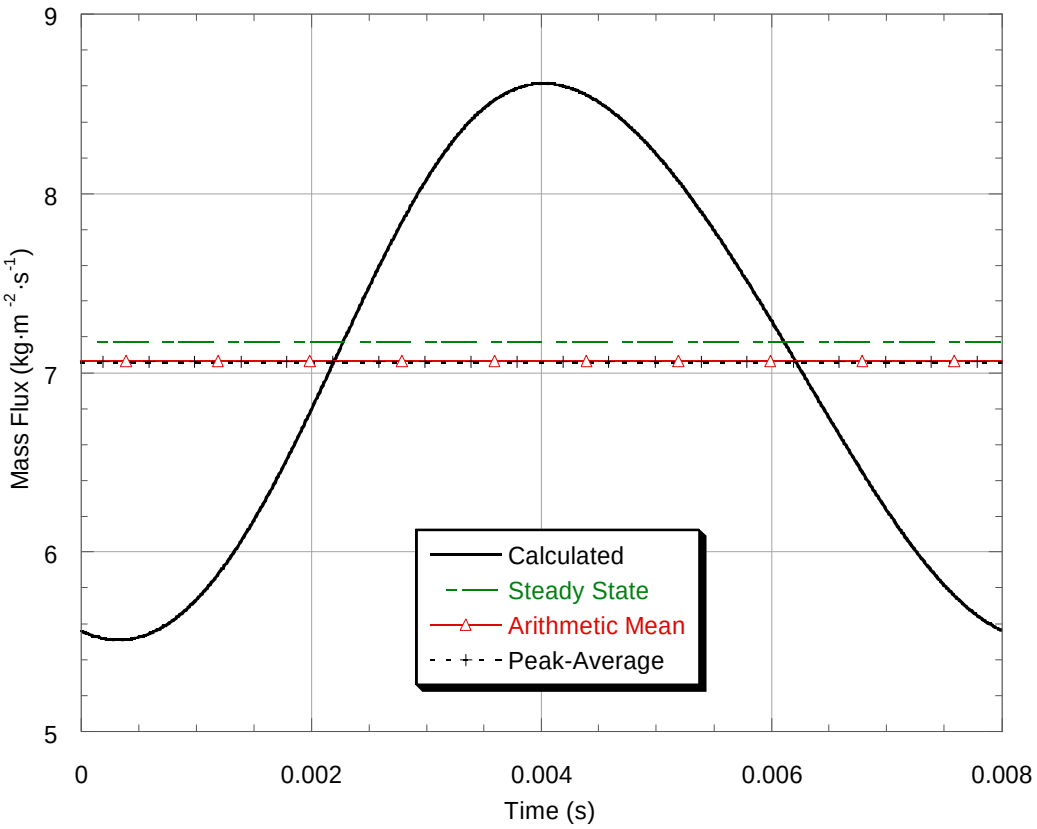

Figure 3.9: Final Oscillation of Mass Flux Under an Oscillatory Pressure Field

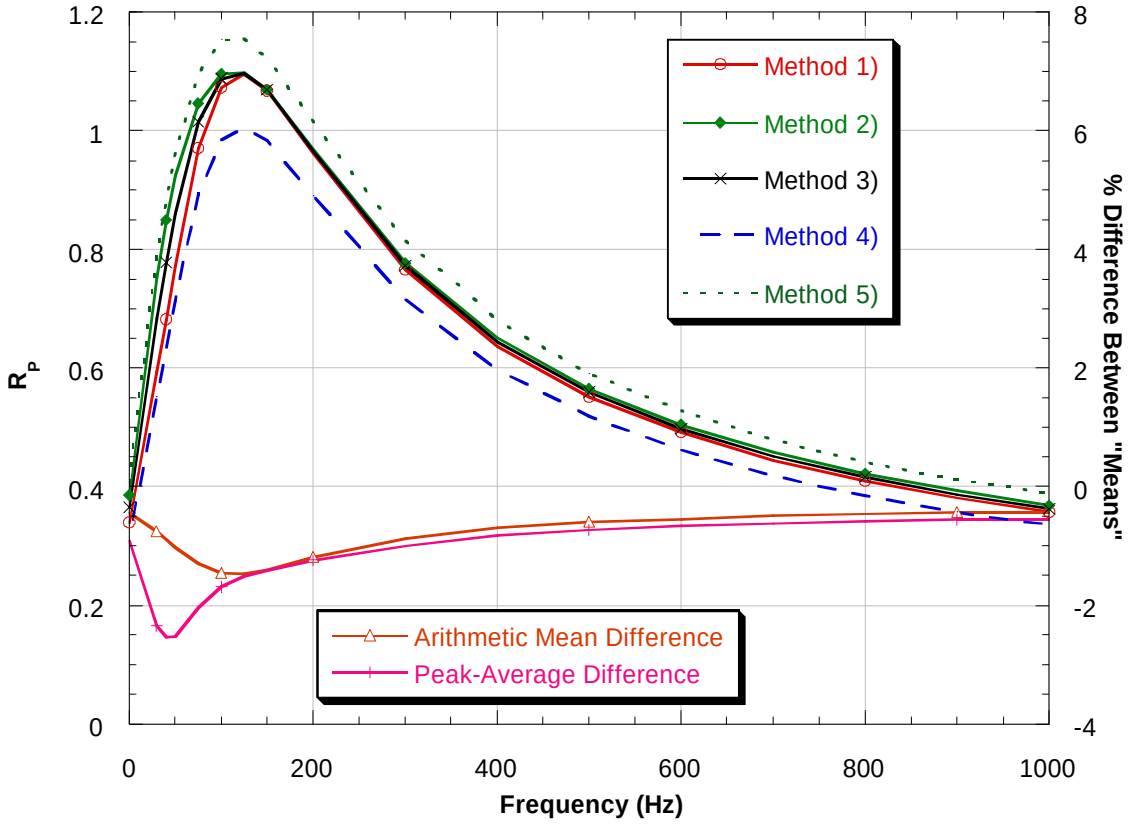

Figure 3.10: R_P vs. Frequency Using Several Calculation Methods

E. Preliminary Nonsteady Results

The following pages contain R_P vs. frequency plots that illustrate the effect of various parameters on the system.

Figure 3.11 is a frequency response plot for 80% AP, 20% HTPB propellants at 298K initial temperature. The driving pressure in all cases is a harmonic function with a mean at 10 bar and 20% pressure oscillations.

Figure 3.12 is a frequency response plot for a (50, 80/20, 298) propellant. The driving pressure in all cases is a harmonic function with 20% oscillation magnitude, but the mean pressure ranges from 10 bar to 100 bar.

Figure 3.13 is a frequency response plot for a (50, 80/20, 298) propellant. The driving pressure in all cases is a harmonic function with a 10 bar mean pressure, but the oscillation magnitude ranges from 5% to 30%.

Figure 3.14 is a frequency response plot for a 50μm AP particle diameter propellant at 298K initial temperature, while the AP mass percentage ranges from 73% to 87%. The driving pressure in all cases is a harmonic function with a mean at 10 bar and 20% oscillation magnitude.

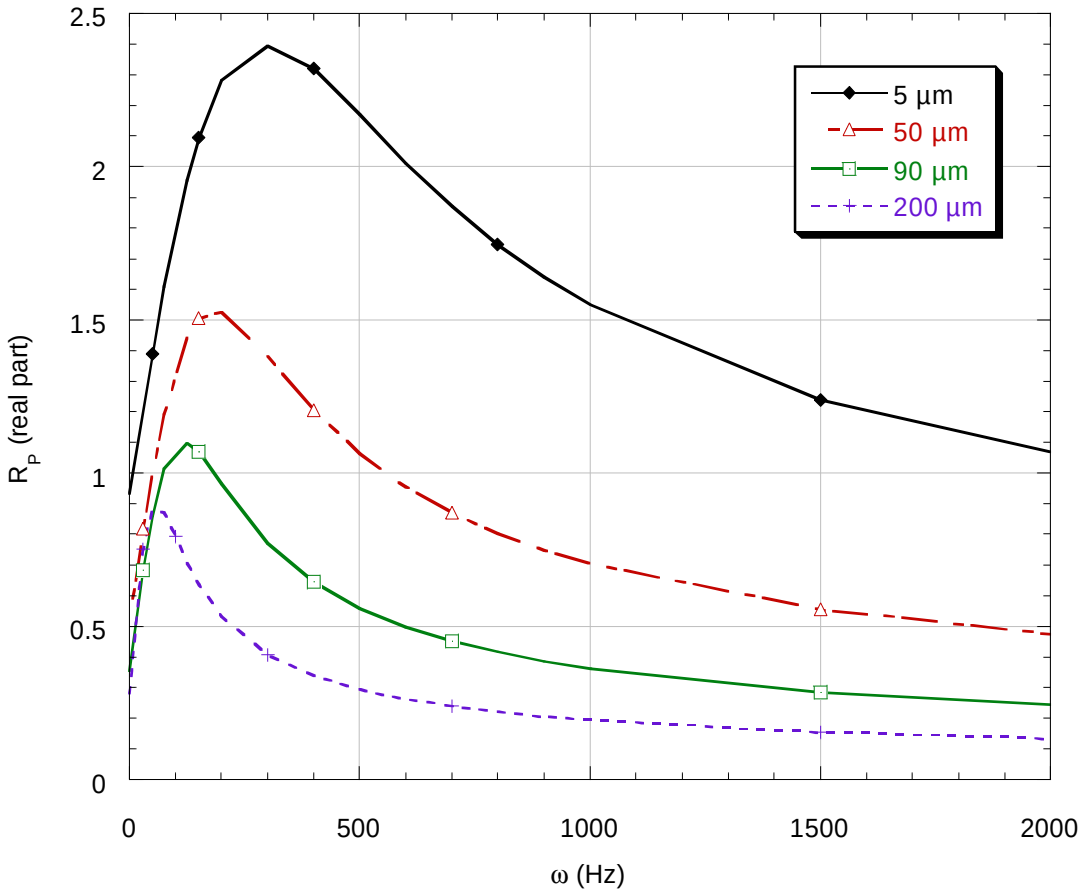

Figure 3.11: Effect of AP Particle Diameter on R_P

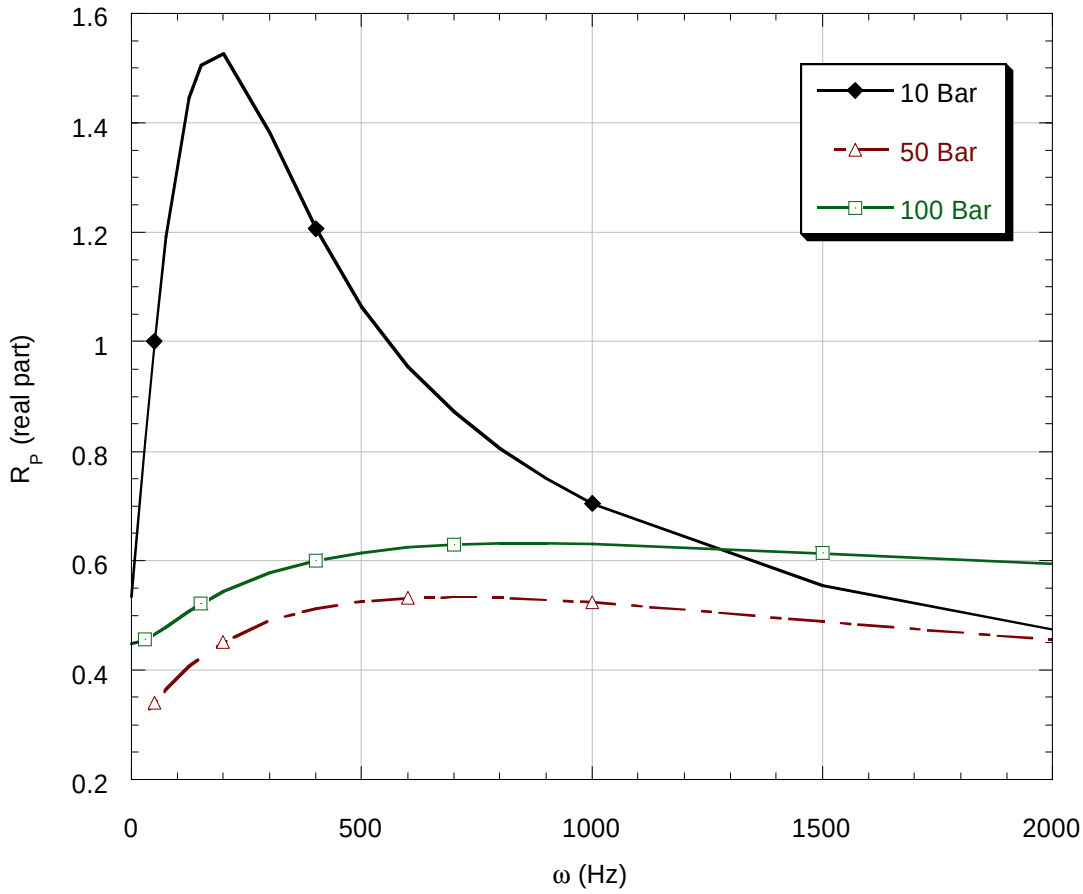

Figure 3.12: Effect of Mean Pressure on R_P

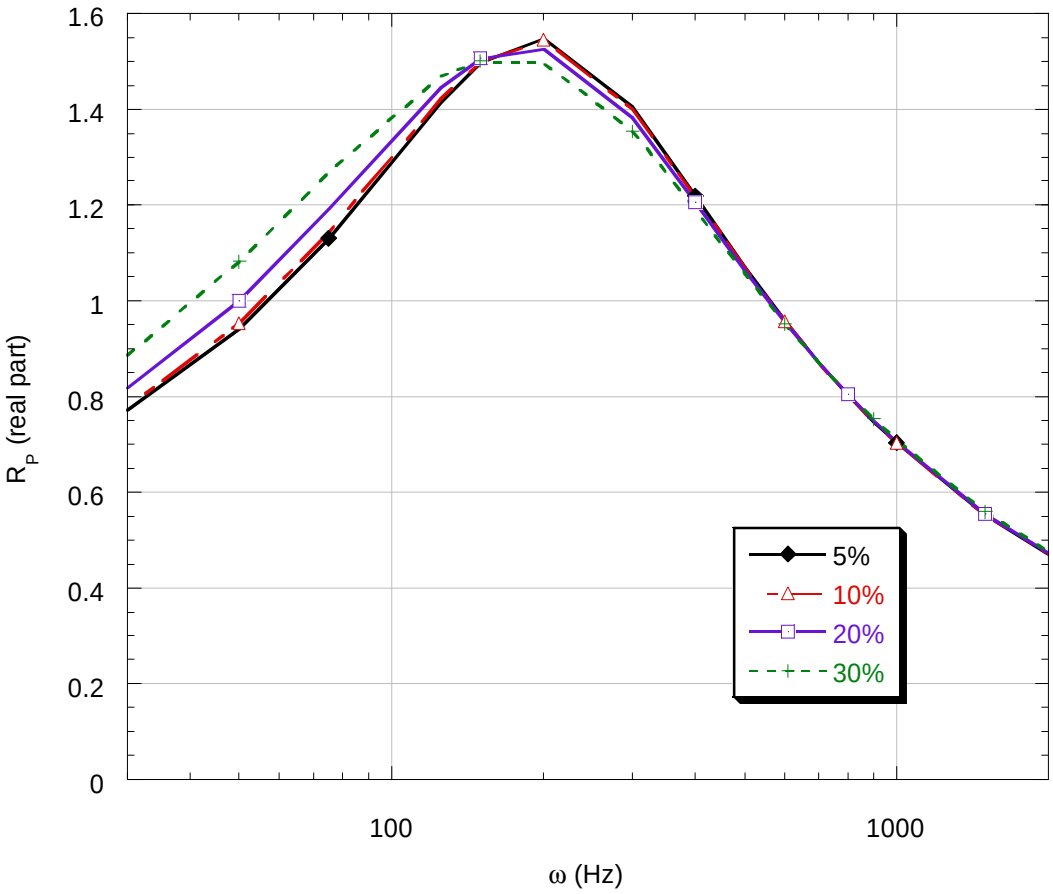

Figure 3.13: Effect of Oscillation Magnitude on R_P

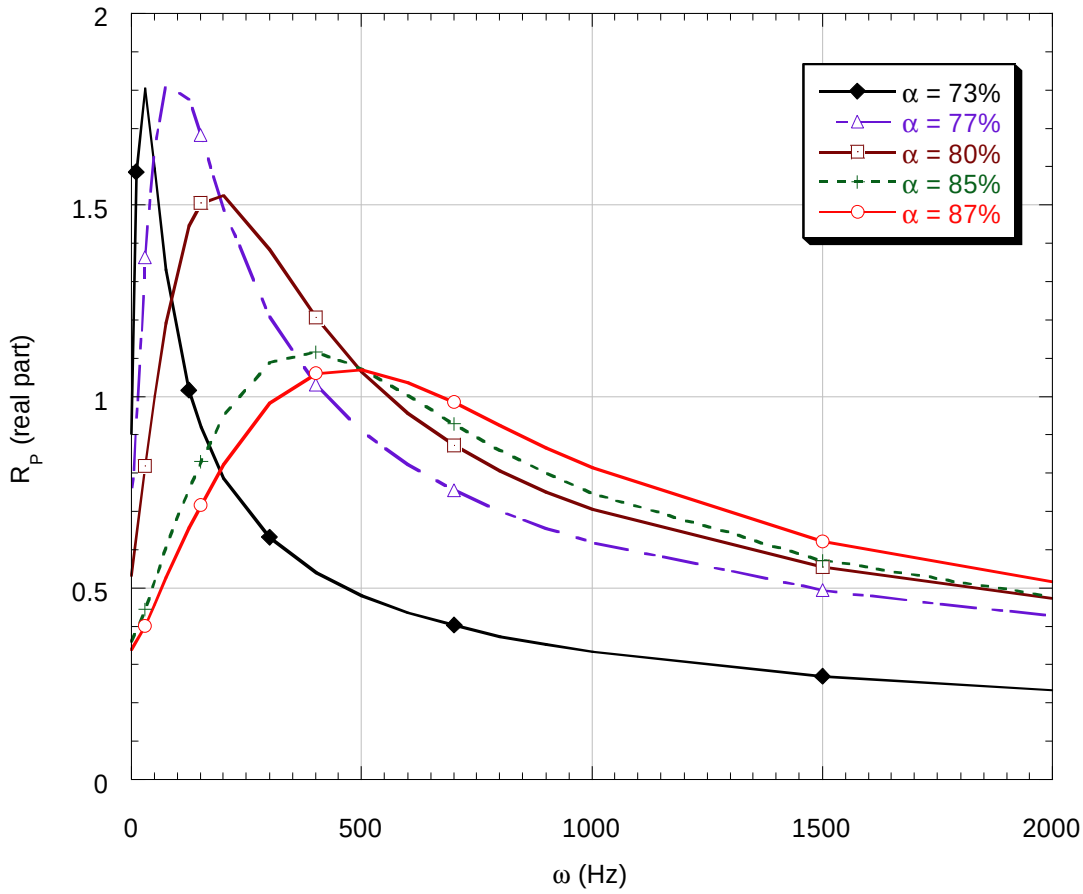

Figure 3.14: Effect of Oxidizer Mass Percentage on R_P

Chapter IV

RESULTS AND DISCUSSION

A. Steady-state

To a motor designer, the most important conditions of the steady-state model are the effect of AP particle diameter, the effect of AP mass percentage, and the initial temperature sensitivity. In addition, the theoretical turbulence modeling developed in this thesis has added some complexity which deserves consideration. The following sections are a discussion of some of the trends and relationships in these four areas.

1. Effect of Particle Diameter

The AP particle diameter size affects the model through the size of the diffusion flame. The surface of a burning solid propellant is analogous to an array of Bunsen burners, where the AP particle diameter controls the size of the burner nozzle. The diffusion flame then causes two effects, both of which slow down the overall propellant burning rate.

First, large diffusion flames pull the total flame height high above the surface. Thus, x_f is larger in Equation 2.15, and the heat flux into the binder surface is smaller.

Second, the diffusion flame indirectly lowers the heat flux into the AP by changing the pre-mixed flame temperature. When x_f is large, the AP flame temperature drops according to Equation 2.23. The heat flux into the AP surface falls because even though $x_{f,ap}$ stays relatively small, the temperature at that point drops significantly.

Figure 4.1 is a plot of diffusion flame height and AP flame temperature for (5, 80/20, 298), (50, 80/20, 298), (90, 80/20, 298), and (200, 80/20, 298) propellants across a wide pressure range. Notice how the smallest-diameter (5μm) propellant has almost no diffusion flame. Consequently, it has the highest AP flame temperature. (See also Figure 2.4.)

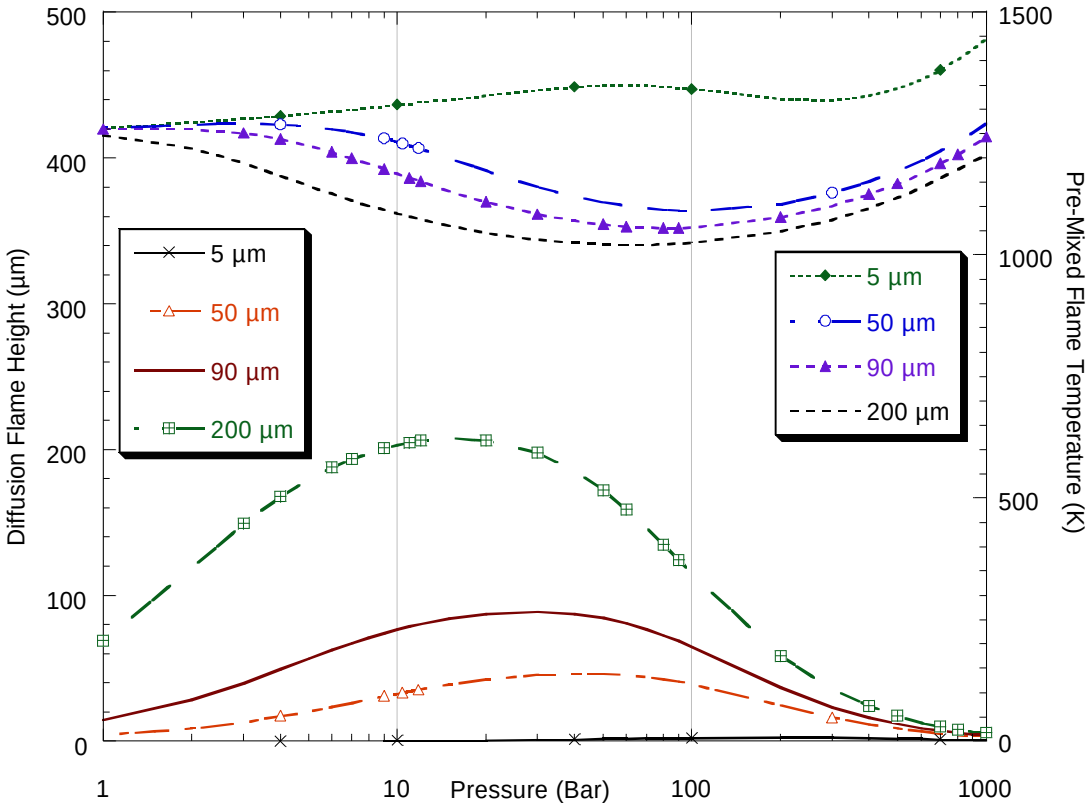

Figure 4.1: Overall Flame Height and Pre-mixed Flame Temperature

2. Effect of Turbulence

The diffusion flame height depends heavily on turbulent mixing at high pressures. The "humps" in Figure 4.1 would have a constant, upward slope if not for the turbulent mixing that kicks in with a low reaction flame height.

This should sound alarm bells in the alert reader's ear. It is possible that the model is "faking out" nature by employing unrealistically low flame heights to make up for deficiencies in other areas. For example, radiation might play an important role in the burning rate, especially at high pressure as the flame heights get lower.

One should remember, though, that the flame heights are really *characteristic* flame heights. They do not represent the actual bright zone of gas that is visible over a strand of burning propellant. They represent the point at which the temperature is the following (over either binder or AP):

$$T(x_f) = T_f - \frac{(T_f - T_s)}{e^n}. \tag{4.1}$$

Therefore, no one can say exactly how small the "flame heights" should be in an actual burning propellant. Moreover, the purpose of the model is to study nonsteady heterogeneous effects, so the gas phase is not as important as the solid phase, where most of the thermal lag resides. As long as the gas model provides a reasonable heat-feedback relation, it is doing its job splendidly.

Figure 4.2 contains two plots. The bottom portion is a plot of burning rate vs. pressure for (90, 80/20, 298) and (5, 80/20, 298) propellants, compared to experimental data. The dotted lines represent the theoretical calculations without turbulence. The top portion is a plot of total flame height for the same cases. The diffusion flame in the plot continues to get higher with pressure when turbulence is neglected. This causes an underestimation of burning rate at high pressures.

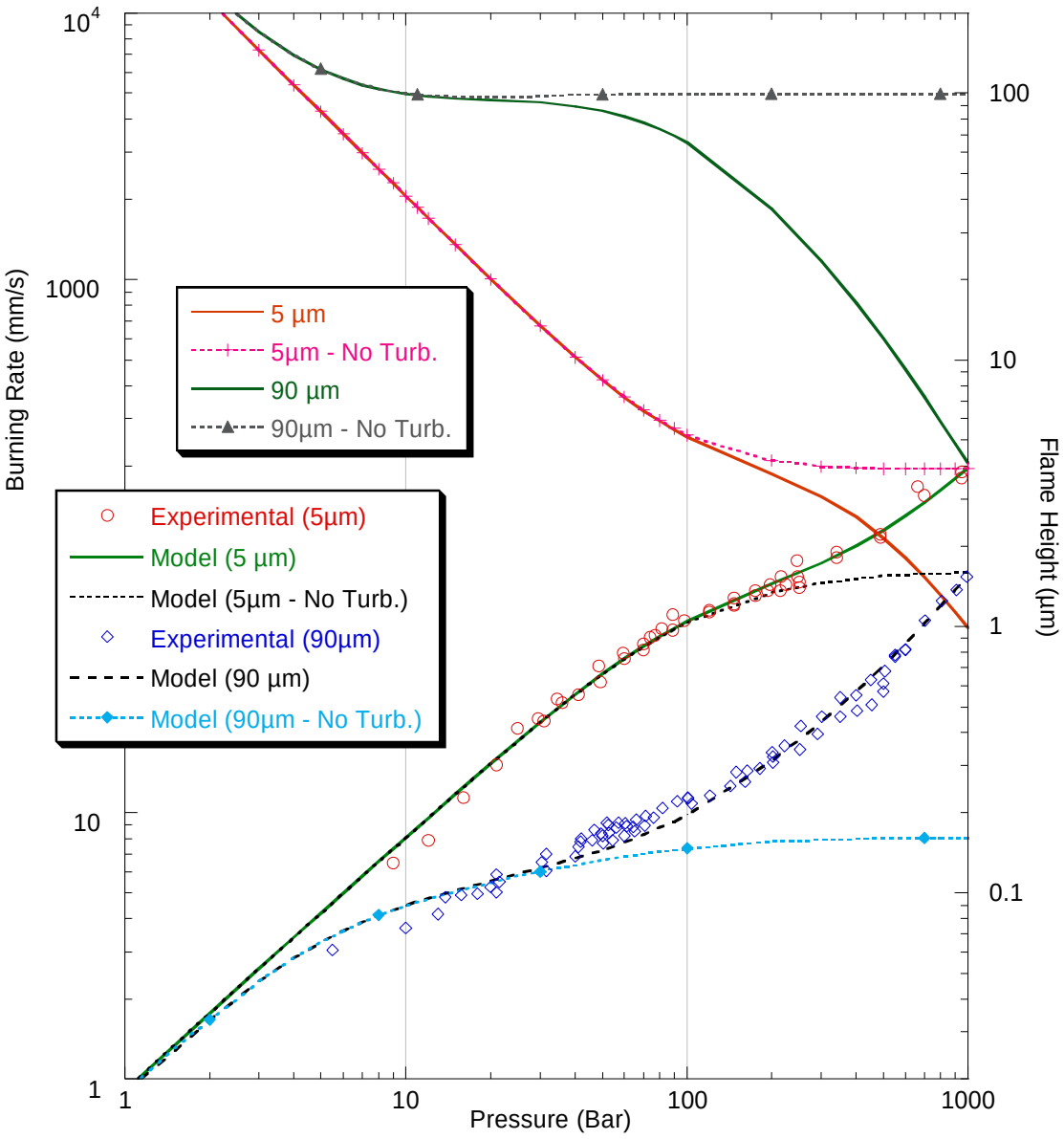

Figure 4.2: Turbulence in the Steady-State Model

3. Effect of AP Mass Percentage

Whereas most of the other parameters change the physics of the system, the AP mass percentage affects the chemistry of the system. The parameters q_f, T_f and $C_{p,g}$ all come from linear, single-variable interpolation of thermo-chemical-equilibrium calculations done at ONERA, where the single variable is oxidizer mass percentage. In addition, the AP mass percentage is a critical component of the total mass flux combination (Equation 2.3) and the total solid propellant density. Figure 4.3 is a plot of the flame temperature and diffusion flame heat release for a propellant at 298K initial temperature.

Raising the AP mass percentage will obviously raise the burning rate, which is why motor designers often try to get a_{ap} as high as possible by using multi-modal propellants. Figure 4.4 shows the effect of AP mass percentage on the burning rate of a 50µm propellant at 298K initial temperature. Higher values of a_{ap} seem to wash out the slowing effect of the diffusion flame, which is why the curves in Figure 4.4 with higher values of a_{ap} seem to have shallower "dips".

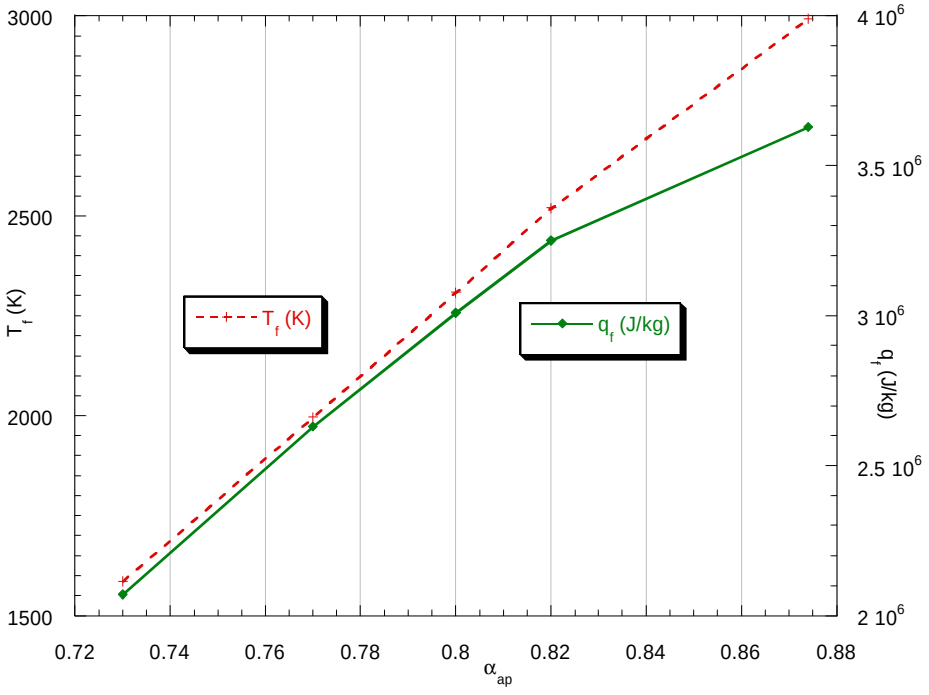

Figure 4.3: Flame Temperature and Heat Release as Functions of a_{ap}

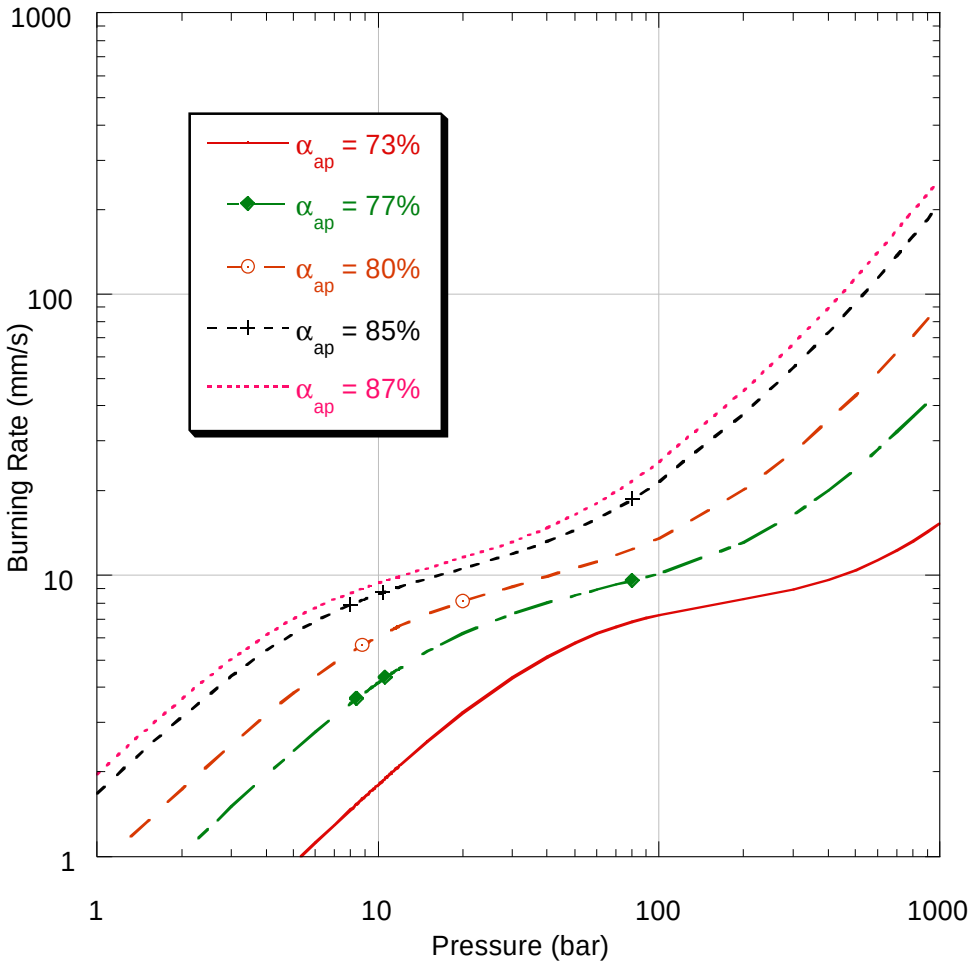

Figure 4.4: Effect of a_{ap} on Burning Rate

4. Effect of Initial Temperature

Initial temperature takes two paths to affect the model. The first, most obvious, path is the T_i term in Equation 2.19 and again in Equation 2.21. These two terms come from the heat capacity times the difference between T_i and T_s. Intuitively, when something is cold, it takes more energy to heat it than it does when the object is already warm.

The other path that T_i takes to affect the model is through the flame temperature. Simply doing an energy balance at steady-state leads to

$$T_f = T_{f,ref} + \frac{C_{p,s,p}}{C_{p,g,p}}\left(T_i - T_{i,ref}\right). \tag{4.2}$$

Because T_f is so far from the surface of both the binder and the AP, the effect of Equation 4.2 on the model is mild. It is a significant contribution, however, and the model must account for it. To see how significant it is, note the correlation between Figure 4.1 and Figure 2.7. As the diffusion flame gets higher, the contribution of T_f to the burning process becomes smaller, and the temperature sensitivity, which depends on T_f though Equation 4.2, goes down. When x_f falls again at higher pressure, the temperature sensitivity goes back up.

B. Frequency Response

The following sections contain a discussion of the nonsteady model and the related, dependent nature of its variables.

1. Effect of Mean Pressure

A rise in the mean pressure changes the nonsteady response in a very direct manner. Higher pressures induce faster burning rates, which in turn shift the frequency response of a propellant in a predictable pattern.

Equation 1.9 shows that the characteristic response time of a propellant is inversely proportional to the square of the burning rate. A propellant with a higher burning rate has a much shorter characteristic response time, and thus the pressure-coupled frequency response peak is shifted toward higher frequencies.

Moreover, the temperature profiles in the binder and AP are much shorter in faster burning propellants. The integral terms in Equations 3.1 and 3.2 are less significant, and the response amplitude should correspondingly be smaller. Figure 4.5 is a plot of steady-state binder and AP temperature profiles for a (50, 80/20, 298) propellant at 10 bar and 100 bar pressure. The profiles at 100 bar are clearly much steeper.

The mean pressure also contributes to the frequency response by changing the zero-crossing of the response curve. This point represents the pressure exponent, which changes with pressure. On a log-log plot of burning rate vs. pressure, the pressure exponent is the slope of the burning rate curve (as in Figure 2.4).

In sum, an increasing pressure should shift the peak of the pressure coupled frequency response curve to higher frequencies while simultaneously diminishing the amplitude of the curve although the whole curve can shift up or down depending on the value of n at the particular pressure. Figure 3.12 shows this predicted trend. The curve at 100 bar is higher than the curve at 50 bar because the pressure exponent is higher for a (50, 80/20, 298) propellant at 100 bar than at 50 bar. Figure 4.6 is a plot of the same data, where each curve is normalized by subtracting the pressure exponent from R_P.

2. Effect of AP Mass Percentage

The AP mass percentage also affects the frequency response through the burning rate and pressure exponent. Higher burning rates lead to response peaks at higher frequency with lower peak amplitude, while the pressure exponent shifts the entire curve either up or down. Figure 4.7 is a plot of the steady-state curves of a 50μm AP particle diameter propellant at around 10 bars and 298K initial temperature. It is essentially a blown-up version of Figure 4.4. Figure 4.8 is an n-normalized plot of the data from Figure 3.14. The expected trends are evident.

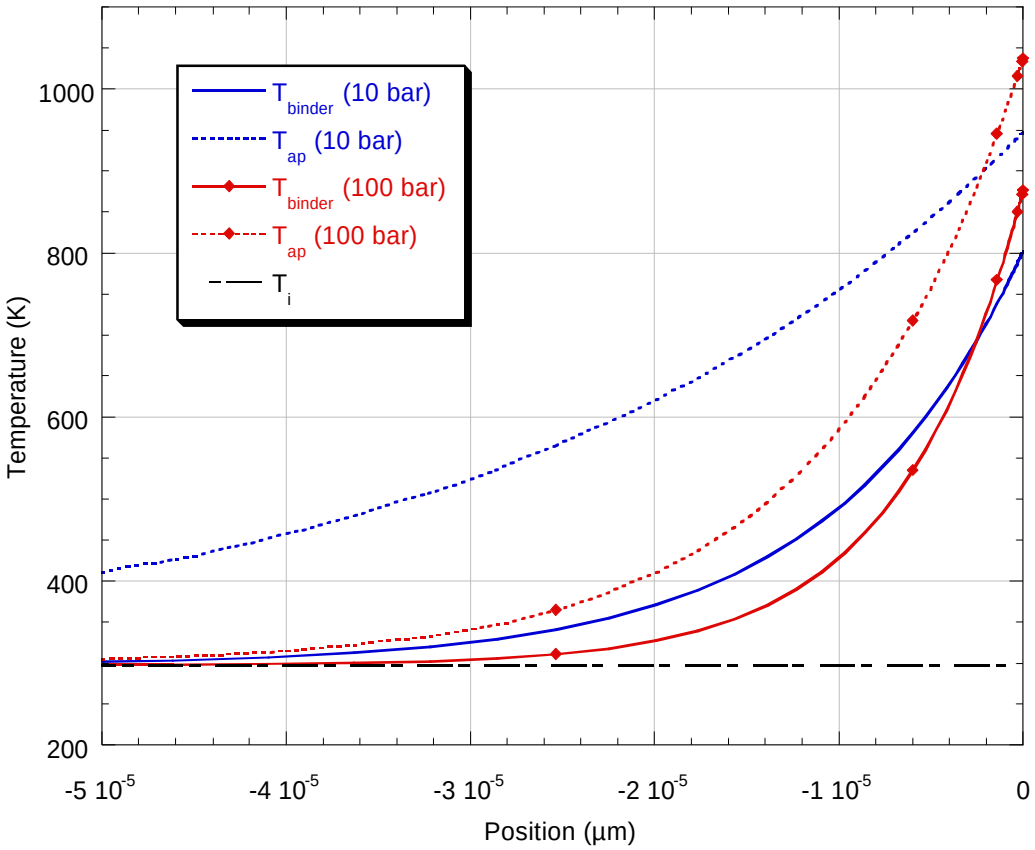

Figure 4.5: Steady-state Temperature Profiles at Two Mean Pressures

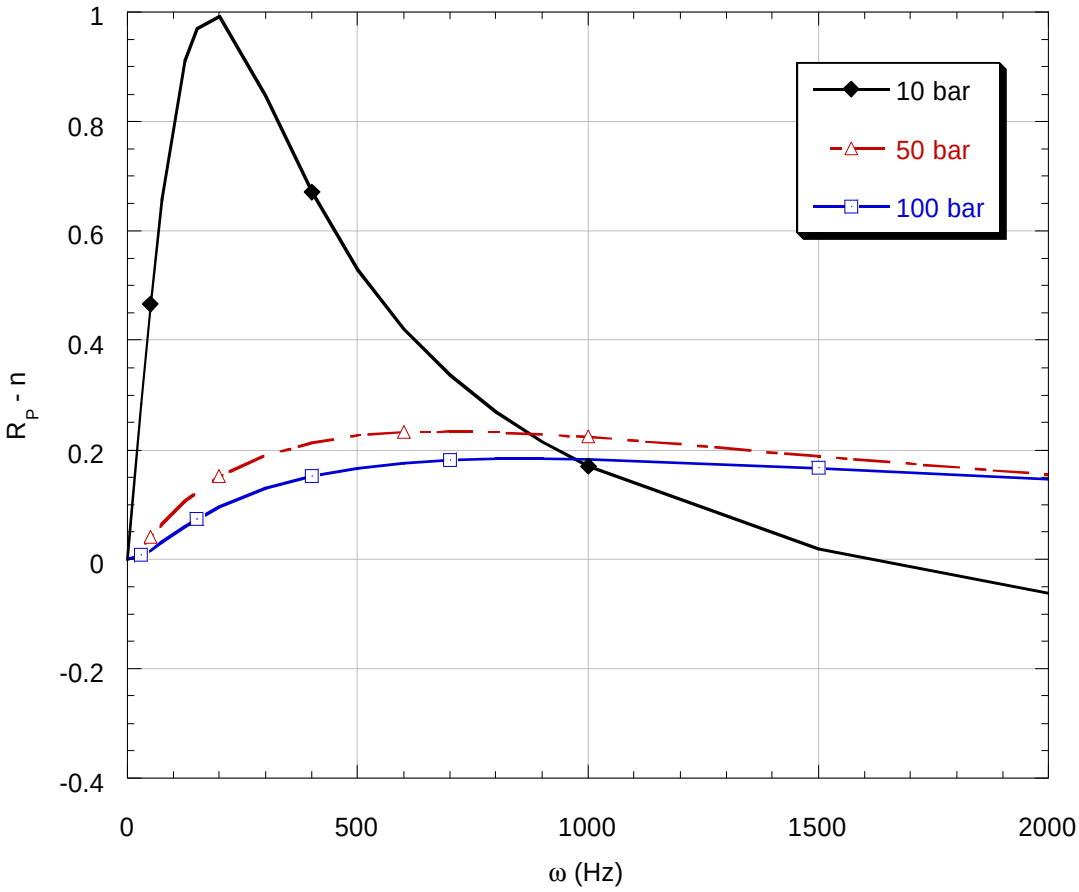

Figure 4.6: Normalized R_P Plot: Effect of Mean Pressure

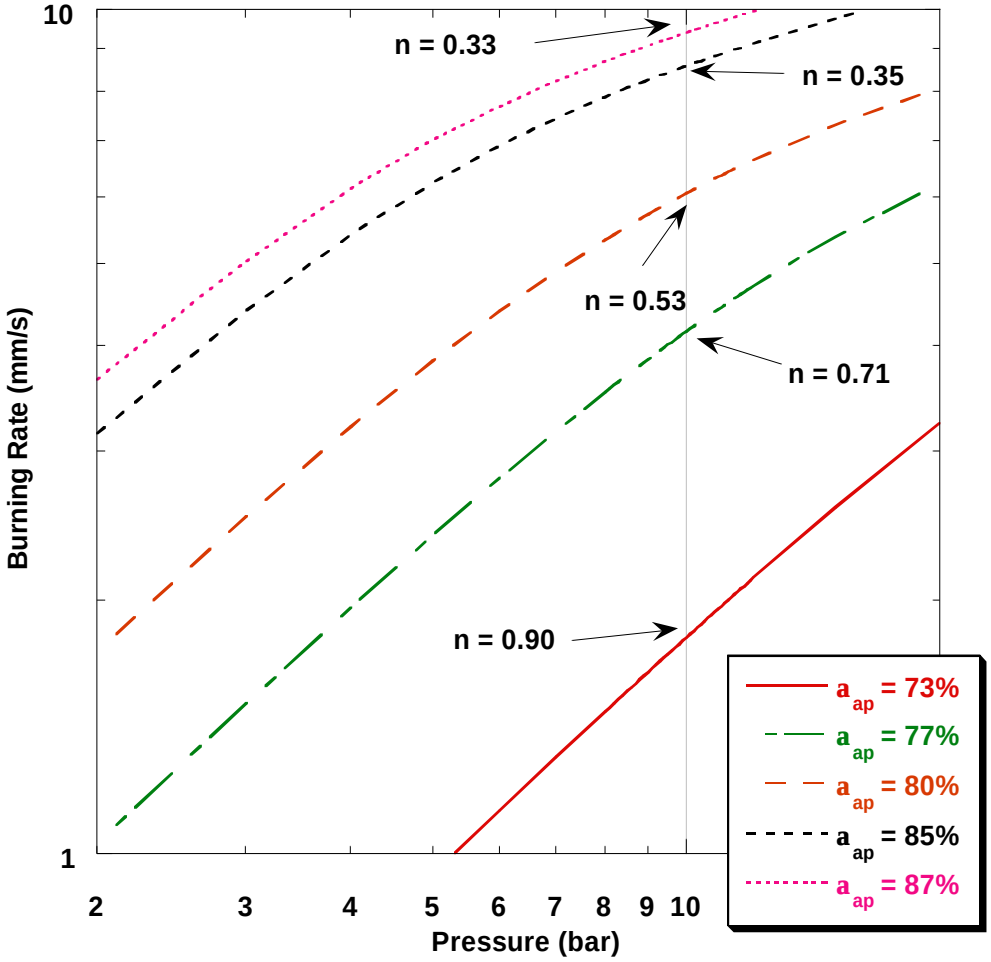

Figure 4.7: Steady-state Curves for Different AP Mass Percentages

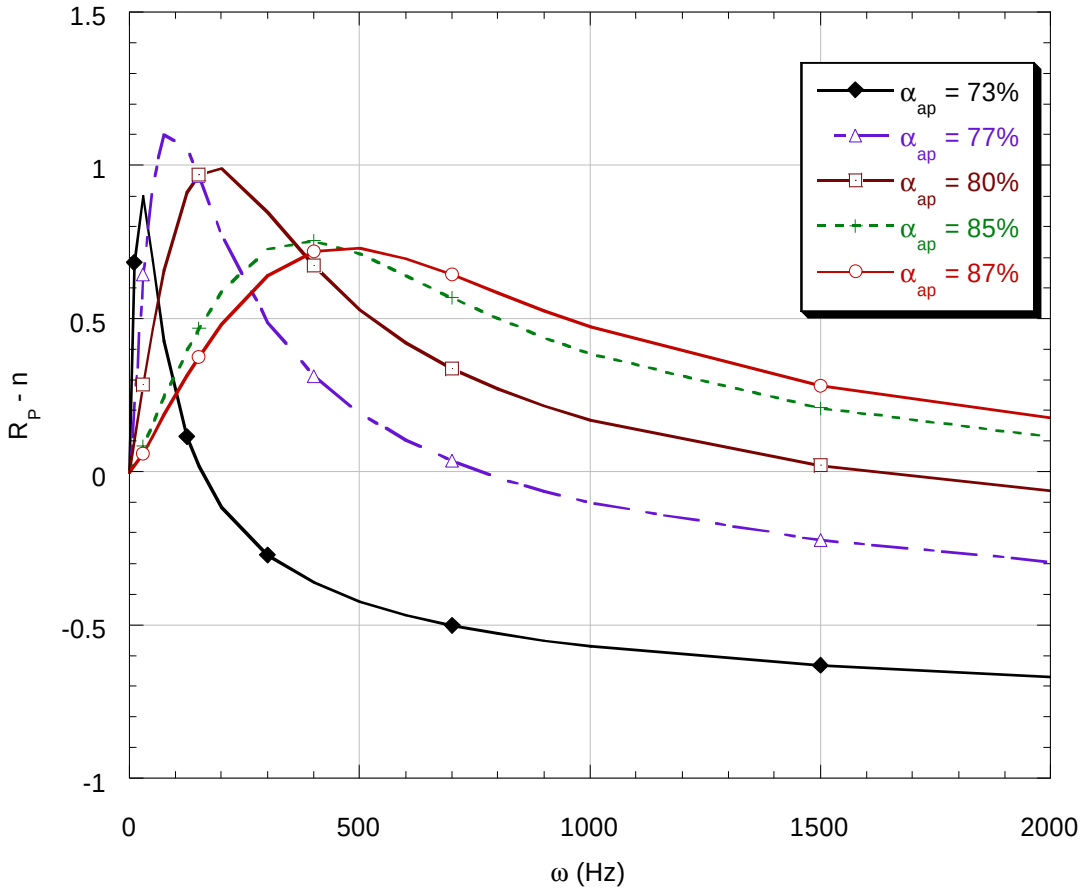

Figure 4.8: Normalized R_P Plot: Effect of AP Mass Percentage at 10 bar

3. Effect of AP Particle Diameter

In the nonsteady-state, just as in the steady-state, the AP particle diameter changes the system mostly through the diffusion flame. Larger AP particle diameters induce lower AP flame temperatures and higher overall flame heights.

Composite propellants with small AP particles typically burn faster than their counterparts with larger AP particles. As in the previous two sections, Equation 1.9 indicates that the characteristic response time is lower. The response peak should therefore occur at higher frequencies with a smaller amplitude.

Oddly enough, Figure 3.11 does not show such a trend. The frequencies are certainly higher for smaller AP particle diameters, but the amplitudes actually increase! The pressure exponent for the 5μm propellant is high compared to the others, but this does not explain the very large peak. Figure 4.9 is an n-normalized version of Figure 3.11.

4. Path of Burning Rate Dependence

The previous three sections lead to some interesting hypotheses about the nature of gas-phase "dragging" done by the burning rate. Faster burning propellants have lower response amplitudes than slower burning propellants, as long as the AP particle diameters are equal. In contrast, a propellant with a smaller AP particle diameter will almost certainly have a higher response amplitude, *even though it burns faster*. All the evidence points toward one culprit for the gas-phase dragging: the diffusion flame.

As the AP particle diameter gets smaller, the combustion model tends to resemble a homogeneous propellant. The diffusion flame, specifically, becomes very small, and the pre-mixed flame temperature becomes larger, almost matching the adiabatic flame temperature. Figure 4.1 shows the effect quite clearly.

Because the response amplitude is higher in smaller AP particle diameter propellants, one would expect the dragging effects to be less significant. Unfortunately, this does not seem to be the case. Figure 4.10 shows that the dragging is just as significant in a (5, 80/20, 298) propellant as it is in a (90, 80/20, 298) or (50, 80/20, 298) propellant. The path through which the gas phase affects the frequency response is therefore not a simple, linear relationship.

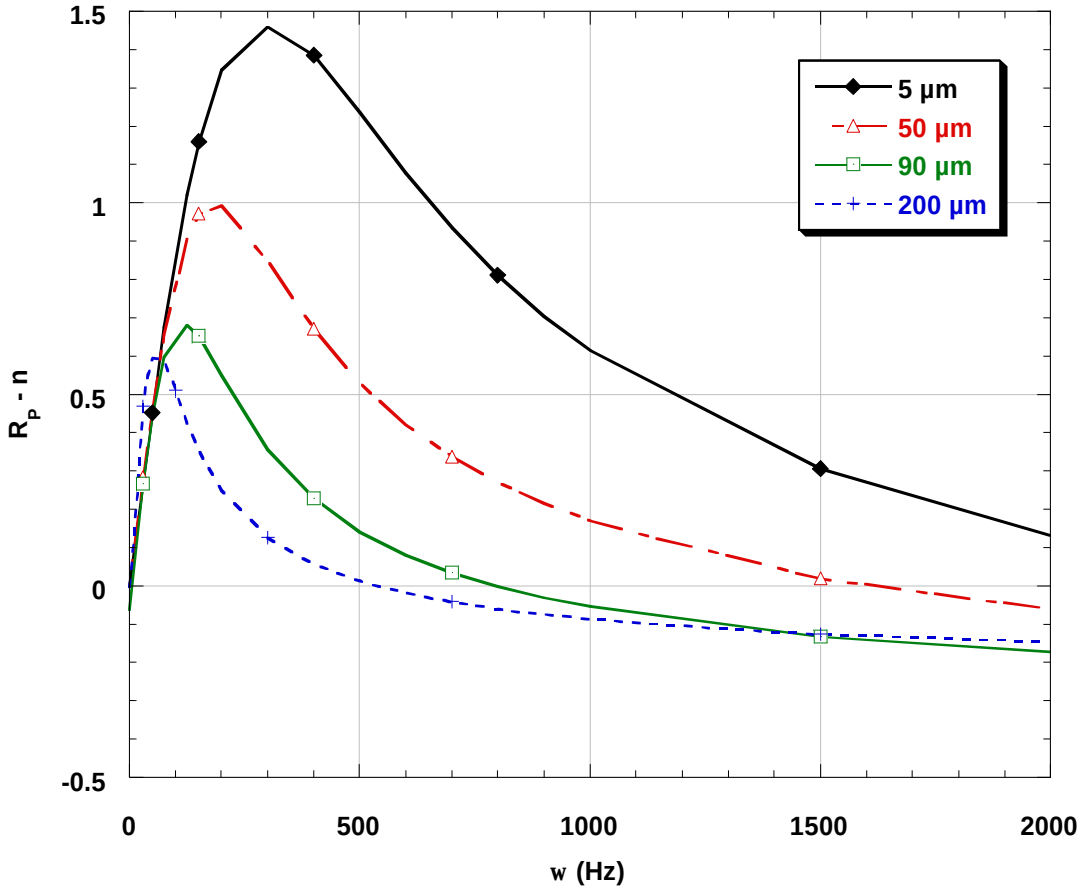

Figure 4.9: Normalized R_P Plot: Effect of AP Particle Diameter at 10 bar

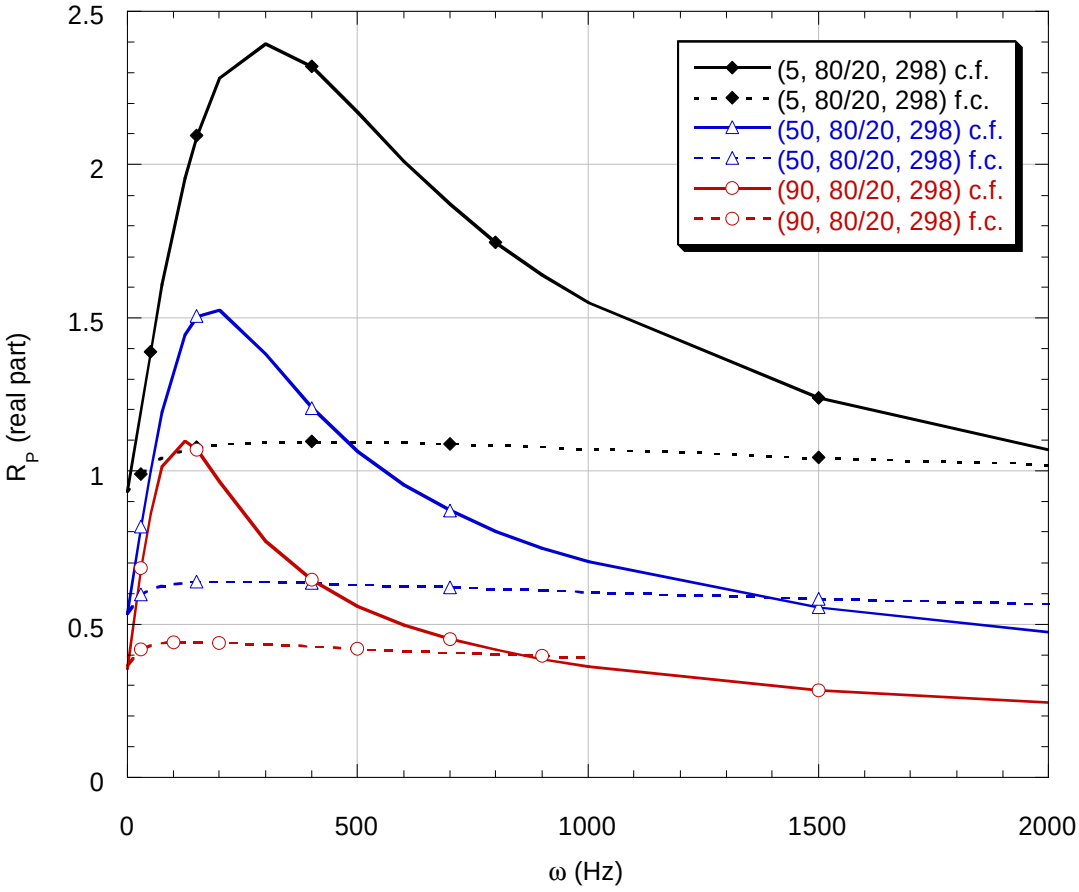

Figure 4.10: Effect of Gas-Phase Dragging on Three Propellants

Another possible explanation for the trend of higher response amplitude with lower AP particle diameter is that propellants with large exponents will show high response peaks, even if the shift is factored out. That is, the pressure exponent amplifies the peak in addition to shifting it.

Consider, for example, a pressure region where the pressure exponent is not necessarily larger with decreasing AP particle diameter. Figure 4.11 is a plot of steady-state burning rate curves for various AP particle diameters of an 80%AP / 20%HTPB propellant at 298K initial temperature around 100 bar pressure. The 200µm propellant has the highest pressure exponent, followed by the 5µm, 90µm, and 50µm propellants in descending order.

Figure 4.12 shows the response calculated with a mean pressure of 100 bar and an oscillation magnitude of 20%. The 5µm curve still has the highest peak, followed by the 200 µm, 90µm, and 50µm propellants. Figure 4.13 is an n-normalized version.

In Figure 4.13, the peak amplitude is definitely higher for the 5µm propellant, even though its pressure exponent is lower than that of the 200µm propellant. The general trend is lower response with smaller AP particle diameter, except in the case of the 5µm propellant. The pressure exponent may cause a slight amplification in addition to the shift, but it is not enough to cause the 200µm propellant to mimic the very high response amplitude of the 5µm propellant. Thus, the diffusion flame remains as a likely culprit in diminishing response amplitude, while the pressure exponent mostly shifts the R_P curve up or down.

There is, as yet, no direct evidence of exactly *how* the diffusion flame or any other aspect of the gas phase influences response amplitude. Neither the pre-mixed flame temperature nor the total flame height alone can account for the problem, as Figures 3.7 and 3.8 illustrate.

One conclusion remains clear —the over-simplified notion of a pressure-dependent-only gas phase is physically unrealistic. Future research in this area must either “fix” the gas phase model or develop a phenomenological explanation of why multiple-flame models resembling the one in this thesis are fundamentally incapable of predicting adequate response amplitudes.

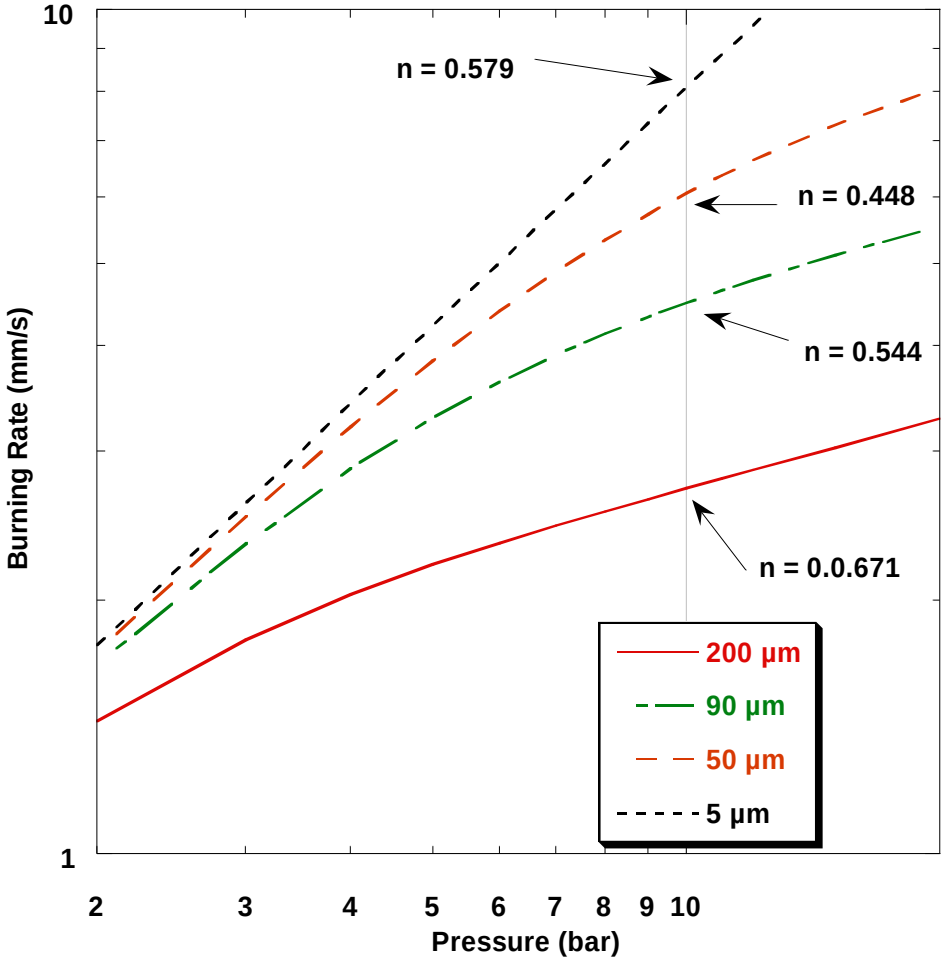

Figure 4.11: Steady-state Curves for Different AP Particle Diameters

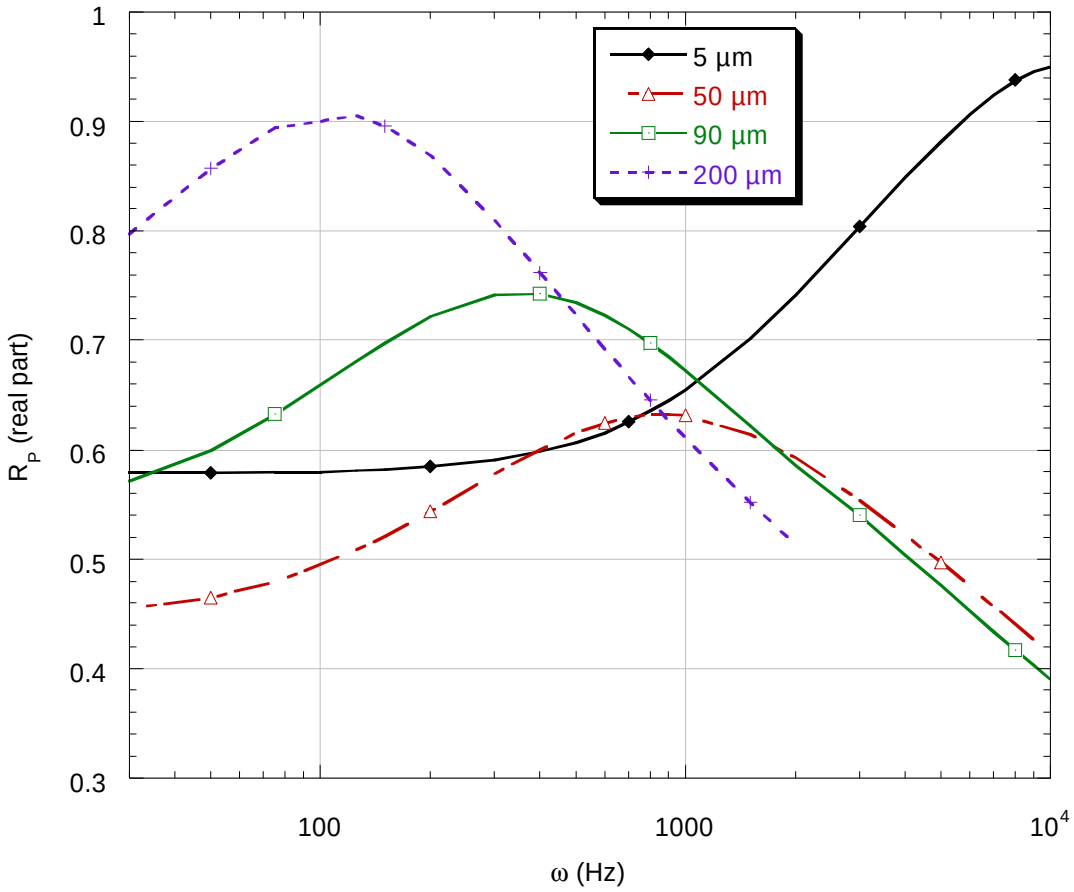

Figure 4.12: Effect of AP Particle Diameter on R_P at 100 bar

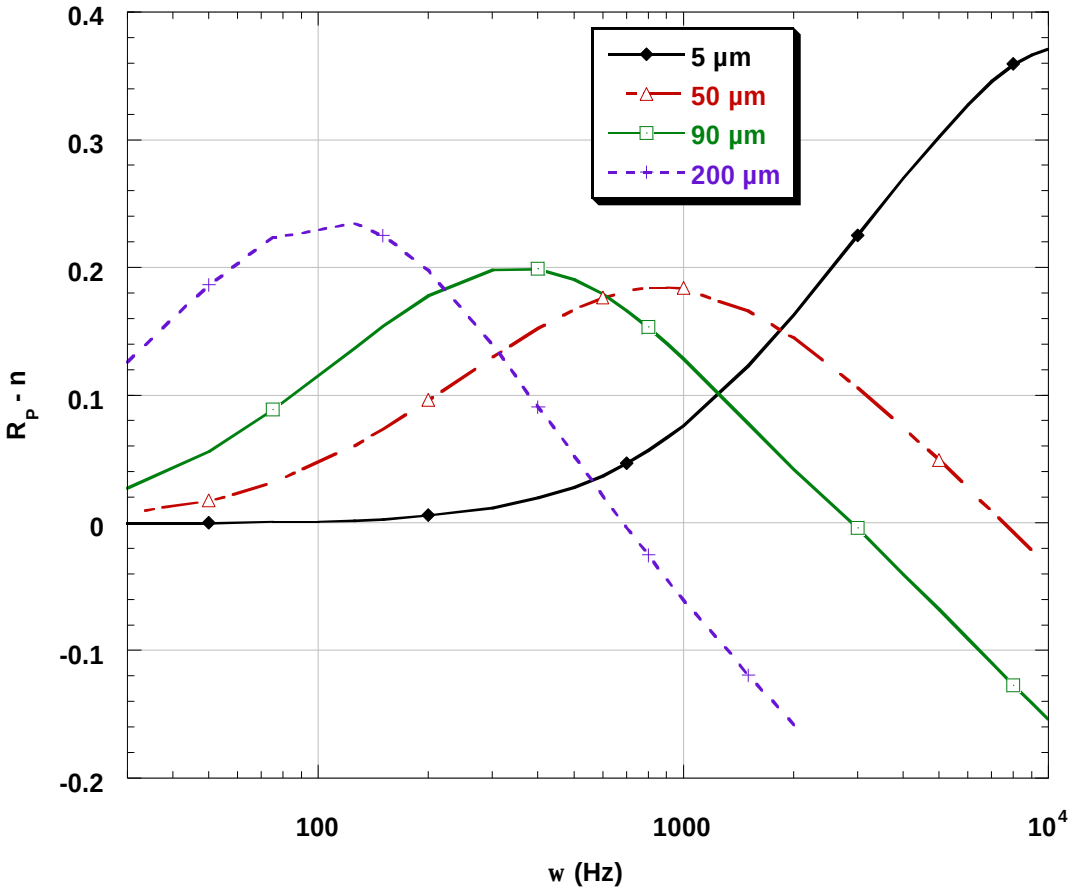

Figure 4.13: Normalized R_P Plot: Effect of AP Particle Diameter at 100 bar

5. Effect of Oscillation Amplitude

Nonlinear effects should show up most profoundly through the oscillation magnitude. In a linear system, the response to a harmonic input is itself harmonic, so the oscillation magnitude is completely irrelevant. In nonlinear systems, however, the response becomes "less harmonic" as the input magnitude goes up. Thus, one should see a definite trend of some sort as the driving pressure magnitude goes from 5% to 30%.

Figure 3.13 does not show much of a trend at all. There may be a simple explanation for its absence; the peak-average method of calculating R_P could be minimizing the nonlinear effects.

Again, the basic problem is that the definition of R_P is inherently linear, so any R_P taken from a nonlinear simulation will be somewhat contrived and arbitrary. The effect of oscillation amplitude could differ greatly, depending on the calculation method. For example, Figures 4.14 and 4.15 are plots of R_P vs. frequency for various oscillation magnitudes. The curves in Figure 4.14 come from method 4, where $\bar{r}$ is the steady-state burning rate and r' is the maximum *positive* change in burning rate over the course of one oscillation. The curves in Figure 4.15 come from method 5, where $\bar{r}$ is also the steady-state burning rate, but r' is the maximum *negative* change in burning rate. They both show a relatively high dependence on oscillation magnitude compared to Figure 3.13. Oddly enough, the trends in Figures 4.14 and 4.15 are reversed. In Figure 4.14, increasing oscillation magnitude diminishes the response peak. In Figure 4.15, it is the opposite.

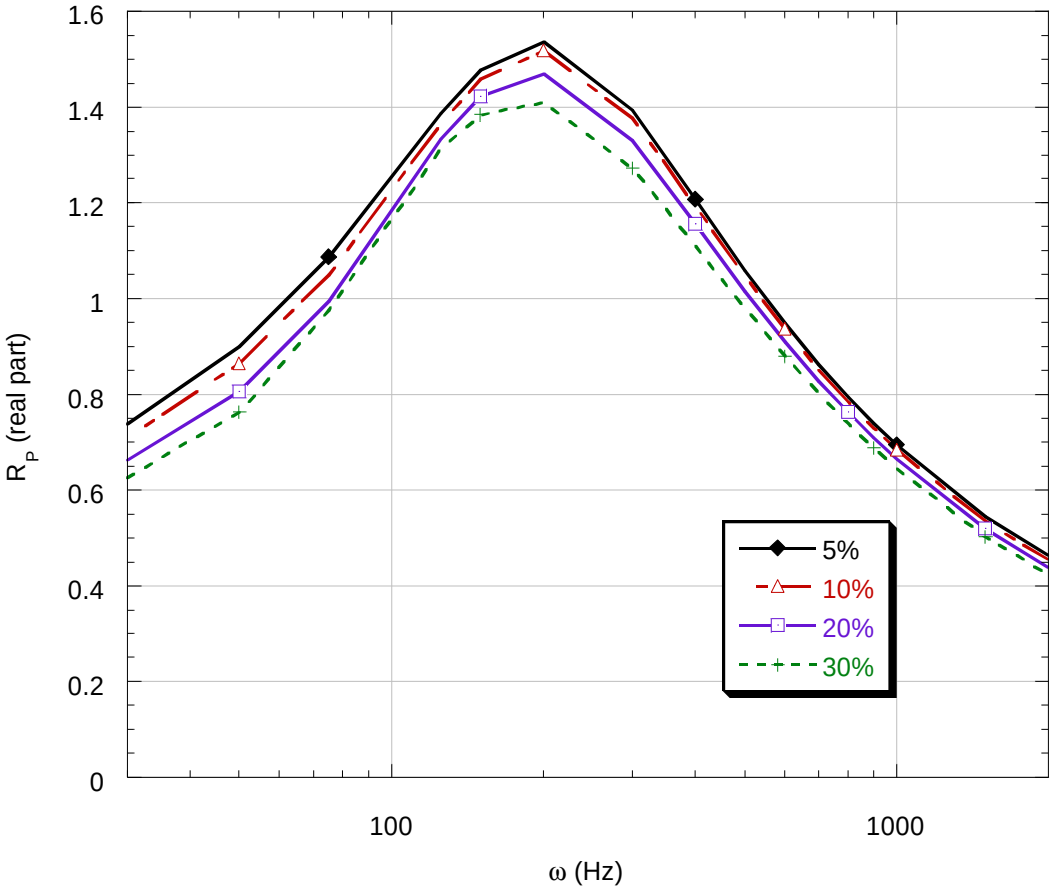

Figure 4.14: Effect of Oscillation Magnitude on R_P Revisited: Method 4

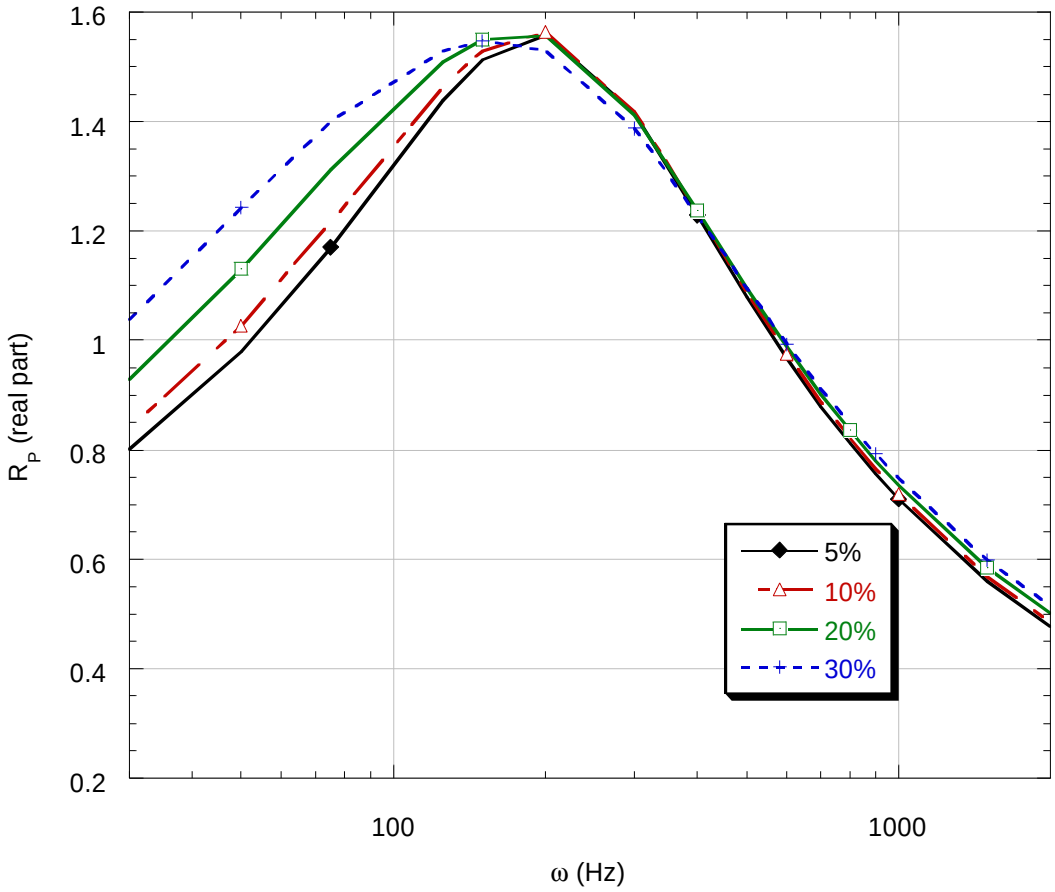

Figure 4.15: Effect of Oscillation Magnitude on R_P Revisited: Method 5

Chapter V

SUMMARY AND CONCLUSIONS

A. Steady-state

In general, the steady-state predictions seem to match the available experimental data very well. Figures 2.5 and 2.6 show that the theoretical predictions are usually within 10% of experimental measurements done at ONERA on a class of mono-modal propellants. Temperature sensitivity data are sparse and not very accurate anyway, so it would be difficult to compare Figure 2.7 to any real propellants. Work is ongoing in this area.

There is a problem, however, in comparing theoretical predictions to experimental data. The chemical properties of HTPB can vary widely, depending on the manufacturer, curative, cure cycle, etc. The molecular weight, for example, can vary from under 1200 gm/mol to over 5500 gm/mol[39]. There is no guarantee that the properties of HTPB used here, which are based on French HTPB, will correspond to HTPB manufactured in the U.S. or anywhere else. The model might require completely different values in Table 2.2, given a different type of binder.

Regardless of these issues, the steady-state part of the model certainly does seem to return excellent results. Although the model may still be mimicking nature with unrealistic parameters rather than solid theoretical reasoning, it seems at least to pass all the obvious checks. As the model makes more steady-state predictions that seem reasonable, it gains credibility. Only further experimentation and validation will tell.

In summary, some of the most important conclusions from the steady-state model are as follows:

- Propellants with smaller AP particle diameters typically burn faster. This is probably due to the lessening effect of the diffusion flame.

- Higher AP mass percentages induce faster burning rates as well.
- Predicted temperature sensitivity, s_P, is on the order of 0.002 K^{-1}, a reasonable value for AP/HTPB, mono-modal composites.
- The model predicts that propellants with larger AP particle diameters will have higher values of s_P at lower pressure, but the effect is not pronounced.

B. Nonsteady-State

The nonsteady regime, in contrast to the steady state, is less encouraging. By far, the most troubling aspect of the nonsteady model is the apparent over-dependence of flame heat feedback on the burning rates. Although the assumption of a solely pressure-dependent gas phase will produce results, this is an unsatisfactory approximation. Models are supposed to grow more accurate with fewer assumptions, not less accurate, and it does seem odd that a more realistic model leads to less realistic results. Some of the most important conclusions from the nonsteady model results are as follows:

- Faster burning propellants typically have a pressure-coupled frequency-response peak at higher frequencies of pressure oscillations. Also, their frequency-response peaks are of lower amplitude.
- The pressure exponent of the propellant tends to shift the R_P curve up or down.
- One exception to the above rules is that propellants with extremely fine AP particle diameters tend to demonstrate a high frequency response. The diffusion flame, or lack thereof, may be responsible for this observed effect.
- Pressure oscillation amplitude has very little effect on frequency response. R_P has an ambiguous definition in nonlinear models, however, so this result may not be too meaningful.

C. Recommendations

The next few paragraphs are recommendations for future work and study in the area of composite propellant combustion modeling.

First, it should be possible to either “fix” the nonsteady model so that it returns higher response amplitudes with full calculation or develop a phenomenological explanation of why

BDP-type models such as these are fundamentally unable to predict reasonable response amplitudes.

Second, future models should include the effect of additives, such as the ubiquitous aluminum. Many researchers have been working on the "aluminum problem" for some time, so this is not going to be an easy feat.

Third, the model should eventually include the effect of multi-modal propellants. Mono-modal propellants are rare in practical motors because of the limited AP mass percentage, so if theoretical models such as the one in this thesis are to exhibit any practical use, they must eventually describe propellants with multiple oxidizer particle diameters.

Fourth, as a philosophical recommendation, researchers should continue to do theoretical modeling because it is a worthy scientific endeavor. Experimental research is an excellent way to catalogue observed physical phenomena and indeed is absolutely essential for scientific progress. Theory, however, contributes to the understanding of physical phenomena, as opposed to the classification of it. This alone makes theory valuable, even if it has no immediate application.

APPENDICES

APPENDIX A

Steady-State Model

The following pages are a direct copy from a Mathcad 7.0.3 sheet. This Appendix contains a version of the steady-state model, shown immediately after a sample calculation.

The sheet is a solution of the system of simultaneous equations that comprise a model of steady-state, composite solid propellant burning. Sheet written by Bryan Rasmussen. bryanras@mae.uah.edu

Get the parameters that represent the particular type of propellant, and the floating parameters.

$$\begin{bmatrix} \alpha_{ap} \\ D_{ap} \\ T_i \\ A_r \\ A_{diff} \\ k \\ A_{g.ap} \\ C_1 \\ C_2 \end{bmatrix} := \begin{bmatrix} 0.80 \\ 90\cdot10^{-6} \\ 298 \\ 8\cdot10^{-5} \\ 10 \\ 2.0 \\ 8\cdot10^{-6} \\ 30 \\ 0.075 \end{bmatrix} \quad defined := \begin{bmatrix} \alpha_{ap} \\ D_{ap} \\ T_i \\ A_r \\ A_{diff} \\ k \\ A_{g.ap} \\ C_1 \\ C_2 \end{bmatrix}$$

Get the pressure. Convert to Pa.

PP := C:\..\pressure.txt

$PP := PP\cdot10^5$

$ii := 0..rows(PP) - 1$

Write the floating parameters to a file for reference.

defined := C:\..\defined.txt

defined

Get the guess values and the previous answer.

guesses := C:\..\guess.txt

prev := C:\..\steadout.txt

$jj := 0..rows(prev) - 1$

Get the experimental data.

fiveμmexp := C:\..\5micexp.txt

ninetyμmexp := C:\..\90micexp.txt

Energy required to vaporize AP is the energy required to force a crystalline phase transition in AP, plus the energy to turn it into a gas. Negative indicates endothermic. The Q_{vap} is a median estimate based on 70% degradation, and 30% sublimation.

$q_{tr} := -87780$ $q_{vap} := 5.1 \cdot 10^5$ $q_{v.ap} := q_{tr} + q_{vap}$ $q_{v.ap} = 4.222 \cdot 10^5$

Energy required to gassify HTPB: $q_{v.b} := -2 \cdot 10^5$ Gas constant: $R := 8.314$

Define the solid-phase specific heats. $T_{tr} := 513$

$C_{or.a} := 1.717$ $C_{or.b} := 586.15$ $C_{cu.a} := 1.717$ $C_{cu.b} := 669.9$ $C_{b.a} := 3.559$ $C_{b.b} := 1047$

$C_{p.or}(T) := C_{or.a} \cdot T + C_{or.b}$ $C_{p.cu}(T) := C_{cu.a} \cdot T + C_{cu.b}$ $C_{p.s.b}(T) := C_{b.a} \cdot T + C_{b.b}$

$$C_{p.s.ap}(T) := \text{if}\left(T < T_{tr}, C_{p.or}(T), C_{p.cu}(T)\right)$$

Define the gas phase specific heats. $C_{p.g.ap} := 1254$ $C_{p.g.b} := 2100$

Reference temperature for constant thermal properties:

$T_{ref} := 500$

Give the thermal conductivity of the gaseous AP, HTPB, and total propellant. This comes from TEP calculations.

$\lambda_{g.p.a} := 1.08 \cdot 10^{-4}$ $\lambda_{g.p.b} := 0.0133$ $\lambda_{g.ap.a} := 7.2 \cdot 10^{-5}$ $\lambda_{g.ap.b} := 6 \cdot 10^{-3}$ $\lambda_{g.b.a} := 4.33 \cdot 10^{-4}$ $\lambda_{g.b.b} := -0.15$

$\lambda_{g.p}(T) := \lambda_{g.p.a} \cdot T + \lambda_{g.p.b}$ $\lambda_{g.ap}(T) := \lambda_{g.ap.a} \cdot T + \lambda_{g.ap.b}$ $\lambda_{g.b}(T) := \lambda_{g.b.a} \cdot T + \lambda_{g.b.b}$

Solid-phase density: $\rho_{ap} := 1950$ $\rho_b := 920$

Pyrolysis parameters for AP come from an average of the ONERA paper and the original BDP paper. Pyrolysis parameters for HTPB come from an average of various values in the literature, mostly Chen & Brill.

$A_{s.ap} := 9.6 \cdot 10^5$ $E_{s.ap} := 9 \cdot 10^4$ $A_{s.b} := e^{3.1} \cdot 10^{-3} \cdot 60 \cdot \rho_b$ $A_{s.b} = 1.225 \cdot 10^3$ $E_{s.b} := 3.43 \cdot 10^4$

For the reaction flame heights (of AP and of the entire propellant) we have the following parameters:

$E_{g.ap} := 62800$ $E_r := 125600$

We need an exponential factor to determine how fast the temperature climbs above the surface. In the original ONERA paper, the assumed factor was 1, but I don't think that's realistic. Call this factor ν, just to be an effete snob about it. Moreover, let ν_b be a factor between the surface of binder and x = ∞, let ν_{ap} be a factor between the surface of the oxidizer and the ap flame standoff (x_{ap}), and let $\nu_{f.ap}$ be the factor from x_{ap} to x = ∞.

$$\nu_b := 2.5 \qquad \nu_{ap} := 2.5 \qquad \nu_{f.ap} := 2.5$$

The diffusion constant below corresponds to 0.16cm²/sec at room temperature and pressure, with the diffusion relationship is as published in the original BDP paper and the ONERA report. Assume that the molecular weight of the combustion products is relatively constant.

$$D_0 := 7.585 \cdot 10^{-5} \qquad M := 0.0262$$

The published relationship is $D_{diff} := D_0 \cdot \frac{T^{1.75}}{P}$

Get the density and specific heat of the propellant (at T = T_i). This may be a measured quantity, or it could be based on volumetric fractions.

$$C_{p.s.p} := \frac{C_{p.s.ap}(T_i) \cdot \alpha_{ap} \cdot \rho_b + C_{p.s.b}(T_i) \cdot (1 - \alpha_{ap}) \cdot \rho_{ap}}{\alpha_{ap} \cdot \rho_b + (1 - \alpha_{ap}) \cdot \rho_{ap}} \qquad \rho_p := \frac{1}{\frac{\alpha_{ap}}{\rho_{ap}} + \frac{(1 - \alpha_{ap})}{\rho_b}}$$

From the mass fraction of ammonium perchlorate, figure out the flame properties. The following is just an interpolation to a thermoequilibrium code. This assumes that the values q_f, T_f, and $C_{p,g}$ are functions of percentage of AP only.

$$C_{vec} := \begin{matrix} \alpha & q_f & T_f & C_{p,g} \end{matrix} \begin{bmatrix} 0.73 & 2.07 \cdot 10^6 & 1587 & 2870 \\ 0.77 & 2.63 \cdot 10^6 & 1996 & 2292 \\ 0.80 & 3.01 \cdot 10^6 & 2309 & 2091 \\ 0.82 & 3.25 \cdot 10^6 & 2520 & 1991 \\ 0.874 & 3.63 \cdot 10^6 & 2993 & 1787 \end{bmatrix}$$

$$q_{vs} := \text{regress}(C_{vec}^{\langle 0 \rangle}, C_{vec}^{\langle 1 \rangle}, 4) \qquad Cvs := \text{regress}(C_{vec}^{\langle 0 \rangle}, C_{vec}^{\langle 3 \rangle}, 4)$$

$$q_f := \text{interp}(q_{vs}, C_{vec}^{\langle 0 \rangle}, C_{vec}^{\langle 1 \rangle}, \alpha_{ap}) \qquad C_{p.g.p} := \text{interp}(Cvs, C_{vec}^{\langle 0 \rangle}, C_{vec}^{\langle 3 \rangle}, \alpha_{ap})$$

$$Tvs := \text{regress}(C_{vec}^{\langle 0 \rangle}, C_{vec}^{\langle 2 \rangle}, 4)$$

$$T_f := \text{interp}(Tvs, C_{vec}^{\langle 0 \rangle}, C_{vec}^{\langle 2 \rangle}, \alpha_{ap}) \qquad T_f := T_f + (T_i - 298) \cdot \frac{C_{p.s.p}}{C_{p.g.p}}$$

$C_{p.s.p} = 1.448 \cdot 10^3$ $C_{p.g.p} = 2.091 \cdot 10^3$ $q_f = 3.01 \cdot 10^6$ $\rho_p = 1.593 \cdot 10^3$ $T_f = 2.309 \cdot 10^3$

Define an equation for the characteristic diameter of an AP crystal.

$$D^*_{ap}(D_{ap}, G_{ap}, G_p) := \frac{2 \cdot D_{ap}}{\sqrt{6 \cdot \frac{\rho_p \cdot G_{ap}}{\rho_{ap} \cdot G_p}}}$$

Define the equation for reaction flame height to make things simpler.

$$x_r(G_p, P) := \frac{G_p}{P^2 \cdot A_r \cdot e^{\left(\frac{-E_r}{R \cdot T_f}\right)}} \cdot 10^6$$

$TOL \equiv 1 \cdot 10^{-6}$

Solve the equations: GIVEN

Algebraic solution of general mass flow rate given the individual mass flow rates of the components:

$$G_p = \frac{1}{\frac{\alpha_{ap}}{G_{ap}} + \frac{1 - \alpha_{ap}}{G_b}}$$

The mass flow rate comes from pyrolysis relationships:

$$G_b = A_{s.b} \cdot e^{\left(\frac{-E_{s.b}}{R \cdot T_{s.b}}\right)} \qquad G_{ap} = A_{s.ap} \cdot e^{\left(\frac{-E_{s.ap}}{R \cdot T_{s.ap}}\right)}$$

The height of the premixed AP flame is related to the inverse square of the pressure.

$$x_{f.ap} = \frac{G_{ap}}{P^2 \cdot A_{g.ap} \cdot e^{\left(\frac{-E_{g.ap}}{R \cdot T_{f.ap}}\right)}} \cdot 10^6$$

Total Flame Height:

$$x_f = G_p \cdot \left[\frac{D^*_{ap}\left(D_{ap}, G_{ap}, G_p\right)^2}{A_{diff} \cdot \left[D_0 \cdot T_{f.ap}^{0.75} \cdot \frac{M}{R} + k \cdot G_p \cdot D^*_{ap}\left(D_{ap}, G_{ap}, G_p\right) \cdot \left[\operatorname{atan}\left(C_1 \cdot C_2\right) + \operatorname{atan}\left[\left(\frac{1}{x_r\left(G_p, P\right)} - C_1 \right) \cdot C_2 \right] \right] \right]} \right] \cdot 10^6 \ldots$$
$$+ x_r\left(G_p, P\right)$$

The final three equations are energy balances.

In the binder:

$$T_{s.b} = \frac{G_b \cdot C_{p.s.b}\left(T_{ref}\right) \cdot T_i + \frac{\lambda_{g.b}\left(T_{s.b}\right) \cdot T_f \cdot \nu_b}{x_f \cdot 10^{-6}} + G_b \cdot q_{v.b}}{G_b \cdot C_{p.s.b}\left(T_{ref}\right) + \frac{\lambda_{g.b}\left(T_{s.b}\right) \cdot \nu_b}{x_f \cdot 10^{-6}}}$$

In the oxidizer:

$$T_{s.ap} = \frac{G_{ap} \cdot C_{p.s.ap}\left(T_{ref}\right) \cdot T_i + \frac{\lambda_{g.ap}\left(T_{s.ap}\right) \cdot T_{f.ap} \cdot \nu_{ap}}{x_{f.ap} \cdot 10^{-6}} + G_{ap} \cdot q_{v.ap}}{G_{ap} \cdot C_{p.s.ap}\left(T_{ref}\right) + \frac{\lambda_{g.ap}\left(T_{s.ap}\right) \cdot \nu_{ap}}{x_{f.ap} \cdot 10^{-6}}}$$

Above the oxidizer, above x_{ap}:

$$T_{f.ap} = T_f - \frac{G_p \cdot q_f}{G_p \cdot C_{p.g.p} + \frac{\nu_{f.ap} \cdot \lambda_{g.p}\left(T_{f.ap}\right)}{\left(x_f - x_{f.ap}\right) \cdot 10^{-6}}}$$

And we solve as a function of four different variables.

$$\text{steady}\left(P, G_p, G_{ap}, G_b, x_f, x_{f.ap}, T_{s.b}, T_{s.ap}, T_{f.ap}\right) := \text{find}\left(G_p, G_{ap}, G_b, x_f, x_{f.ap}, T_{s.b}, T_{s.ap}, T_{f.ap}\right)$$

Solve it over the entire range of pressures. Use the programming loop for error returns.

$$
\begin{aligned}
sol := \;& \text{for } jj \in 0..7 \\
& \quad sol_{jj,0} \leftarrow \left(guesses^{T}\right)_{jj+2} \\
& \text{for } jj \in 1..rows(PP) \\
& \quad \text{on error } sol^{\langle jj \rangle} \leftarrow steady\left(PP_{jj-1}, sol_{0,jj-1}, sol_{1,jj-1}, sol_{2,jj-1}, sol_{3,jj-1}, sol_{4,jj-1}, sol_{5,jj-1}, sol_{6,jj-1}, sol_{7,jj-1}\right) \\
& \qquad sol \leftarrow submatrix(sol, 0, rows(sol)-1, 1, cols(sol)-1)^{T} \\
& \qquad \text{return } sol \\
& sol \leftarrow submatrix(sol, 0, rows(sol)-1, 1, cols(sol)-1)^{T}
\end{aligned}
$$

Fill in the blanks.

If the solution failed at some point, then the number of rows in PP will be larger than the number of rows in sol.

$ii := 0..rows(sol) - 1$

$kk := 0..7$

$ans_{ii,0} := PP_{ii}$ $\quad ans^{\langle 1 \rangle} := \dfrac{sol^{\langle 0 \rangle}}{\rho_p} \cdot 1000$ $\quad ans_{ii,10} := x_r\left(sol_{ii,0}, PP_{ii}\right)$

$ans_{ii,kk+2} := sol_{ii,kk}$

Make a bunch O' plots.

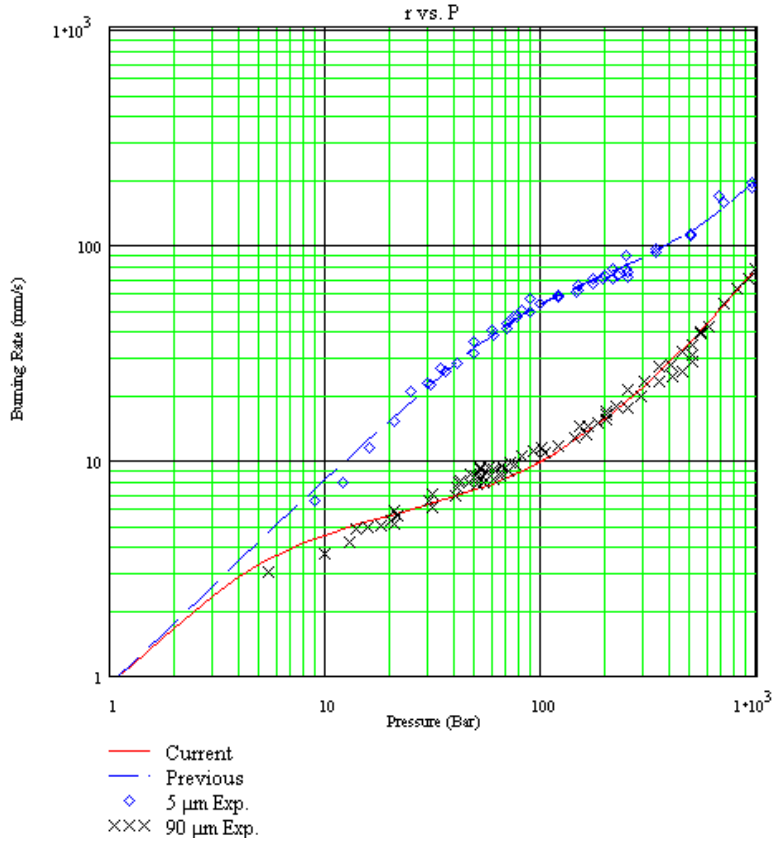

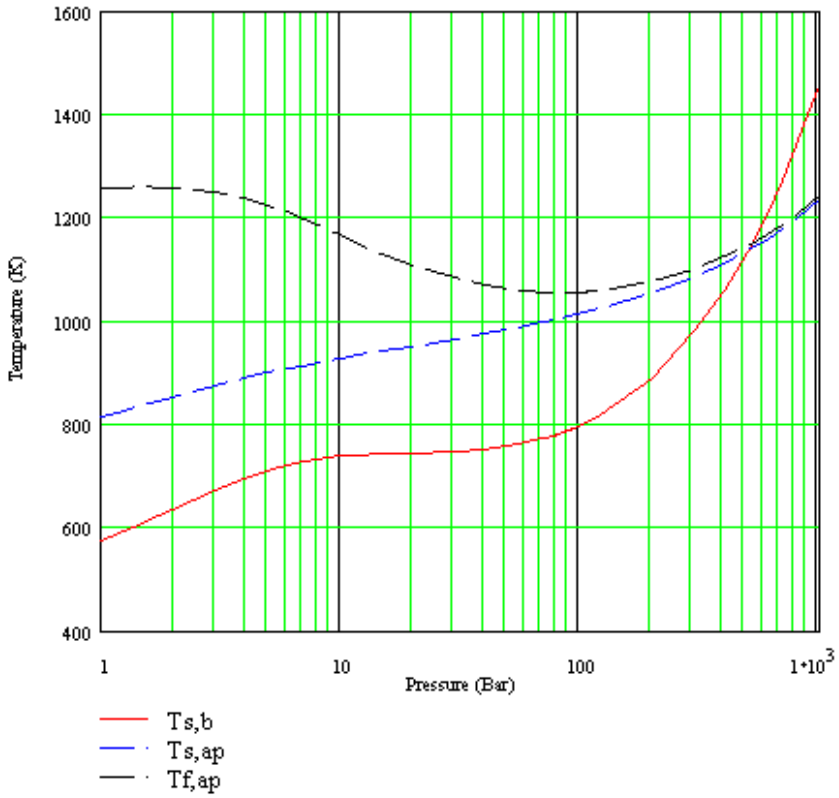
1600
1400
1200
1000
800
600
400
Temperature (K)
1
10
100
1*10^3
Pressure (Bar)
Ts,b
Ts,ap
Tf,ap

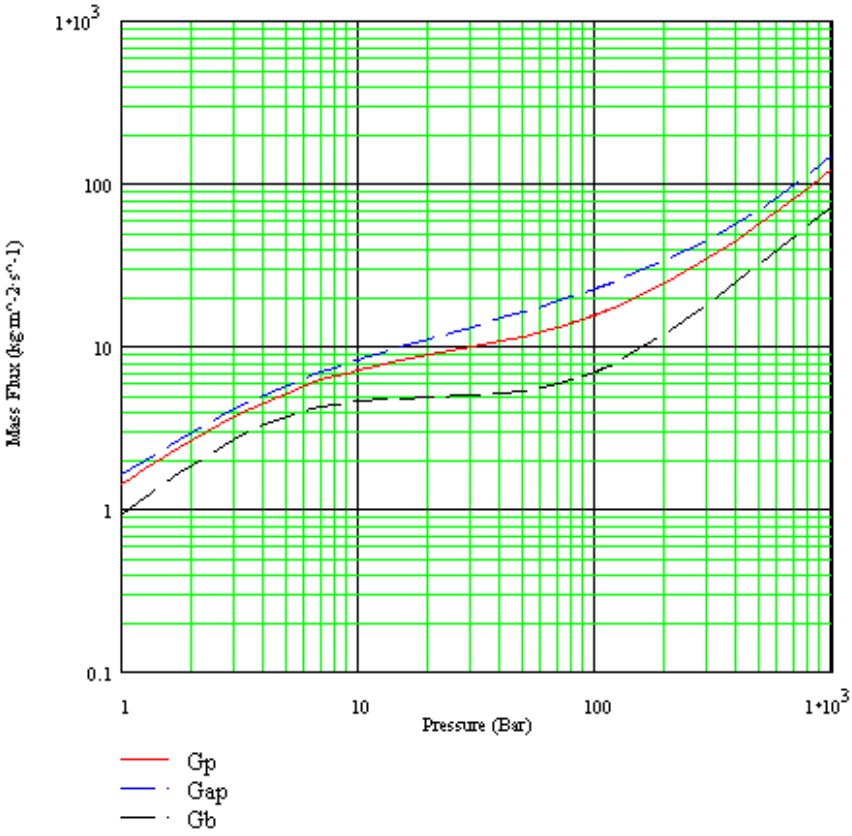
1*10^3
100
10
1
0.1
Mass Flux (kg·m^-2·s^-1)
1
10
100
1*10^3
Pressure (Bar)
Gp
Gap
Gb

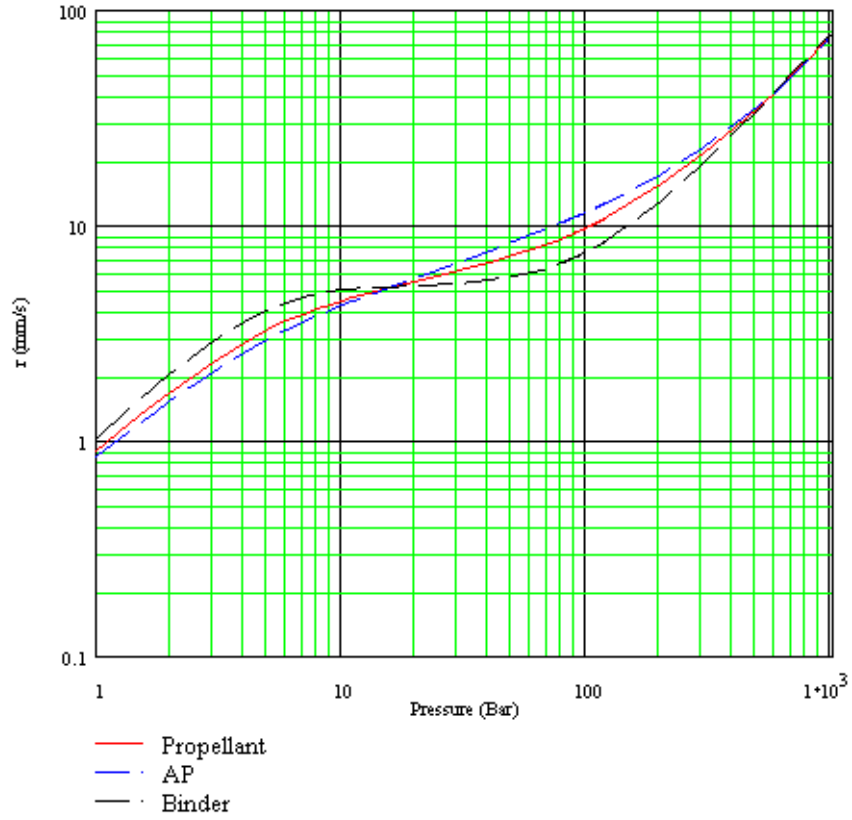
100
10
1
0.1
r (mm/s)
1
10
100
1·10^3
Pressure (Bar)
Propellant
AP
Binder

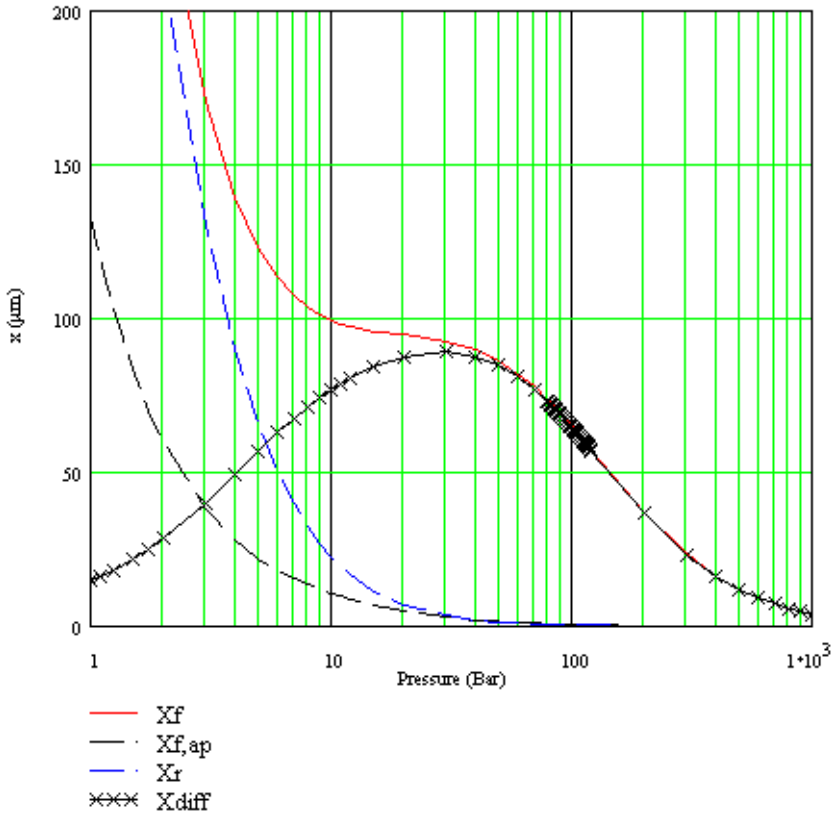
200
150
100
50
0
x (µm)
1
10
100
1·10^3
Pressure (Bar)
Xf
Xf,ap
Xr
Xdiff

Plot out the mass fractions. $V_{ap} := \alpha_{ap} \cdot \frac{\rho_p}{\rho_{ap}}$

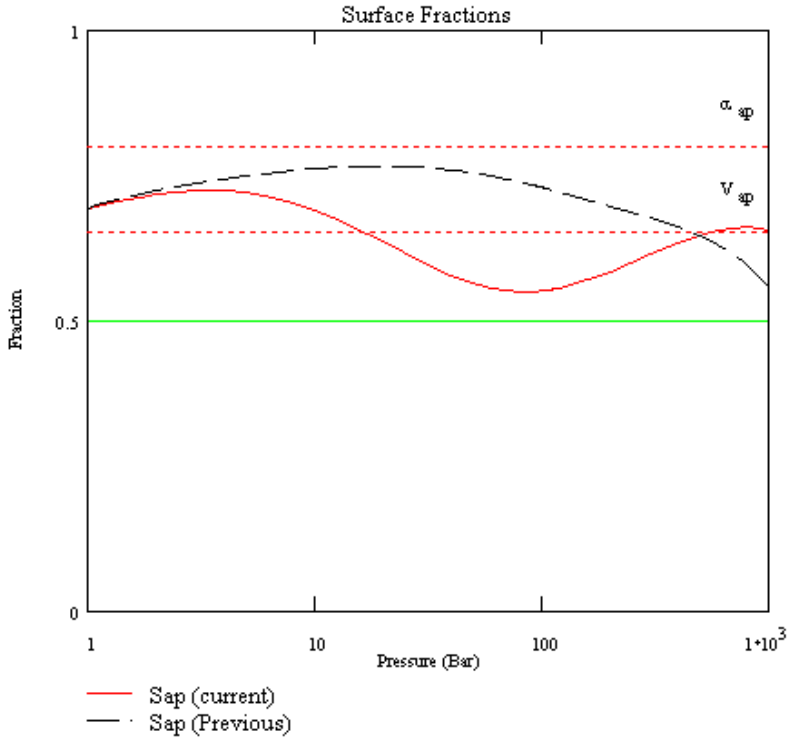

Put it all out to the file "steadout.txt".

C:\..\steadout.txt

ans

Put out all the material properties to a file for use by the "nonstead.mcd" file.

$$params := \begin{bmatrix} C_{p.s.p} & C_{p.g.p} & q_f & \rho_p & T_f & q_{v.ap} \\ q_{v.b} & q_{tr} & q_{vap} & C_{p.g.ap} & C_{p.g.b} & \rho_{ap} \\ \rho_b & A_{s.ap} & E_{s.ap} & A_{s.b} & E_{s.b} & E_{g.ap} \\ E_r & \nu_b & \nu_{ap} & \nu_{f.ap} & D_0 & M \\ \lambda_{g.b.a} & \lambda_{g.b.b} & \lambda_{g.ap.a} & \lambda_{g.ap.b} & \lambda_{g.p.a} & \lambda_{g.p.b} \\ C_{b.a} & C_{b.b} & C_{cu.a} & C_{cu.b} & C_{or.a} & C_{or.b} \\ T_{tr} & T_{ref} & 0 & 0 & 0 & 0 \end{bmatrix}$$

C:\..\params.txt

params

APPENDIX B

Nonsteady-State Model

The following pages are a direct copy from a Mathcad 7.0.3 sheet. This Appendix contains a version of the nonsteady-state model, shown immediately after a sample calculation.

God, I hope this works. Bryan Rasmussen- bryan@rasmussen.org

Get the steady-state data. steadat := C:\..\steadout.txt TOL≡1·10^-6

Enter the mean pressure: $P_{bar} := 10 \cdot 10^5$

Get the defined properties (user-defined and floating params).

defs := C:\..\defined.txt

Enter the oscillation magnitude (Pa): $mag := 0.2 \cdot P_{bar}$

Parse the steady-state data to get the steady-state information. Use a cubic spline fit to the steady state data.

$ii := 0 .. cols(steadat) - 1 \qquad spliner_{ii} := cspline(steadat^{\langle 0 \rangle}, steadat^{\langle ii \rangle})$

$$bar(P) := \left| \begin{array}{l} bar_0 \leftarrow P \\ \text{for } kk \in 1 .. cols(steadat) - 1 \\ \quad bar_{kk} \leftarrow interp(spliner_{kk}, steadat^{\langle 0 \rangle}, steadat^{\langle kk \rangle}, P) \\ bar \end{array} \right.$$

$$\begin{bmatrix} P_{bar} \\ r_{bar} \\ G_{p.bar} \\ G_{ap.bar} \\ G_{b.bar} \\ x_{f.bar} \\ x_{f.ap.bar} \\ T_{s.b.bar} \\ T_{s.ap.bar} \\ T_{f.ap.bar} \\ x_{r.bar} \end{bmatrix} := bar(P_{bar}) = \begin{bmatrix} P_{bar} \\ r_{bar} \\ G_{p.bar} \\ G_{ap.bar} \\ G_{b.bar} \\ x_{f.bar} \\ x_{f.ap.bar} \\ T_{s.b.bar} \\ T_{s.ap.bar} \\ T_{f.ap.bar} \\ x_{r.bar} \end{bmatrix} = \begin{bmatrix} 1 \cdot 10^6 \\ 4.5035866212 \\ 7.1753413841 \\ 8.3169457925 \\ 4.6320920524 \\ 99.5753301407 \\ 10.7144593237 \\ 739.6208491409 \\ 928.6846994811 \\ 1.1678467202 \cdot 10^3 \\ 22.639652276 \end{bmatrix}$$

$$\begin{bmatrix} \alpha_{ap} \\ D_{ap} \\ T_i \\ A_r \\ A_{diff} \\ k \\ A_{g.ap} \\ C_1 \\ C_2 \end{bmatrix} := defs = \begin{bmatrix} \alpha_{ap} \\ D_{ap} \\ T_i \\ A_r \\ A_{diff} \\ k \\ A_{g.ap} \\ C_1 \\ C_2 \end{bmatrix} = \begin{bmatrix} 0.8 \\ 9 \cdot 10^{-5} \\ 298 \\ 2.2 \cdot 10^{-4} \\ 11 \\ 2 \\ 5 \cdot 10^{-4} \\ 30 \\ 0.075 \end{bmatrix}$$

$G_{p.bar} = 7.17534$

Get the propellant properties from what the steady-state program put out. Gas constant: $R := 8.314$

params :=

C:\..\params.txt

$$\begin{bmatrix} C_{p.s.p} & C_{p.g.p} & q_f & \rho_p & T_f & q_{v.ap} \\ q_{v.b} & q_{tr} & q_{vap} & C_{p.g.ap} & C_{p.g.b} & \rho_{ap} \\ \rho_b & A_{s.ap} & E_{s.ap} & A_{s.b} & E_{s.b} & E_{g.ap} \\ E_r & \nu_b & \nu_{ap} & \nu_{f.ap} & D_0 & M \\ \lambda_{g.b.a} & \lambda_{g.b.b} & \lambda_{g.ap.a} & \lambda_{g.ap.b} & \lambda_{g.p.a} & \lambda_{g.p.b} \\ C_{b.a} & C_{b.b} & C_{cu.a} & C_{cu.b} & C_{or.a} & C_{or.b} \\ T_{tr} & T_{ref} & dummy1 & dummy2 & dummy3 & dummy4 \end{bmatrix} := params$$

Define the thermal properties:

$\lambda_{s.b}(T) := T \cdot \left(5.443 \cdot 10^{-5}\right) + 0.184$

$\lambda_{s.b}(T_{ref}) = 0.211$

$\lambda_{s.ap}(T) := T \cdot \left(-3.852 \cdot 10^{-4}\right) + 0.628$

$\lambda_{s.ap}(T_{ref}) = 0.435$

$T_{ref} = 500$

$C_{p.or.ap}(T) := C_{or.a} \cdot T + C_{or.b}$ $C_{p.cu.ap}(T) := C_{cu.a} \cdot T + C_{cu.b}$ $C_{p.s.b}(T) := C_{b.a} \cdot T + C_{b.b}$

$C_{p.s.ap}(T) := \text{if}\left(T < T_{tr}, C_{p.or.ap}(T), C_{p.cu.ap}(T)\right)$

$d_b(T) := \dfrac{\lambda_{s.b}(T)}{\rho_b \cdot C_{p.s.b}(T)}$ $d_b(T_{ref}) = 8.122 \cdot 10^{-8}$

$d_{ap}(T) := \dfrac{\lambda_{s.ap}(T)}{\rho_{ap} \cdot C_{p.s.ap}(T)}$ $d_{ap}(T_{ref}) = 1.546 \cdot 10^{-7}$

Gas-phase: $\lambda_{g.ap}(T) := \lambda_{g.ap.a} \cdot T + \lambda_{g.ap.b}$ $\lambda_{g.b}(T) := \lambda_{g.b.a} \cdot T + \lambda_{g.b.b}$

$\lambda_{g.p}(T) := \lambda_{g.p.a} \cdot T + \lambda_{g.p.b}$

Get the steady-state temperature profile in the binder and the AP.

Define the points for integration. Split it up into "points" different points stretching from the surface to the AP particle radius. Moreover, use a Δx that decreases exponentially near the surface.

Run out the profile until the temperature is nearly T_i.

$deep := -1500 \cdot 10^{-6}$ $\nu_{xx} := 0.12$

$points \equiv 100$ $ii := 0 .. points - 1$ $xx_{ii} := deep \cdot e^{(ii+1-points)\cdot \nu_{xx}} - deep \cdot e^{-\nu_{xx}\cdot(points-1)}$

Generate the x-steps for use in the integral.

$\Delta x_0 := \frac{xx_0 - xx_1}{2}$ $jj := 1 .. points - 2$ $\Delta x_{jj} := \frac{xx_{jj-1} - xx_{jj+1}}{2}$ $\Delta x_{points-1} := \frac{xx_{points-2} - xx_{points-1}}{2}$

Lay out the temperature profile in the binder and AP and plot it.

$Tprof_{b.bar_{ii}} := T_i + \left(T_{s.b.bar} - T_i\right) \cdot e^{\frac{\left(xx_{ii} \cdot G_{b.bar}\right)}{d_b \left(T_{ref}\right) \cdot \rho_b}}$ $Tprof_{ap.bar_{ii}} := T_i + \left(T_{s.ap.bar} - T_i\right) \cdot e^{\frac{\left(xx_{ii} \cdot G_{ap.bar}\right)}{\rho_{ap} \cdot d_{ap}\left(T_{ref}\right)}}$

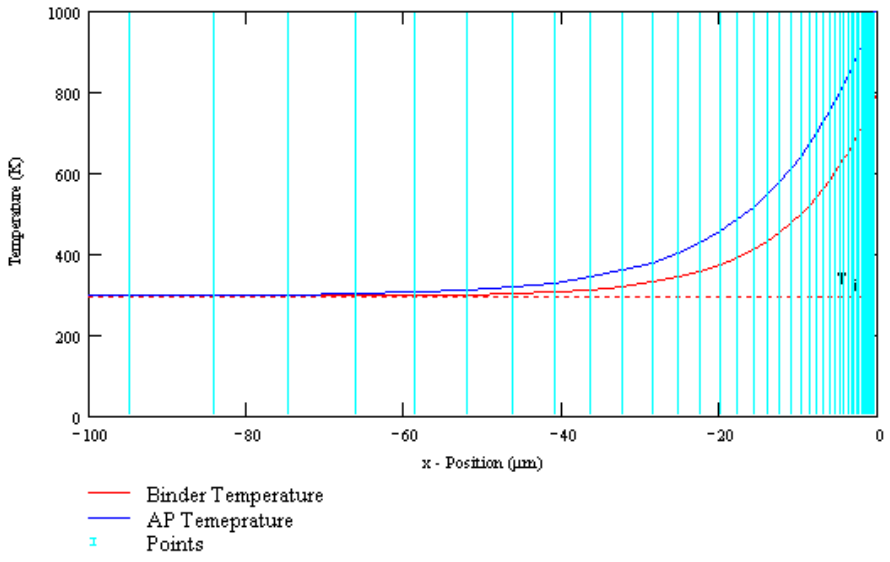

Get the time step size.

Get an approximate characteristic response time for the system.

$$\tau_{min} := \min\left(\left[\frac{d_b\langle T_{ref}\rangle \cdot \rho_b^{\,2}}{G_{b.bar}^{\,2}} \quad \frac{d_{ap}\langle T_{ref}\rangle \cdot \rho_{ap}^{\,2}}{G_{ap.bar}^{\,2}}\right]\right) \qquad \tau_{min} = 1.135 \cdot 10^{-3}$$

$$\tau_{max} := \max\left(\left[\frac{d_b\langle T_{ref}\rangle \cdot \rho_b^{\,2}}{G_{b.bar}^{\,2}} \quad \frac{d_{ap}\langle T_{ref}\rangle \cdot \rho_{ap}^{\,2}}{G_{ap.bar}^{\,2}}\right]\right) \qquad \tau_{max} = 1.4 \cdot 10^{-3}$$

$\Delta t \equiv 8 \cdot 10^{-6}$

$\Delta t = 8 \cdot 10^{-6}$

Enter some preliminary functions that we will use in the main "loop" of problem solving. The idea is to reduce the system of eight equations to a system of four equations through simple algebra.

Reaction flame height:

$$x_r\langle T_{s.ap}, T_{s.b}, P\rangle := \frac{10^6}{\left[P^2 \cdot A_r \cdot e^{\left(\frac{-E_r}{R \cdot T_f}\right)}\right] \cdot \left[\frac{\alpha_{ap}}{A_{s.ap} \cdot e^{\left(\frac{-E_{s.ap}}{R \cdot T_{s.ap}}\right)}} + \frac{1 - \alpha_{ap}}{A_{s.b} \cdot e^{\left(\frac{-E_{s.b}}{R \cdot T_{s.b}}\right)}}\right]}$$

$$x_r\langle T_{s.ap}, T_{s.b}, P\rangle := \text{interp}\left(\text{spliner}_{10}, \text{steadat}^{\langle 0\rangle}, \text{steadat}^{\langle 10\rangle}, P\right)$$

AP mass flux:

$$G_{ap}\langle T_{s.ap}\rangle := A_{s.ap} \cdot e^{\left(\frac{-E_{s.ap}}{R \cdot T_{s.ap}}\right)}$$

Binder mass flux:

$$G_b\langle T_{s.b}\rangle := A_{s.b} \cdot e^{\left(\frac{-E_{s.b}}{R \cdot T_{s.b}}\right)}$$

Total mass flux:

$$G_p\langle T_{s.ap}, T_{s.b}\rangle := \frac{1}{\frac{\alpha_{ap}}{A_{s.ap} \cdot e^{\left(\frac{-E_{s.ap}}{R \cdot T_{s.ap}}\right)}} + \frac{1 - \alpha_{ap}}{A_{s.b} \cdot e^{\left(\frac{-E_{s.b}}{R \cdot T_{s.b}}\right)}}}$$

AP Flame height:

$$x_{f.ap}\langle P, T_{s.ap}, T_{f.ap}\rangle := \frac{A_{s.ap} \cdot e^{\left(\frac{-E_{s.ap}}{R \cdot T_{s.ap}}\right)}}{P^2 \cdot A_{g.ap} \cdot e^{\left(\frac{-E_{g.ap}}{R \cdot T_{f.ap}}\right)}} \cdot 10^6$$

$$x_{f.ap}\langle P, T_{s.ap}, T_{f.ap}\rangle := \text{interp}\left(\text{spliner}_6, \text{steadat}^{\langle 0\rangle}, \text{steadat}^{\langle 6\rangle}, P\right)$$

Characteristic diameter of an AP crystal.

$$D^*_{ap}\left(D_{ap}, T_{s.ap}, T_{s.b}\right) := \frac{2 \cdot D_{ap}}{\sqrt{6 \cdot \frac{\rho_p \cdot \left[\alpha_{ap} + \frac{\left(1 - \alpha_{ap}\right) \cdot \left[A_{s.ap} \cdot e^{\left(\frac{-E_{s.ap}}{R \cdot T_{s.ap}}\right)}\right]}{A_{s.b} \cdot e^{\left(\frac{-E_{s.b}}{R \cdot T_{s.b}}\right)}}\right]}{\rho_{ap}}}}$$

This is a little routine for finding the solution of a tri-diagonal matrix system. It is a modification of the example in *Numerical Recipes*. A is the "left diagonal", B is the main diagonal, and C is the "right diagonal".

$$\begin{aligned}
&\text{mtridiag}(A, B, C, v) := \left|\begin{array}{l}
\beta \leftarrow B_0 \\
U_0 \leftarrow \frac{v_0}{\beta} \\
\text{for } kk \in 1 .. \text{points} - 1 \\
\quad \left|\begin{array}{l}
\gamma_{kk} \leftarrow \frac{C_{kk-1}}{\beta} \\
\beta \leftarrow B_{kk} - A_{kk} \cdot \gamma_{kk} \\
U_{kk} \leftarrow \frac{v_{kk} - A_{kk} \cdot U_{kk-1}}{\beta}
\end{array}\right. \\
\text{for } kk \in \text{points} - 2, \text{points} - 3 .. 1 \\
\quad U_{kk} \leftarrow U_{kk} - \gamma_{kk+1} \cdot U_{kk+1} \\
U
\end{array}\right.
\end{aligned}$$

Replaced by C function "tridiag". 1 Nov. 98.

This is the program for calculating a new temperature profile, given the previous temperature profile, new surface temperature, and mass flux. It uses the tridiag function to do the linear solution.

Note: v= Solution vector

$$
\begin{aligned}
&mnp\left(Tprof, T_s, r, r_\pi, d, \Delta t, xx\right) := \\
&\quad v_0 \leftarrow T_s \\
&\quad v_{points-1} \leftarrow Tprof_{points-1} \\
&\quad A_{points-1} \leftarrow \left[C_{points-1} \leftarrow \left\langle C_0 \leftarrow 0 \right\rangle\right] \\
&\quad B_{points-1} \leftarrow \left\langle B_0 \leftarrow 1 \right\rangle \\
&\quad \text{for } kk \in 1..points-2 \\
&\qquad delx \leftarrow xx_{kk-1} - xx_{kk+1} \\
&\qquad v_{kk} \leftarrow \frac{d}{delx}\cdot\left(\frac{Tprof_{kk-1} - Tprof_{kk}}{xx_{kk-1} - xx_{kk}} - \frac{Tprof_{kk} - Tprof_{kk+1}}{xx_{kk} - xx_{kk+1}}\right) \ldots \\
&\qquad\quad + \frac{Tprof_{kk}}{\Delta t} - \frac{r_\pi}{2\cdot delx}\cdot\left\langle Tprof_{kk-1} - Tprof_{kk+1}\right\rangle \\
&\qquad A_{kk} \leftarrow \frac{r}{2\cdot delx} - \frac{d}{\left\langle xx_{kk-1} - xx_{kk}\right\rangle \cdot delx} \\
&\qquad B_{kk} \leftarrow \frac{1}{\Delta t} + \frac{d}{delx}\cdot\left(\frac{1}{xx_{kk-1} - xx_{kk}} + \frac{1}{xx_{kk} - xx_{kk+1}}\right) \\
&\qquad C_{kk} \leftarrow \frac{-r}{2\cdot delx} - \frac{d}{\left\langle xx_{kk} - xx_{kk+1}\right\rangle \cdot delx} \\
&\quad np \leftarrow mtridiag(A, B, C, v) \\
&\quad np
\end{aligned}
$$

Replaced by function "np" 11/11/98.

$$
npb(plus) := mnp\left(Tprof_{b.bar}, T_{s.b.bar} + plus, \frac{G_b\left\langle T_{s.b.bar} + plus\right\rangle}{\rho_b}, \frac{G_{b.bar}}{\rho_b}, d_b\left\langle T_{ref}\right\rangle, \Delta t, xx\right)
$$

$$
npap(plus) := mnp\left(Tprof_{ap.bar}, T_{s.ap.bar} + plus, \frac{G_{ap}\left\langle T_{s.ap.bar} + plus\right\rangle}{\rho_{ap}}, \frac{G_{ap.bar}}{\rho_{ap}}, d_{ap}\left\langle T_{ref}\right\rangle, \Delta t, xx\right)
$$

GIVEN

Algebraic solution of general mass flux given the individual mass fluxes of the components:

$$x_f = \text{interp}\left(\text{spliner}_s, \text{steadat}^{\langle 0 \rangle}, \text{steadat}^{\langle 5 \rangle}, P\right)$$

Total flame height:

$$x_f = G_p\left(T_{s.ap}, T_{s.b}\right)\cdot\left[\frac{D^*_{ap}\left(D_{ap}, T_{s.ap}, T_{s.b}\right)^2}{A_{diff}\cdot\left[\left(D_0\cdot T_{f.ap}^{0.75}\cdot\frac{M}{R}\right)\cdots + k\cdot G_p\left(T_{s.ap}, T_{s.b}\right)\cdot D^*_{ap}\left(D_{ap}, T_{s.ap}, T_{s.b}\right)\cdot\left[\operatorname{atan}\left(C_1\cdot C_2\right)\cdots + \operatorname{atan}\left[\left(\frac{1}{x_r\left(T_{s.ap}, T_{s.b}, P\right)} - C_1\right)\cdot C_2\right]\right]\right]}\right]\cdot 10^6 \cdots + x_r\left(T_{s.ap}, T_{s.b}, P\right)$$

Binder surface temperature:

$$T_{s.b} = \frac{G_b\left(T_{s.b}\right) C_{p.s.b}\left(T_{ref}\right)\cdot T_i + \frac{\lambda_{g.b}\left(T_{s.b}\right)\cdot T_f\cdot \nu_b}{x_f\cdot 10^{-6}} + G_b\left(T_{s.b}\right)\cdot q_{v.b}\cdots + \frac{-\rho_b\cdot C_{p.s.b}\left(T_{ref}\right)}{\Delta t}\cdot\Delta x\cdot\left(\text{np}\left(\text{Tprof}_{b.p}, T_{s.b}, \frac{G_b\left(T_{s.b}\right)}{\rho_b}, r_{b.p}, d_b\left(T_{ref}\right), \Delta t, xx\right) - \text{Tprof}_{b.p}\right)}{C_{p.s.b}\left(T_{ref}\right)\cdot G_b\left(T_{s.b}\right) + \frac{\lambda_{g.b}\left(T_{s.b}\right)\cdot \nu_b}{x_f\cdot 10^{-6}}}$$

Oxidizer surface temperature:

$$T_{s.ap} = \frac{G_{ap}\left(T_{s.ap}\right)\cdot C_{p.s.ap}\left(T_{ref}\right)\cdot T_i + \frac{\lambda_{g.ap}\left(T_{s.ap}\right)\cdot T_{f.ap}\cdot \nu_{ap}}{x_{f.ap}\left(P, T_{s.ap}, T_{f.ap}\right)\cdot 10^{-6}} + G_{ap}\left(T_{s.ap}\right)\cdot q_{v.ap}\cdots + \frac{-\rho_{ap}\cdot C_{p.s.ap}\left(T_{ref}\right)}{\Delta t}\cdot\Delta x\cdot\left(\text{np}\left(\text{Tprof}_{ap.p}, T_{s.ap}, \frac{G_{ap}\left(T_{s.ap}\right)}{\rho_{ap}}, r_{ap.p}, d_{ap}\left(T_{ref}\right), \Delta t, xx\right) - \text{Tprof}_{ap.p}\right)}{G_{ap}\left(T_{s.ap}\right)\cdot C_{p.s.ap}\left(T_{ref}\right) + \frac{\lambda_{g.ap}\left(T_{s.ap}\right)\cdot \nu_{ap}}{x_{f.ap}\left(P, T_{s.ap}, T_{f.ap}\right)\cdot 10^{-6}}}$$

AP flame temperature:

$$T_{f.ap} = \text{interp}\left(\text{spliner}_9, \text{steadat}^{\langle 0 \rangle}, \text{steadat}^{\langle 9 \rangle}, P\right)$$

$$T_{f.ap} = T_f - \frac{G_p\left(T_{s.ap}, T_{s.b}\right)\cdot q_f}{G_p\left(T_{s.ap}, T_{s.b}\right)\cdot C_{p.g.p} + \frac{\nu_{f.ap}\cdot\lambda_{g.p}\left(T_{f.ap}\right)}{\left(x_f - x_{f.ap}\left(P, T_{s.ap}, T_{f.ap}\right)\right)\cdot 10^{-6}}}$$

This is the iterative solver. It takes the previous temperature profiles and other variables.

$$\text{unsteady}\left(P, x_{f}, T_{s.b}, T_{s.ap}, T_{f.ap}, \text{Tprof}_{ap.p}, \text{Tprof}_{b.p}, r_{ap.p}, r_{b.p}, \Delta t\right) := \text{find}\left(x_{f}, T_{s.b}, T_{s.ap}, T_{f.ap}\right)$$

This is the big-daddy solver.

$$\text{sol}(P, \Delta t) := \left|\begin{array}{l}
\text{sol}^{\langle 0\rangle} \leftarrow \begin{bmatrix} x_{f.bar} \\ T_{s.b.bar} \\ T_{s.ap.bar} \\ T_{f.ap.bar} \\ 0 \\ 0 \end{bmatrix} \\
PP_{0} \leftarrow P_{bar} \\
\text{Tprof}_{ap} \leftarrow \text{Tprof}_{ap.bar} \\
\text{Tprof}_{b} \leftarrow \text{Tprof}_{b.bar} \\
\text{for } jj \in 1 .. \text{rows}(P) \\
\quad \left|\begin{array}{l}
\text{on error} \\
\quad \left|\begin{array}{l}
\text{sol}^{\langle jj\rangle} \leftarrow \text{unsteady}\left(P_{jj-1}, \text{sol}_{0,jj-1}, \text{sol}_{1,jj-1}, \text{sol}_{2,jj-1}, \text{sol}_{3,jj-1}, \text{Tprof}_{ap}, \text{Tprof}_{b}, \dfrac{G_{ap}\left(\text{sol}_{2,jj-1}\right)}{\rho_{ap}}, \dfrac{G_{b}\left(\text{sol}_{1,jj-1}\right)}{\rho_{b}}, \Delta t\right) \\
\text{ans} \leftarrow \text{submatrix}(\text{sol}, 0, \text{rows}(\text{sol}) - 1, 1, \text{cols}(\text{sol}) - 1)^{T} \\
\text{return ans}
\end{array}\right. \\
\text{Tprof}_{ap.new} \leftarrow \text{np}\left(\text{Tprof}_{ap}, \text{sol}_{2,jj}, \dfrac{G_{ap}\left(\text{sol}_{2,jj}\right)}{\rho_{ap}}, \dfrac{G_{ap}\left(\text{sol}_{2,jj-1}\right)}{\rho_{ap}}, d_{ap}\left(T_{ref}\right), \Delta t, xx\right) \\
\text{Tprof}_{b.new} \leftarrow \text{np}\left(\text{Tprof}_{b}, \text{sol}_{1,jj}, \dfrac{G_{b}\left(\text{sol}_{1,jj}\right)}{\rho_{b}}, \dfrac{G_{b}\left(\text{sol}_{1,jj-1}\right)}{\rho_{b}}, d_{b}\left(T_{ref}\right), \Delta t, xx\right) \\
\text{sol}_{4,jj} \leftarrow \dfrac{\rho_{ap} \cdot C_{p.s.ap}\left(T_{ref}\right)}{\Delta t} \cdot \Delta x \cdot \left(\text{Tprof}_{ap.new} - \text{Tprof}_{ap}\right) \\
\text{sol}_{5,jj} \leftarrow \dfrac{\rho_{b} \cdot C_{p.s.b}\left(T_{ref}\right)}{\Delta t} \cdot \Delta x \cdot \left(\text{Tprof}_{b.new} - \text{Tprof}_{b}\right) \\
\text{Tprof}_{ap} \leftarrow \text{Tprof}_{ap.new} \\
\text{Tprof}_{b} \leftarrow \text{Tprof}_{b.new}
\end{array}\right. \\
\text{ans} \leftarrow \text{submatrix}(\text{sol}, 0, \text{rows}(\text{sol}) - 1, 1, \text{cols}(\text{sol}) - 1)^{T}
\end{array}\right.$$

Use this section to solve for only one point on the response function curve.

Frequency (Hz): $\omega := 5000$

$start := 3 \cdot 10^{-5}$

$\Delta t := \min\left(\begin{bmatrix} \frac{1}{\omega \cdot 59} \\ 10^{-5} \\ \frac{\tau_{min}}{37} \end{bmatrix}\right)$

$steps := \max\left(\begin{bmatrix} ceil\left(\frac{\tau_{max} \cdot 10}{\Delta t}\right) \\ ceil\left(\frac{3}{\omega \cdot \Delta t}\right) \end{bmatrix}\right) + ceil\left(\frac{start}{\Delta t}\right)$

$\Delta t = 3.39 \cdot 10^{-6}$ $\tau_{min} = 1.135 \cdot 10^{-3}$ $steps = 4.138 \cdot 10^{3}$

$\tau_{max} = 1.4 \cdot 10^{-3}$

$nn := 0 .. steps - 1$ $tt_{nn} := \Delta t \cdot nn$

Model the pressure function.

Step function: $P_{nn} := P_{bar} + P_{bar} \cdot \Phi\left(tt_{nn} - start\right)$

Ramp: $P_{nn} := P_{bar} + \frac{tt_{nn} - start}{0.005} \cdot P_{bar} \cdot \Phi\left(tt_{nn} - start\right)$

Sine wave: $P_{nn} := P_{bar} + \Phi\left(tt_{nn} - start\right) \cdot \left[mag \cdot \sin\left[2 \cdot \pi \cdot \left(tt_{nn} - start\right) \cdot \omega\right]\right]$

Exponential: $P_{nn} := P_{bar} + P_{bar} \cdot \left(1 - e^{\frac{-tt_{nn}}{resptime}}\right)$

Get the previous solution: $ugh :=$ C:\..\oscout.txt $kk := 0 .. rows(ugh) - 1$

Plot the pressure function.

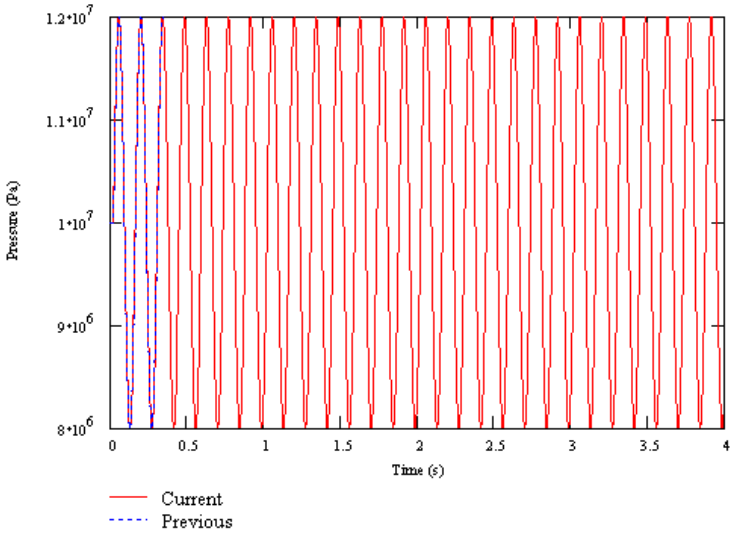

Solve. ans := sol(P, Δt) ii := 0.. rows(ans) – 1

Plot the mass fluxes:

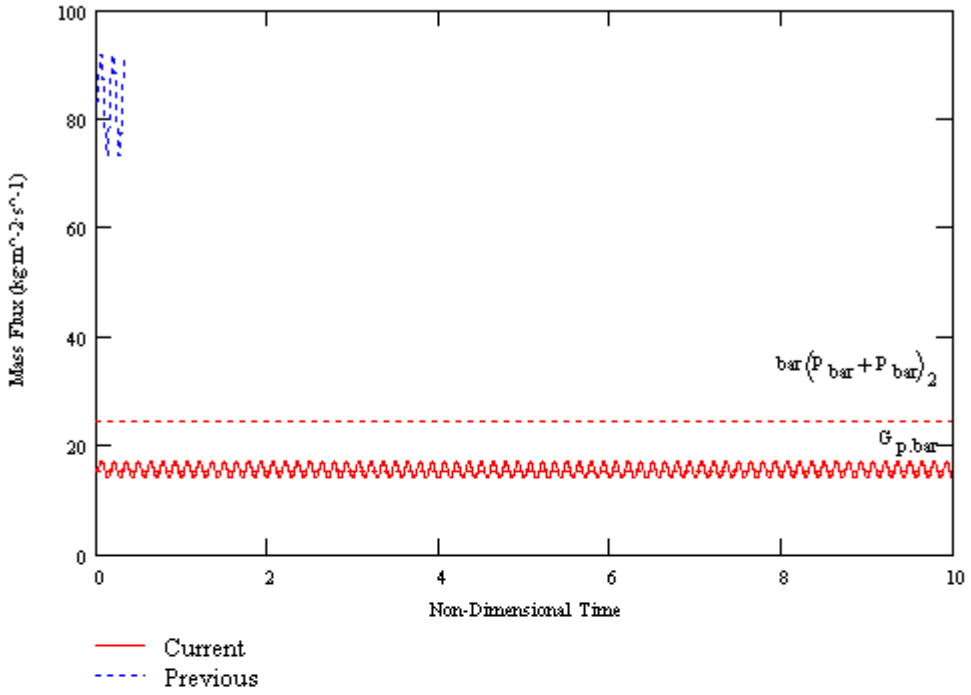

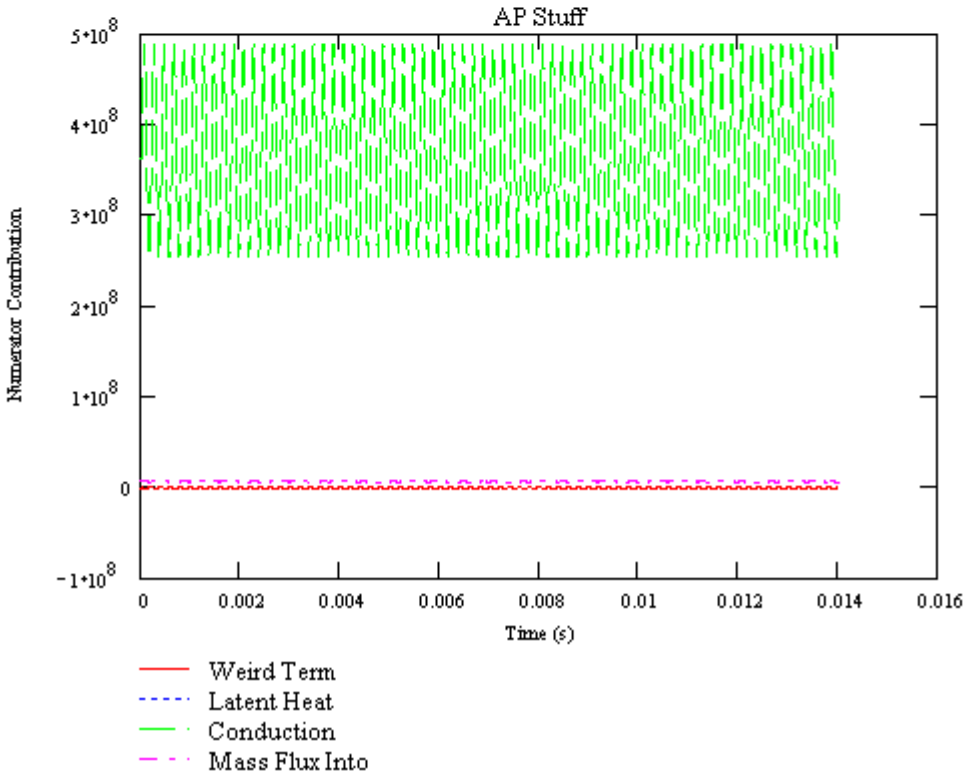

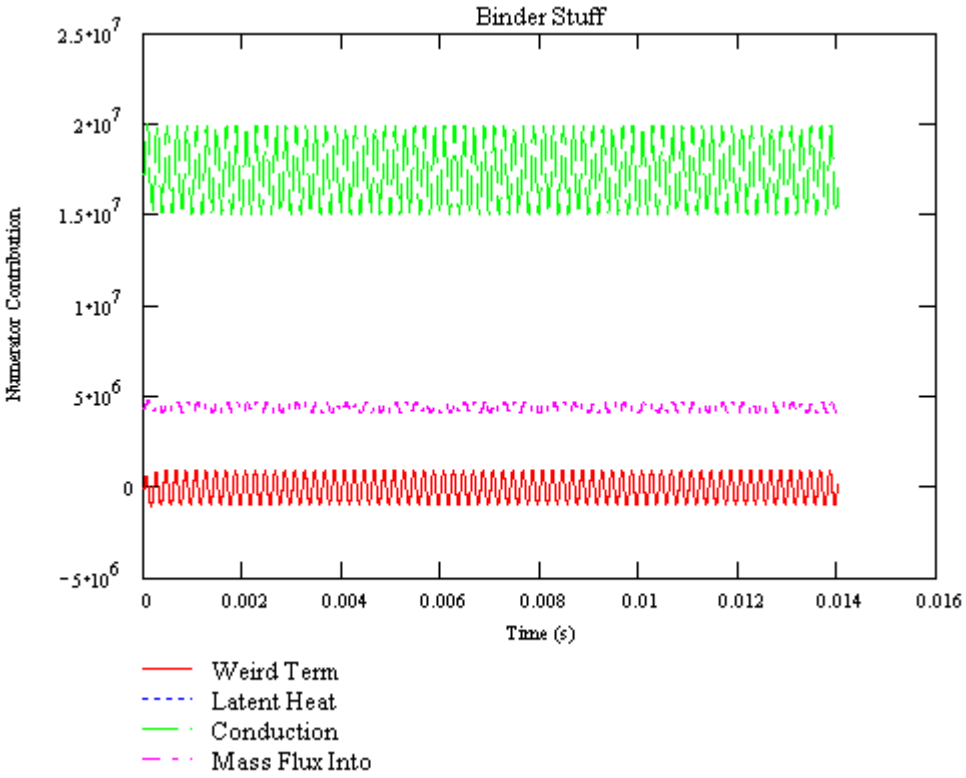
Binder Stuff
Numerator Contribution
2.5•10^7
2•10^7
1.5•10^7
1•10^7
5•10^6
0
-5•10^6
0
0.002
0.004
0.006
0.008
0.01
0.012
0.014
0.016
Time (s)
Weird Term
Latent Heat
Conduction
Mass Flux Into

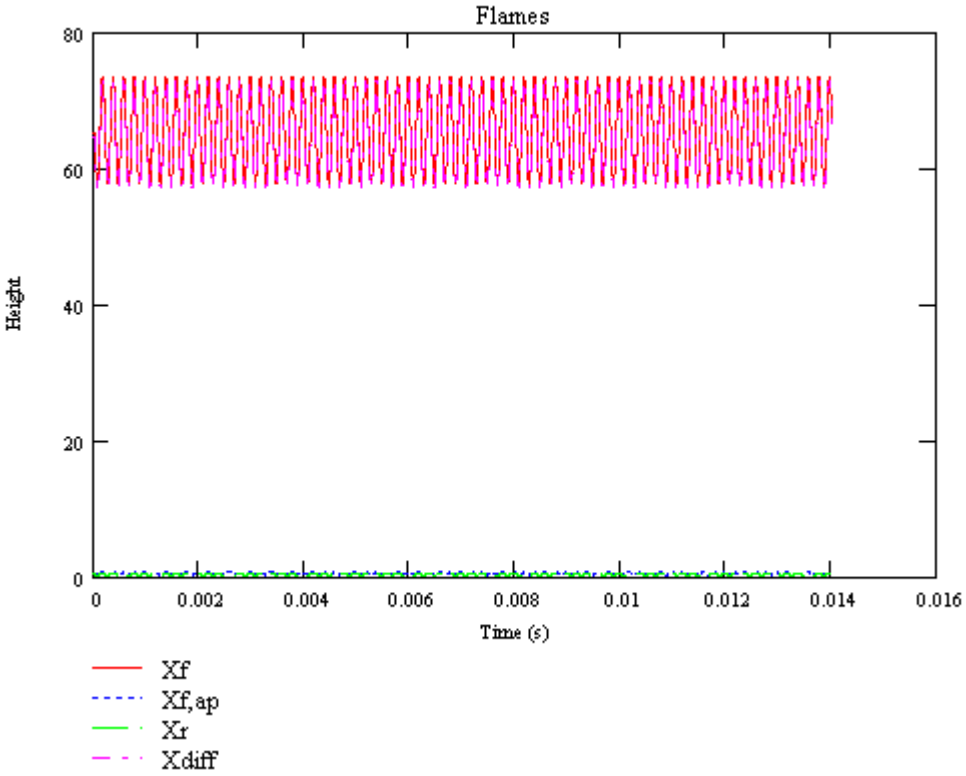
Flames
Height
80
60
40
20
0
0
0.002
0.004
0.006
0.008
0.01
0.012
0.014
0.016
Time (s)
Xf
Xf,ap
Xr
Xdiff

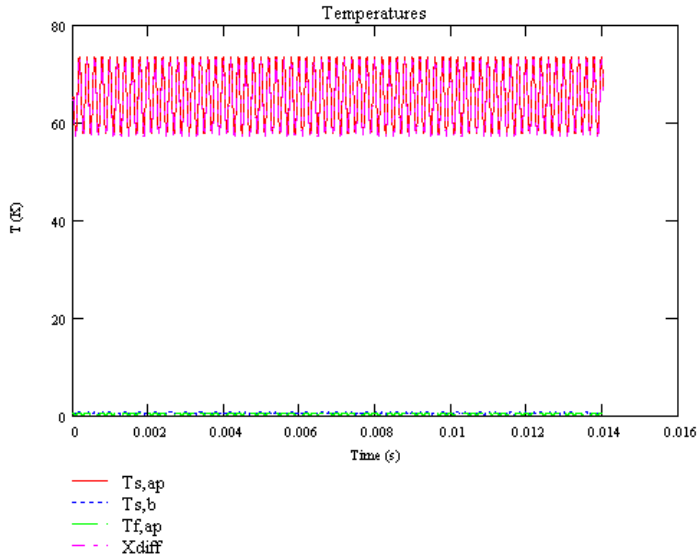

Get the response function. $pp := steps - 1, steps - 2 .. ceil\left(steps - \frac{1}{\omega \cdot \Delta t}\right)$

$$iggy_{steps-1-pp} := G_p\left[\left\langle ans^{\langle 2\rangle}\right\rangle_{pp}, \left\langle ans^{\langle 1\rangle}\right\rangle_{pp}\right]$$

$$igbar := mean(iggy) \quad igbar2 := \frac{max(iggy) + min(iggy)}{2}$$

$$R_p := \left[\frac{\frac{max(iggy) - igbar}{igbar}}{\frac{mag}{P_{bar}}} \quad \frac{\frac{igbar - min(iggy)}{igbar}}{\frac{mag}{P_{bar}}} \quad \frac{igbar - G_{p.bar}}{G_{p.bar}} \quad \frac{\frac{igbar2 - min(iggy)}{igbar2}}{\frac{mag}{P_{bar}}} \quad \frac{igbar2 - G_{p.bar}}{G_{p.bar}} \quad \frac{\frac{max(iggy) - G_{p.bar}}{G_{p.bar}}}{\frac{mag}{P_{bar}}} \quad \frac{\frac{G_{p.bar} - min(iggy)}{G_{p.bar}}}{\frac{mag}{P_{bar}}}\right]$$

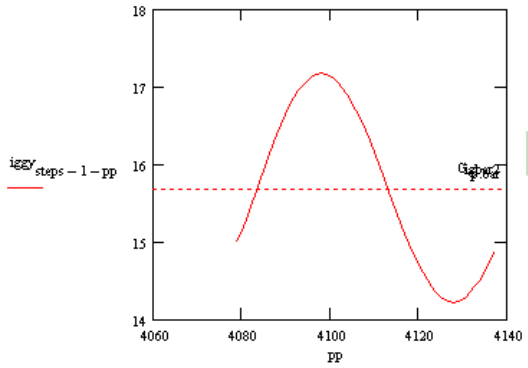

$$R_p = \begin{bmatrix} 0.47 & 0.47 & 2.973 \cdot 10^{-4} & 0.47 & 3.023 \cdot 10^{-4} & 0.472 & 0.469 \end{bmatrix}$$

Write the solution out to a file.

C:\..\oscout.txt

augment(submatrix(P, 0, rows(ans) – 1, 0, 0), augment(submatrix(tt, 0, rows(ans) – 1, 0, 0), ans))

SOLUTION SECTION II:

Use this section for calculating an entire response function curve. Define the ω vector and let that baby run.

$$\omega := (30 \;\; 50 \;\; 75 \;\; 125 \;\; 150 \;\; 200 \;\; 300 \;\; 400 \;\; 500 \;\; 600 \;\; 700 \;\; 800 \;\; 900 \;\; 1000 \;\; 1500 \;\; 2000)^{T}$$

$$kk := 0 .. rows(\omega) - 1 \qquad \Delta t_{kk} := \min\left(\left[\frac{1}{\omega_{kk} \cdot 59} \;\; 10^{-5} \;\; \frac{\tau_{min}}{37}\right]^{T}\right)$$

$$steps_{kk} := \max\left(\left[ceil\left(\frac{\tau_{max} \cdot 10}{\Delta t_{kk}}\right) \;\; ceil\left(\frac{10}{\omega_{kk} \cdot \Delta t_{kk}}\right)\right]^{T}\right) + ceil\left(\frac{start}{\Delta t_{kk}}\right)$$

$$P(\omega, steps, \Delta t) := \left| \begin{array}{l} \text{for } jj \in 0 .. steps - 1 \\ \quad P_{jj} \leftarrow P_{bar} + \Phi(\Delta t \cdot jj - start) \cdot mag \cdot \sin(2 \cdot \pi \cdot (\Delta t \cdot jj - start) \cdot \omega) \\ P \end{array} \right.$$

Solve for the full response function.

$$R_P := \left| \begin{array}{l} \text{for } kk \in 0..\text{rows}(\omega) - 1 \\ \quad ans \leftarrow \text{sol}\left(P\left(\omega_{kk}, steps_{kk}, \Delta t_{kk}\right), \Delta t_{kk}\right) \\ \quad iggy \leftarrow 0 \\ \quad \text{for } pp \in steps_{kk} - 1, steps_{kk} - 2..\text{ceil}\left(steps_{kk} - \frac{1}{\omega_{kk} \cdot \Delta t_{kk}}\right) \\ \quad\quad iggy_{steps_{kk} - 1 - pp} \leftarrow G_p\left[\left\langle ans^{\langle 2 \rangle}\right\rangle_{pp}, \left\langle ans^{\langle 1 \rangle}\right\rangle_{pp}\right] \\ \quad igbar \leftarrow \text{mean}(iggy) \\ \quad igbar2 \leftarrow \frac{\min(iggy) + \max(iggy)}{2} \\ \quad R_P^{\langle kk \rangle} \leftarrow \left[\frac{\frac{\max(iggy) - igbar}{igbar}}{\frac{mag}{P_{bar}}} \quad \frac{\frac{igbar - \min(iggy)}{igbar}}{\frac{mag}{P_{bar}}} \quad \frac{igbar - G_{p.bar}}{G_{p.bar}} \quad \frac{\frac{\max(iggy) - igbar2}{igbar2}}{\frac{mag}{P_{bar}}} \quad \frac{igbar2 - G_{p.bar}}{G_{p.bar}} \quad \frac{\frac{\max(iggy) - G_{p.bar}}{G_{p.bar}}}{\frac{mag}{P_{bar}}} \quad \frac{\frac{G_{p.bar} - \min(iggy)}{G_{p.bar}}}{\frac{mag}{P_{bar}}}\right]^T \\ \text{return } R_P \end{array} \right.$$

$$R_P := R_P^T$$

And here is the answer.

$$kk := 0..\text{rows}\left(R_P\right) - 1$$

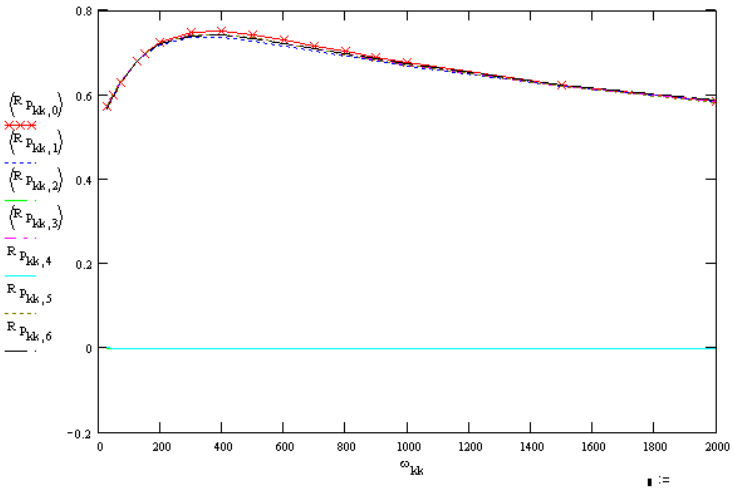

$$\blacksquare := \blacksquare$$

C:\Rp20080298201OO.txt

$$\text{augment}\left(\omega, R_P\right)$$

REFERENCES

[1] Kubota, N. 1984. "Survey of Rocket Propellants and Their Combustion Characteristics," *Fundamentals of Solid Propellant Combustion*, Kuo, K., and M. Summerfield (Eds.). AIAA Progress in Aeronautics and Astronautics, Vol. 90, pp. 1-52.

[2] Strand, L., and R. Brown. 1992. "Laboratory Test Methods for Combustion-Stability Properties of Solid Propellants," *Nonsteady Burning and Combustion Stability of Solid Propellants*, De Luca, L., E. Price and M. Summerfield, (Eds.). AIAA Progress in Aeronautics and Astronautics, Vol. 143, pp. 689-718.

[3] Crawford, B. L., Jr., C. Huggett, F. Daniels and R. E. Wilfong. 1947. "Direct Determination of Burning Rates of Propellant Powders," *Analytical Chemistry*, Vol. 19, No. 9, pp. 630-633.

[4] Cauty, F. and J. Demarais. 1990. "Ultrasonic Measurement of The Uncured Solid Propellant Burning Rate," *Proceedings of the 21st ICT International Congress*, Karlsruhe, Germany. ONERA TP 1990-90.

[5] McQuade, W. 1998. *Ultrasound Technique Resolution for Solid Propellant Burning Rate Measurement*, M.S. Thesis, University of Alabama in Huntsville, Huntsville, AL.

[6] Razdan, M., and K. Kuo. 1984. "Erosive Burning of Solid Propellants," *Fundamentals of Solid Propellant Combustion*, Kuo, K., and M. Summerfield (Eds.). AIAA Progress in Aeronautics and Astronautics, Vol. 90, pp. 515-598.

[7] Cohen, N., and D. Flanigan. 1983. *A Literature Review of Solid Propellant Burn Rate Temperature Sensitivity* Morton Thiokol Corporation, Huntsville, AL. AFRPL-TR-83-042.

[8] Price, E. 1992. "Solid Rocket Combustion Instability- An American Historical Account," *Nonsteady Burning and Combustion Stability of Solid Propellants*, De Luca, L., E. Price and M. Summerfield, (Eds.). AIAA Progress in Aeronautics and Astronautics, Vol. 143, pp. 1-16.

[9] Strand, L., A. Schultz and G. Reedy. 1974. "Microwave Doppler Shift Technique for Determining Solid Propellant Regression Rates," *Journal of Spacecraft and Rockets*, Vol. 11, No. 2, pp.75-80.

[10] Traineau, J., M. Prévost, and P. Tarrin. 1994. "Experimental Low and Medium Frequency Determination of Solid Propellants Pressure-Coupled Response Function," AIAA 94-3043.

[11] Cauty, F., P. Comas, F. Vuillot and M. Micci. 1996. "Magnetic Flow Meter Measurement of Solid Propellant Pressure-Coupled Responses Using an Acoustic Analysis," *Journal of Propulsion and Power*, Vol. 12, No. 2, pp.436-438.

[12] Beckstead, M., R. Derr and C. Price. 1970. "A Model of Solid-Propellant Combustion Based on Multiple Flames," *AIAA Journal*, Vol. 8, No. 12, pp.2200-2207.

[13] Cohen, N. 1980. "Review of Composite Burn Rate Modeling," *AIAA Journal*, Vol. 18, No. 3, pp. 277-293.

[14] Cohen, N., and L. Strand. 1982. "An Improved Model for the Combustion of AP Composite Propellants," *AIAA Journal*, Vol. 20, No. 12, pp.1739-1746.

[15] Condon, J., J. Osborn and R. Glick. 1976. "Statistical Analysis of Polydisperse, Heterogeneous Propellant Combustion: Steady-state," 13th JANNAF Combustion Meeting, CPIA Publication 281, Vol. 2, pp.313-345.

[16] Condon, J., J. Renie and J. Osborn. 1979. "Oxidizer Size Distribution Effects on Propellant Combustion," *AIAA Journal*, Vol. 17, No. 8, pp.878-883.

[17] Sutton, G. P. 1992. *Rocket Propulsion Elements*. Wiley, New York.

[18] Ramohalli, K. 1984. "Steady-State Burning of Composite Propellants under Zero Cross-Flow Situation," *Fundamentals of Solid Propellant Combustion*, Kuo, K., and M. Summerfield (Eds.). AIAA Progress in Aeronautics and Astronautics, Vol. 90, pp. 409-477.

[19] Denison, M., and E. Baum. 1961."A Simplified Model of Unstable Burning in Solid Propellants," *Journal of the American Rocket Society*, Vol. 31, 1961, p.1112.

[20] Novozhilov, B. 1992. "Theory of Nonsteady Burning and Combustion Stability of Solid Propellants Using the Zeldovich-Novozhilov Method," *Nonsteady Burning and Combustion Stability of Solid Propellants*, De Luca, L., E. Price and M. Summerfield, (Eds.). AIAA Progress in Aeronautics and Astronautics, Vol. 143, pp. 601-639.

[21] Barrère, M. 1992. "Introduction to Nonsteady Burning and Combustion Instability," *Nonsteady Burning and Combustion Stability of Solid Propellants*, De Luca, L., E. Price and M. Summerfield, (Eds.). AIAA Progress in Aeronautics and Astronautics, Vol. 143, pp. 17-58.

[22] Brewster, Q, and S. Son. 1995. "Quasi-Steady Combustion Modeling of Homogeneous Solid Propellants," *Combustion and Flame*, Vol. 103, pp. 11-26.

[23] Lengellé, G. 1970. "Thermal Degradation Kinetics and Surface Pyrolysis of Polymers," *AIAA Journal*, Vol. 8 No. 11, pp. 1989-1998.

[24] Group discussions at a meeting for the Multidisciplinary University Research Initiative (MURI), Cleveland, OH; July 1998.

[25] Cohen, N. 1981. "Response Function Theories That Account for Size Distribution Effects— a Review," *AIAA Journal*, Vol. 19, No. 7, pp. 907-912.

[26] Condon, J., J. Osborn and R. Glick. 1976. "Statistical Analysis of Polydisperse, Heterogeneous Propellant Combustion: Nonsteady-state," 13th JANNAF Combustion Meeting, CPIA Publication 281, Vol. 2, pp.209-223.

[27] Brown, R., and R. Muzzy. 1970. "Pressure-Coupled Combustion Instability," *AIAA Journal*, Vol. 8, No. 8, pp. 1492-1500.

[28] Galfetti, L., G. Riva and C. Bruno. 1992. "Numerical Computations of Solid-Propellant Nonsteady Burning in Open or Confined Volumes," *Nonsteady Burning and Combustion*

Stability of Solid Propellants, De Luca, L., E. Price and M. Summerfield, (Eds.). AIAA Progress in Aeronautics and Astronautics, Vol. 143, pp. 643-687.

[29] Louwers, J., and G. Gaidot. 1997. "Model for the Nonlinear Transient Burning of Hydrazinium Nitroformate," International Workshop: Combustion Instability of Solid Propellants and Rocket Motors, Milano, Italy.

[30] Louwers, J. and G. Gaidot. 1996. "Nonlinear Transient Burning of Composite Propellants: The Effect of Solid Phase Reactions," Proceedings of the 4th International Symposium on Special Topics in Chemical Propulsion: Challenges in Propellants & Combustion 100 Years after Nobel, Stockholm, Sweden.

[31] Chiaverini, M., G. Harting, L. Yeu-Cherng, K. Kuo, A. Peretz, S. Jones, B. Wygle and J. Arves. 1997. "Pyrolysis Behavior of Hybrid Rocket Solid Fuels Under Rapid Heating Conditions," AIAA 97-3078.

[32] Chen, J., and T. Brill. 1991. "Chemistry and Kinetics of Hydroxyl-terminated Polybutadiene (HTPB) and Diisocyanate-HTPB Polymers during Slow Decomposition and Combustion-Like Conditions," *Combustion and Flame*, Vol. 87, pp. 217-232.

[33] Burke, S., and T. Schumann. 1928. "Diffusion Flames," *Industrial and Engineering Chemistry*, Vol. 20, p. 998.

[34] Penner, S. S. 1957. *Chemistry Problems in Jet Propulsion*. Wiley, Los Angeles.

[35] *Mathcad User's Guide.* (Version 6.0). 1995. MathSoft, Inc. Cambridge, MA.

[36] Holman, J. 1927. *Heat Transfer*. McGraw Hill, New York..

[37] Kreyszig, E. 1993. *Advanced Engineering Mathematics*. John Wiley & Sons, New York.

[38] Press, W., B. Flannery, S. Teukolsky and W. Vetterling. 1987. *Numerical Recipes*. Cambridge University Press, New York, p. 40.

[39] Jeppson, M., M. Beckstead and Q. Jing. 1998. "A Kinetic Model for the Premixed Combustion of a Fine AP/HTPB Propellant," AIAA 98-0447.

BILBIOGRAPHY

1. Beckstead, M. 1981. "A Model for Solid Propellant Combustion," *18th Symposium (International) on Combustion*, The Combustion Institute, pp. 175-185.

2. Bellec, R., J. Duterque and G. Lengellé. 1996. *Modélisation de la Combustion des Propergols Solides Aluminisés*, ONERA Rapport Technique 37/7128 EN.

3. Condon, J. 1978. *The Effect of Oxidizer Particle Size on the Steady-state Combustion, Erosive Burning and Nonsteady Combustion of Polydisperse Composite Solid Propellants*, Ph.D. Dissertation, Purdue University, May.

4. King, M. 1996. "Examination of Chemical Approaches to Stabilizing Composite-Propellant Combustion" *Journal of Propulsion and Power*, Vol. 12, No. 3, pp. 554-563.

5. Renie, J. 1982. *Combustion Modeling of Composite Solid Propellants*, Ph.D. Dissertation, Purdue University.

6. Rasmussen, B., and R. A. Frederick, Jr. 1998. "Issues in Nonlinear, Nonsteady Solid Combustion Modeling" 1998 JANNAF CS/PSHS/APS Joint Meeting; Tucson, AZ.

7. Rasmussen, B., R. A. Frederick, Jr., M. D. Moser and G. Lengellé. "A Theoretical Pressure-Driven Response Function for Composite Solid Propellants," 1998 JANNAF Propulsion Meeting; Cleveland, OH.

8. Rasmussen, B., R. A. Frederick, Jr. and G. Lengellé. 1997. "Pressure-Coupled Frequency Response Models of Solid Propellants," 1997 JANNAF CS/PSHS/APS Joint Meeting; W. Palm Beach, FL.